Updated understanding of landslides kinematics along the Thompson River Valley using satellite InSAR

by

Amir Soltanieh

A thesis submitted in partial fulfillment of the requirements for the degree of

Master of Science

in

Geotechnical Engineering

Department of Civil and Environmental Engineering

University of Alberta

Abstract

Geohazards threaten human's well-being in many different ways. Landslide, as a common geohazard in both natural and anthropogenic man-made features all around the world, generally, damage many infrastructures, nature balance, animal habitat and cause even loss of lives for many creatures as well as human beings when they occur.

Transportation corridors along valleys are example of the most vulnerable areas in landslide occurrences. The Thompson River Valley South of town of Ashcroft in British Columbia, Canada is one of the most important transportation corridors within Canada which connects the Port of Vancouver to other parts of Canada to haul goods from and into this port by Canadian Pacific and Canadian National Railways. This corridor hosts several landslides along the valley. Monitoring the landslides along this valley can reduce risk of landslide on the transportation system of Canada by alerting of the existence of any possible landslide in this area or their acceleration. Improvements in remote sensing helps geotechnical engineers to monitor massive areas by using satellite radar interferometry (InSAR). This technology helps to observe terrain movements near real time with milimeter accuracy for massive aerial extents and revisiting times of less than a week.

The aerial coverage of Insar, and having different sensors monitoring the same location from different angles o view, provide an opportunity to better understand the 3-dimentional motion of the ground surface that can allow an enhanced kinematic interpretation of the landslide.

In this research updating interpretation of kinematic of landslides along the Thompson River valley south of the town of Ashcroft in British Columbia, Canada is presented. For this purpose, I used the data gathered from the Sentinel 1 satellite's constellation, that it is a radar-based technology for measuring ground movement. I estimated the true ground displacement vector

through geometric combination of different LOS and general assumptions of the expected kinematics of landslides in this thesis. The recorded 2 years LOS changes from different orbits of Sentinel 1 constellations are used in this research to have better understanding of ground's movements in the area of investigation . First, this method is applied for the Ripley landslide, which has been investigated by pervious researchers and the results of recorded data by installed GPS system is used , to validate the accuracy and reliability of the result of this method. The results of the applied method agreed with the reported displacement of the Ripley landslide by GPS system both in magnitudes and directions of movements. , The method is then used to estimate the true ground displacement vectors for other landslides along the Thompson River valley with more impacts on the railways along the valley. The monitoring results of the research allowed for an enhancement in the understanding of the kinematics of the landslides in the study area. Furthermore, this method was tested and validated for this area and provides a tool to extract useful information from Satellite InSAR data.

Preface

This thesis is an original work by Amir Soltanieh at University of Alberta which is supervised by Dr.Renato Macciotta Pulisci. The data used in this thesis were gathered from Sentinel 1 satellite which were pre-processed and provided by TRE Altamira group. The method of calculations is lunched to Updated understanding of landslides kinematics along the Thompson River Valley using satellite InSAR.

Dedication

To my Mom and Dad for saying my appreciation to give me the opportunity for living and for My reasons of my life, Mahya, Nirvan And Niki.

Acknowledgments

I, Amir Soltanieh, would like highly to acknowledge Dr. Macciotta for his kind advice and support to push this research ahead. Without his help I could not be successful to finish this project undoubtedly.

I also would like to acknowledge Canadian Pacific Railway (CP) and TRE Altamira for providing the InSAR monitoring data used in this research. This study was performed within the umbrella of the Railway Ground Hazards Research Program (RGHRP), which is funded by the Natural Sciences and Engineering Research Council of Canada (NSERC), Canadian Pacific Railway, Canadian National Railway, and Transport Canada; and is a collaboration that incudes Queen's University, the Canadian Geological Survey and the University of Alberta.

I also acknowledge my wife, Dr.Mahya Roustaei too, for supporting me in this path.

Table of content

List of Tables

List of Figures

1.Introduction

landslides, as a kind of geohazard, all around the world menace people's lives and infrastructure and create massive economical loss. Many historical landslides have been reported in Canada (Charrière et al., 2015; Cruden & Martin, 2007; Mei et al., 2008; Vallee, 2019). Hundreds of lives and millions of Dollars have been lost from 1771 due to landslide and their damages to infrastructure within Canada (Choe et al., 2021). Recently, climate change and global warming have increased the frequency of triggers for landslide's activities in cold region areas in Canada (Choe et al., 2021). Landslide in British Columbia's Highway 99 in November 2021 is a recent catastrophic landslide, which caused some fatilities and damaged infrastructure in Canada (Simon Little, Global News, November 20, 2021).

The Transportation system in Canada is vulnerable in landslide scenarios due to the path of railways and highways along the valleys. For instance, Thompson River valley is one of the most important transportation corridors for both Canadian Pacific and Canadian National Railways (CPR and CNR) which is employed to transport goods between Vancouver port and other parts of country (Clague & Evans, n.d.). The Thompson River valley hosts several landslides which are located on cut terrace by southward flowing Thompson River. These landslides, formed during postglacial period and are up to 150 meters high along the valley (Porter et al. 2002; Journault 2018).

There are 14 known landslides in the Thompson river valley which 12 of them traversed by one or both of CNR and CPR (Hendry et al., 2015). Landslides in this valley are different in size and the volume of the landslides in this area, vary between 0.75 million to 15 million cubic meters (Journault et al., 2018).

Monitoring activity of known landslides is one of the most effective risk management technics to predict possible landslide acceleration in susceptible areas when stabilization or avoidance are technically challenging or even impossible. This technic can help to manage and scheduling infrastructure's maintenance activities and also it can be applied for early warning systems to inform terrain's movements actively (Huntley et al., 2019b; Rodriguez et al., 2020) and it reduces the negative economic damage and possibility of fatalities due to landslide events. Particularly, using remote sensing technology helps to monitor landslide's movements near real-time for extensive areas with reasonable cost and adequate accuracy, and it helps to have better understanding of landslide's kinematic and probable triggers to enhance landslide risk management strategies (Dean et al. 2020, Macciotta et al. 2020, Woods et al. 2020, Lan et al. 2021, Rodriguez et al. 2021, Macciotta and Hendry 2021).

In this thesis, continuous improvement in landslide monitoring are been made. I am proposing a methodology to work with satellite radar data to improve some of interpretation of landslide's activity and doing an update of the kinematic of some of landslides along the Thompson River Valley.

1.1. Thesis objective

This MSc. project focused on the identified landslides in the Thompson River Valley south of town of Ashcroft, British Columbia, Canada with the global objective of developing interpretation of the kinematics of the landslides in this area. The specific objectives of this MSc. project are summarized as follow:

- To develop a method using data from two satellite orientations and assumptions on plausible kinematic characteristics (e.g. general horizontal direction) to estimate the true displacement vectors of landslides.
- Test the method for validation at the Ripley landslide which has in-place monitoring instrument's data.
- Using the validated method for other landslides along the Thompson River valley to better understanding the landslides' kinematics.

1.2.Methodology:

The Data which is used in this research, were collected by Sentinel-1 Satellite and processed by TRE Altamira Group for CPR. The SqueeSAR method, which is an advanced SAR method, was developed for the data to produce adequate data to cover the area of study within the Thompson River Valley.

At the first step of this study, the data was considered to find any possible time gaps during the data gathering time frame. Based on the gaps exist in the data, time frame between May 2015 and May 2017 was selected to detect the ground displacement in the area of research and understand the temporal and spatial ground displacement trends. Data from both descending and ascending orbits of Sentinel 1 satellite are used in this research to estimate the real displacement of each landslide through geometric calculations based on the orientations of the line of sight between the ground and the satellite (LOS) for two orientations and based on some kinematic assumptions. Although there is some asynchronization between selected time frames for ascending and descending orbits, the effect of this factor was estimated to be negligible in the final result.

The differences between the radar readings during the selected timeline for each point, reflect the projection of ground displacement on the LOS of the satellite. Using the projection for each orbit and employing an assumption about horizontal movement in the direction of average slope's aspect, I derive the estimated real displacement vector for each point within the area of research. A limitation is the preconceived assumption that the sector of landslide being analyzed would move subparallel to the azimuth of its slope, which then becomes the basis for the vertical components. This is expected to be valid for most landslides sectors, however, topographic variations could impact this assumption depending on the scale of the area analyzed and the scale of the topographic feature.

Each landslide in this investigation was divided to several sectors based on the size of the landslide, and average of readings for LOS within each sector reflects the changes of LOS for the sector. The sectors were selected to contain enough data from both satellite orbits to find the real displacement vector.

Finally, the results for the Ripley landslide along the Thompson River valley were verified by GPS result from the other research in different timeline by other researchers. The evaluated method then was employed for other landslides along the valley and the results are presented in other chapters of this research. The details of the method developed and the validation approach are included in more detail in the next chapters of the thesis as part of the publications published or under review.

1.3.Outline of thesis:

This thesis is organized into Four main chapters (Chapter 2 through 5). Two of the main chapters are under review for journal publication. The chapters have been organized in a relative

chronological fashion with each being unique in focus. Some similarities are observed within the chapters, as each journal article needs to be comprehensive in itself and the reader will observe the successively enhanced analysis through extended research.

Chapter 2 introduces a brief literature review of the area of research on landslides along the corridors, landslides located on the Thompson River valley and landslide remote sensing using satellite InSAR.

Chapter 3 presents the method developed and how it is used to improve the interpretation of landslide's movement, with an update of kinematic of the Ripley landslide on the Thompson river valley using satellite InSAR and evaluation of this method using exist in-place monitoring GPS system's data.

Chapter 4 illustrates the results of the validated method for other landslides along the Thompson river valley and presents an update for the kinematic of landslides in this area.

Chapter 5 presents general conclusions of the research and also recommendations for future research.

2.Literature review

This section presents a general literature review on the topics addressed in this thesis. Specific literature review for the steps of the work presented here are included in Chapter 3 and Chapter 4, which are a version of articles submitted for publication.

2.1. Landslides along transportation corridors:

Landslides are common elements of valleys around the world. Streams incise the ground surface and the erosion of ground and other factors lead to shallow to deep landslides, depending on the age of river, ground materials, climate, amongst other factors. Landslides along the river can divert the path of water which can, in turn, create new landslides. The location of landslides in valley's can depend on the vegetation, land use, geology, hydrology, seismology, lithology and climatology of the area which hosts landslides (Levy et al., 2011).

Multiple types of landslides have been reported in different locations around the world and many landslide triggers and contributing factors have been identified. The Grohovo landslide in December 1996 on the Rjecina River valley is identified as a complex retrogressive landslide with $1.0 \times 10^6\ m^3$ of debris which buried the Rjecina River's bed in Croatia (Arbanas et al., 2014), rockfalls, which are categorized as fast-moving landslides with a component of material falling airborne, have caused the largest catastrophic landslide in the Umbria Region of central Italy (Guzzetti et al., 2004), different sized rock falls as well as rotational and compound slides, Flexural toppling on mountain slopes and large rock avalanches are common in southwestern British Columbia (Hunger et al., 1999), relatively slow-moving rotational slumps with multiple back-tilted slide blocks, relatively slow-moving slides involving translational movement with

little rotation and sudden-onset, rapid flow slides in which the debris undergoes considerable disaggregation and flow on a gentle slope have been reported in the Thompson River valley in British Columbia, Canada (Clague et al., 2003). These are just some examples to illustrate the variety of landslides kinematics and mechanisms.

Valleys have always attracted urban and economic development or for use as transportation corridors. The village of St-Leon-le Grand with about 1000 inhabitants and the town of Louiseville with more than 7700 people are two of the most populated areas on the Chacoura River banks in Quebec Canada (Levy et al., 2011), Grohovo village, on the Rjecina River near the City of Rijeka, is the largest Croatian port on the north-eastern Adriatic coast and has experienced numerous historical landslides in past 250 years (Arbanas et al., 2014), The most important railways of Canada have traversed along the valley's to transport goods in extensive lands of Canada and the Thompson River valley is a vital strategic corridor for Canadian transportation system which has seen many occurrences of landslide activity so far (Clague et al., 2003), The Serchio River valley is a famous tourism area between the Alps and Apennines in Italy and usually experiences shallow landslides which caused reported damages and fatalities (Ginnecchini et al., 2012), Several roads and urban development are exposed to rockfalls and other landslide types near the village of Triponzo in Valnerina, Central Italy, along the Nera Valley (Guzzetti et al., 2004) and National highway NH-67 and 17 km of railway tracks declared as a 'world heritage railway route' by UNESCO connecting Mettupalayam to Coonoor Nilgiri of India which is threatened by many possible landslide (Jaiswal et al., 2012). All are some examples of the importance of transportation corridors along vales, and which are exposed to landslide hazards.

Landslides threaten human lives and cause damage to infrastructures (Levy et al., 2011; Herrera et al., 2012; Weidner et al., 2019; Arbanas et al., 2014; Porter et al 2015; Giannecchini et al., 2012; Tonini et al., 2014; Bradley et al., 2019; Wang et al., 2009). Maintenance of railways and roads in British Colombia, Canada already cost over $10 million per year by the end of last century (Hunger et al., 1999). Historically, there are many reported cases of loss of life and damage to infrastructure in Canada as a consequence of landslides (Charrière et al., 2015; Cruden & Martin, 2007; Mei et al., 2008; Vallee, 2019). Since 1771 there have been hundreds of fatalities and damage to infrastructures due to landslides in Canada, which have cost millions of dollars annually (Choe et al., 2021). A recent reminder of the harmful potential of landslides in Canada was the four fatalities confirmed in a recent landslide in British Columbia's Highway 99 in November 2021 (Simon Little, Global News, November 20, 2021).

Although landslides are recognized as very complex events, good risk assessment programs try to combine estimates of the likely location and time of future landslides and mitigation of consequences; with the highest possible reliability. Well-designed risk assessment programs also endeavor to estimate the volume of potential landslides (for proper consequence estimation) and also the frequency of landslide events in the areas of study (Guzzetti et al., 2004).

Data of previous landslides in the area of study are great resources to inform estimates of likelihood, timing and the volume and of future landslides (Hunger et al., 1999). Mapping and developing landslide inventories, in combination with ground monitoring provide a robust basis for the analyses required for landslide risk management and can also be helpful to schedule any maintenance required for infrastructures exposed to landslide movement (Arbanas et al., 2014). In this regard, deploying a near real-time monitoring system is considered as one of the most beneficial strategies for identification and management of landslide risks. In this thesis, satellite

InSAR data is used to have insight on activity and kinematics of landslides along the Thompson River Valley which has experienced several historical landslides, as a means to enhance the understanding of these landslides and provide for enhanced management strategies.

2.2. Landslides along the Thompson River valley:

The Thompson River Valley is one of the most important corridors for the Canadian transportation system. Both Canadian Pacific Railway (CPR) and Canadian National Railway (CNR) use this corridor since 1885 regularly to transport goods between the Port of Vancouver and the rest of Canada. Twenty-five to thirty trains every day carry different essential products each way, including products such as wheat, coal, and petrochemical products for export to the Pacific Rim, imported automobiles for the Canadian market, and intermodal cargo. The Thompson River is the largest tributary of Fraser River, vital for the life cycle of Pacific salmons and up to 4 million sockeye salmon and one million of pink salmon use the Thompson River as their migration path which support their market with more than $100 million in commercial value. The banks of the Thompson River valley are also used as farmlands (Clague & Evans, n.d.).

The importance of the Thompson River Valley made this corridor as a monitoring priority for Natural Resources Canada (NRCAN), the Geological Survey of Canada (GSC), and Transport Canada (TC) due to its possible impacts and effects on transportation services, human life and th environment; as it is vital to understand and manage the risks associated with landslides that threaten the corridor (Huntley et al., 2021).

The Thompson River valley stratigraphy consists of a series of glacial deposits, down cut by the southward moving Thomson River stream that developed slopes of 75 to 125 meter high and

slope angle between 15 to 30 degrees. The glacial deposits contain a wide range of materials from poorly sorted sand and gravel to rhythmically interbedded silt and clay, deposited by multiple glacial advance and retreat intervals in the Pleistocene period. The local bedrock in this area was formed by Triassic and Jurassic volcanic and sedimentary rocks (Clague and Evans 2003; Huntley and Bobrowsky 2014; Journault 2018; Porter et al., 2000).

The Thompson River flow led to several landslides of different heights and volumes by cutting the glacial deposited sediments along the valley and eroding the toes of the cut slopes. (Porter et al. 2002; Journault 2018). The presence of a weak silt and clay layer has been identified as the main geomorphological feature for the formation of these landslides, providing a basal sliding surface for the movement kinematics. These landslides are recognized by multiple graben and horst features as well as steep internal shear and basal through-going surfaces along these weak materials (Clague and Evans 2003; Eshraghian et al. 2007; Journault 2018). The Friction angle for this weak silt and clay layer has been estimated between 9 and 16 degrees (Hendry et al., 2015; Stark and Eid, 1994; Porter et al.,2000). Figure 2-1 illustrates the location of the valley and shows the extents of 12 of the identified landslides traversed by CNR and CPR railways along the valley. The sizes of these landslides vary between 0.75 million cubic meters for the Ripley landslide to more than 15 million cubic meters for North landslide. The landslides' velocities have been reported between 10 mm/year which is classified as extremely slow to accelerated episodes of up to 50 mm/s which is classified as very rapid landslide, historically in the area of study (Journault et al., 2018).

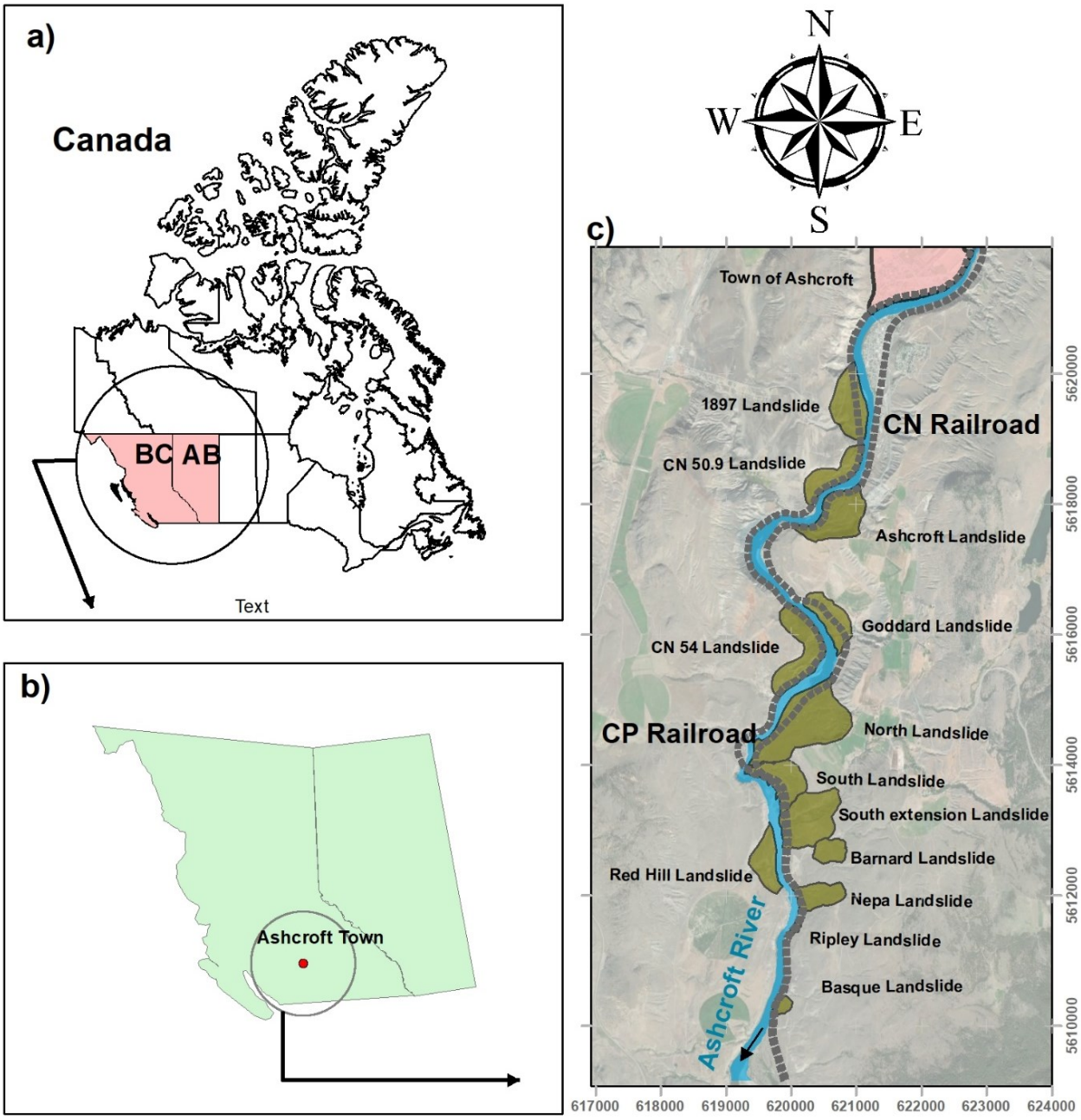

FIGURE 2-1. Thompson River Valley location (a,b) plan-view and active landslides across the valley (c). Coordinates in UTM (units in meters for scale purposes). BC and AB in (a) correspond to the provinces of British Columbia and Alberta, respectively.

Some of these landslides have been active in past and are currently dormant or move slow enough not to impact railway operations in this the corridor. Table 2-1 summarized the slope angles and movement rates of 6 landslides along Thompson River valley that were identified as posing high hazard on the infrastructure along the corridor (Journault et al., 2018).

Landslide	Area (m^2)	Average Slope Aspect (Degrees)	Average Slope (Degrees)	Average Downslope rate (mm/year)	Max Downslope rate (mm/year)
Ripley Landslide	23500	298	-13.2	49	77
South Extension Landslide	181000	235	-17.8	21	60
Goddard Landslide (Toe)	20000	209	-16.9	31	120
North Landslide (Toe)	49000	335	-16.7	25	81
Barnard Landslide	175000	272	-14.1	10	50
Red Hill landslide (Toe)	78500	85	-21.5	37	89

Table 2-1- Summarized characteristics of landslides along the Thompson River valley (Journault et al., 2018).

2.3 Landslide remote sensing with Satellite Interferometric Synthetic Aperture Radar (InSAR):

Innovative monitoring technologies in recent decades help engineers to have better understanding of earth crust movement which help to identify and manage possible landslides.

Great data availability from several lunches of both radar and optical space-borne platforms such as European ERS-1 and ERS-2 satellites, Japanese JERS-1, Canadian RADARSAT, United States LANDSAT TM, European ENVISAT, as well as commercial satellites such as IKONOS, QUICKBIRD and the improved capabilities of the space sensors as well as the development of more advanced Earth Observation data processing techniques have led to an increase in slope deformation and landslide monitoring using satellite imagery in recent years, together with other remote sensing techniques (Colesanti et al., 2006).

Remote sensing, GPS monitoring, geophysical imaging as part of geotechnical investigation are some new methods which are commonly employed for landslide movement characterization to enhance good understanding of landslide kinematic and behavior (Xu et al., 2016). Satellites that carry Synthetic Aperture Radar (SAR) sensors in Interferometric Synthetic Aperture Radar (InSAR) have been used in many applications to detect surface displacements of crustal deformation, glacier motion and landslides by utilizing wavelength information to calculate distance to the surface and that can be used for calculating relative change (Abe et al., 2020).

SAR records the electromagnetic echo backscattered from the Earth surface by sending microwave to the Earth crust and arranges a 2D image map, whose dimensions are the distance between sensor and its target and also the platform flight direction (azimuth). Although SAR offers several unique opportunities respect to its optical sensors, there are also considerable data processing and interpretation difficulties in this technique. The SAR system is independent of Sun illumination because it is an active method that emits energy as microwaves from its sensor that can penetrate clouds, vegetated canopies, and snow to some extent up to several centimeters based on its operation frequency. Different SAR radars can acqure the information of earth surface with different wave lengths. The revisiting time of SAR radar is also different based on

its orbit distance and its speed. Each SAR image pixel represents the coherent sum of all scattering elements within a resolution cell, therefore, there is some overestimation distance for some areas as well as underestimation for some other areas within each cell (Colesanti et al., 2006).

In the Interferometric Synthetic Aperture (InSAR) method, the movement of the earth crust is measured using the changes between signal phase which is reflected from each point to the Radar. Movements on the ground changes the distance between each point and the sensor in the satellite for each subsequent image and produces a corresponding shift in signal phase which is used to calculate changes in distance between the ground and the sensor. The result of this method can be affected by topographic distortions, atmospheric effects, and other sources of noise. To remove the topographic noises the Differential InSAR (DInSAR) process uses a Digital Elevation Model (DEM) of the area of interest. However, the result of DInSAR is still impacted by atmospheric effects. Permanent Scatterer SAR Interferometry process (PS-InSAR) which is an advanced form of DInSAR can minimize the atmospheric effects (filter them out) on the signal phases reflected from the ground by using multiple interferograms created from a stack of at least 15 radar images. This process can measure the ground deformation with millimeter accuracy (TRE Group report for the Thompson River Valley., 2018).

Application of remote sensing methods such as InSAR, Light Detection and Ranging (LiDAR), and Unmanned Aerial Vehicle (UAV) photogrammetry to monitor cut slopes and natural slopes in routine geohazard monitoring programs nowadays support engineers to have enough data over large areas with high spatial resolution in comparison to in-place instruments such as slope inclinometers or survey monuments with reasonable cost (Rodriguez et al., 2020).

InSAR has been recognized as a reliable, accurate and near real time method for monitoring and identifying the potential for landslide events, particularly useful in remote areas where in-place ground monitoring instruments are technically or economically challenging. Despite of extensively using InSAR for landslide monitoring in last three decades, particularly for slow-moving landslides, there are still challenges to find adequate radar data to generate InSAR information to monitor and predict rapid landslide's movement due to the costs of images at the required resolutions and revisiting times, or the possibility that the area had not been captured, therefore preventing a historical view of past landslide performance. These, however, have become less of a challenge in recent years with the increase in availability of high resolution, cost-effective satellite information and processing tools. There are also some other challenges that need to be considered at a particular site, such as atmospheric noise, vegetation cover, and seasonal effects, such as rainfall and snow cover, which impact the results of this method (Choe et al., 2021). Even with these challenges, the ability of InSAR to provide ground deformation measurements with high accuracy, has made this method an effective technique in many applications focused on deformation phenomena that occur on the Earth surface (Mancini et al., 2021).

Using InSAR information in combination with other monitoring information such as precipitation and ground water, can provide a robust understanding of landslide mechanisms that can inform possible landslide behaviour in the near future and evaluate the likelihood of sudden acceleration (e.g. velocity measures to predict time to failure). One of the most considerable InSAR limitations is the revisiting times, which has been reduced to 3 days for some constellations. Revisiting time impacts the temporal resolution of this monitoring method. This means that the approach would not provide adequate warning for failure modes that lead to rapid

acceleration followed by collapse, as there could only be less than a handful of InSAR data points during the evolution of the failure (Huntley, 2021).

3. Updated understanding of the Ripley landslide kinematics using satellite InSAR

A version of this chapter is Accepted for publication in the journal "Geosciences"

Abstract: The Thompson River valley hosts 14 landslides along a 10-km section, which threaten the two major railroads connecting the Port of Vancouver and interior provinces in Canada. The Ripley landslide is one of the active landslides in this section of the valley. Previous research at this site included an analysis of landslide deformations using satellite radar interferometry focusing on deformations measured in the line of sight between the satellite and the slopes, and average downslope displacement (deformations projected in the average downslope direction). Since then, further stratigraphic interpretation has provided an enhanced understanding of the Ripley landslide. In this update, the new stratigraphic interpretation is supplemented with satellite InSAR data from May 2015 to May 2017 to enhance the current understanding of the landslide kinematics. The results indicate that the Ripley landslide has been moving at a rate between 2 and 82 mm per year, corresponding to a Very slow to Slow landslide. It is also observed that the movements tend to be near-horizontal on areas closer to the toe of the landslide, while the vertical component of deformation increases near the scarp of the landslide. This, together with the interpreted stratigraphy, indicates the kinematics corresponds to a compound landslide. This is consistent with interpreted landslide kinematics of older, more

mature landslides in the area that have shown episodes of retrogression, and suggests the possibility of a similar future behaviour of the Ripley Landslide.

Keywords: InSAR; landslides; kinematics; remote sensing

3.1. Introduction

Geohazards threaten many infrastructures as well as lives all around the world. Historically, there are many reported cases of loss of life and damage to infrastructure in Canada as a consequence of landslides(Charrière et al., 2015; Cruden & Martin, 2007; Mei et al., 2008; Vallee, 2019) Since 1771 there have been hundreds of fatalities and damage to infrastructures due to landslides in Canada, which have cost millions of dollars annually (Choe et al., 2021). A recent reminder of the harmful potential of landslides in Canada was the four fatalities confirmed in a recent landslide in British Columbia's Highway 99 in November 2021 (Simon Little, Global News, November 20, 2021). In addition, climate change and accelerated glacier melting and retreat can increase landslide activity in northern regions in Canada (Choe et al., 2021), therefore continued monitoring and understanding of landslide phenomena becomes important for resilience against Climate Change.

Identification of landslides and monitoring the terrain's movement is one of the most effective risk management approaches for areas susceptible to landslides, particularly when stabilization or avoidance are technically or economically challenging. Monitoring can help to adapt to these landslide phenomena and inform adequate maintenance scheduling of infrastructures. Monitoring can also provide robust early warning systems (Huntley et al., 2019b;

Rodriguez et al., 2020) . Particularly, remote monitoring information can be used to increase our understanding of landslide kinematics and triggers, therefore enhancing landslide risk management strategies (Dean et al. 2020, Macciotta et al. 2020, Woods et al. 2020, Lan et al. 2021, Rodriguez et al. 2021, Macciotta and Hendry 2021).This paper presents an updated understanding of the landslide kinematics using satellite InSAR for the Ripley landslide in the province of British Columbia, Canada. The Ripley landslide has been studied by a number of researchers (Hendry et al. 2015, Macciotta et al. 2016, Jornault et al. 2018, Huntley et al. 2019a). Previous research included an analysis of landslide deformations using satellite radar interferometry focusing on deformations measured in the line of sight between the satellite and the slopes and average downslope displacement (deformations projected in the average downslope direction) (Jornault et al. 2018). Since then, further stratigraphic interpretation has provided an enhanced understanding of the geometry of the shear surfaces in the Ripley landslide (Schafer 2016, Huntley et al. 2019a, 2019b, 2020, Sattler et al. 2021). In this update, the new stratigraphic interpretation is supplemented with satellite InSAR data from May 2015 to May 2017 (Sentinel 1) to enhance the current understanding of the landslide kinematics

3.1.1. Landslide remote sensing and satellite InSAR

New technologies facilitate geotechnical engineers real time observation of terrain's movement. Remote sensing, GPS monitoring, geophysical imaging and geotechnical investigation is commonly applied for landslides characterization (Xu et al., 2016). Remote sensing methods like Interferometric Synthetic Aperture Radar (InSAR), Light Detection and Ranging (LiDAR), and Unmanned Aerial Vehicle (UAV) photogrammetry are applied to monitor cut slopes and natural slopes in routine geohazard monitoring programs nowadays. These technologies help engineers to acquire data over large areas with high spatial resolution in

comparison to in-place instruments such as slope inclinometers or survey monuments (Rodriguez et al., 2020).

Interferometric Synthetic Aperture Radar (InSAR) has been used in many worldwide applications to detect surface displacements of crustal deformation, glacier motion, infrastructure's displacement and landslides in recent decades (Herrera et al., 2012, Colesanti et al., 2006, Vadivel et al., 2020, Abe et al., 2020, Motagh et al., 2017, Hooper et al., 2011, Chen et al., 2022, Liu et al., 2022, Mastro et al., 2022, Abdel-Hamid et al., 2021, Dumka et al., 2020, Castellazzi et al., 2020).

In this method, Radar Satellites carry SAR sensors which utilize wavelength information to calculate distance to the surface and that can be used for calculating relative change (Abe et al., 2020).

InSAR has become a reliable, accurate and near real time method to monitor of potential landslide events, particularly useful in remote areas where in-place ground monitoring instruments are technically or economically challenging. Although InSAR has been extensively used for monitoring landslides in last three decades, particularly slow-moving landslides, it is still challenging to find adequate data to generate InSAR calculations for rapid landslide acceleration. Other challenges include atmospheric noise, vegetation cover, and seasonal effects, such as rainfall and snow cover (Choe et al., 2021). Notwithstanding these limitations, the ability of InSAR to provide ground deformation measurements with high accuracy, makes this method an effective technique in many applications focused on deformation phenomena that occur on the Earth surface (Mancini et al., 2021). Satellite InSAR has been proven as an effective method for identifying and monitoring ground displacement of slow to extremely slow moving slopes. InSAR information can be used for enhanced understanding of landslide

mechanisms when complemented with other monitoring information such as precipitation and ground water fluctuation. The resolution of InSAR monitoring (sub-cm/year) and its significant ability to capture massive areas make it very useful for widespread surface monitoring of landslides. It is important to note that satellite revisiting times (now between 1 day and 1 week) limit the temporal resolution of InSAR monitoring. Ground based InSAR can provide adequate high frequency data for forecasting rapid acceleration that develops in a window of hours. No sites will have access to more frequent than one day revisiting time. In this regard, the information is valuable for identifying initiation of ground displacements, changes in displacement trends, seasonal displacements; however, would not provide adequate warning for failure modes that lead to rapid acceleration followed by collapse that develop in just a few days as the variability of monitoring points could mask reliable identification of acceleration (D. Huntley, 2021).

3.1.2. The Thompson River valley landslides south of Ashcroft and the Ripley Landslide

The Thompson River valley south of Ashcroft hosts one of the most important transportation corridors in Canada. Both Canadian Pacific Railway (CP) and Canadian National Railway (CN) use this corridor to transport goods between the Port of Vancouver and the rest of Canada (Clague & Evans, n.d.). The Thompson River valley became a monitoring priority for Natural Resources Canada (NRCAN), the Geological Survey of Canada (GSC), and Transport Canada (TC) due to its economic importance and effects on transportation services in Canada and it is considered essential to understand and manage the risks associated with the landslides that threaten the corridor (Huntley et al., 2021)

The Thompson River valley was formed by a series of glaciations, later exposed to river erosion and incision. The valley is infilled with a complex sequence of a wide range of deposits, from poorly sorted sand and gravel to rhythmically interbedded silt and clay. This corresponds to multiple glacial advance and retreat intervals in the Pleistocene (Clague and Evans 2003; Huntley and Bobrowsky 2014; Journault 2018). The extensive terrace which hosts several landslides was formed during postglacial times when the southward flowing Thompson River down-cut 150 m of deposited sediments gradually along the valley (Porter et al. 2002; Journault 2018). In these landslides, the existence of steep internal shears and basal through-going shear surfaces, as well as presence of multiple graben and horst features, confirm the presence of a weak silt and clay layer that is considered responsible for the instability of many of these landslides (Clague and Evans 2003; Eshraghian et al. 2007; Journault 2018). This weak layer contains pre-sheared surfaces with residual shear strengths characterized by no cohesion and friction angles between 9 and 16 degrees, according to landslide back-analyses (Hendry et al., 2015).

14 landslides have been identified in the Thompson River Valley, 12 of them traversed by one or both railway companies. The first reported landslide dates to the 1860s and periodic reactivation and slope movements have occurred since then. The location and extents of the landslides are shown in Figure 3-1 (Hendry et al., 2015).

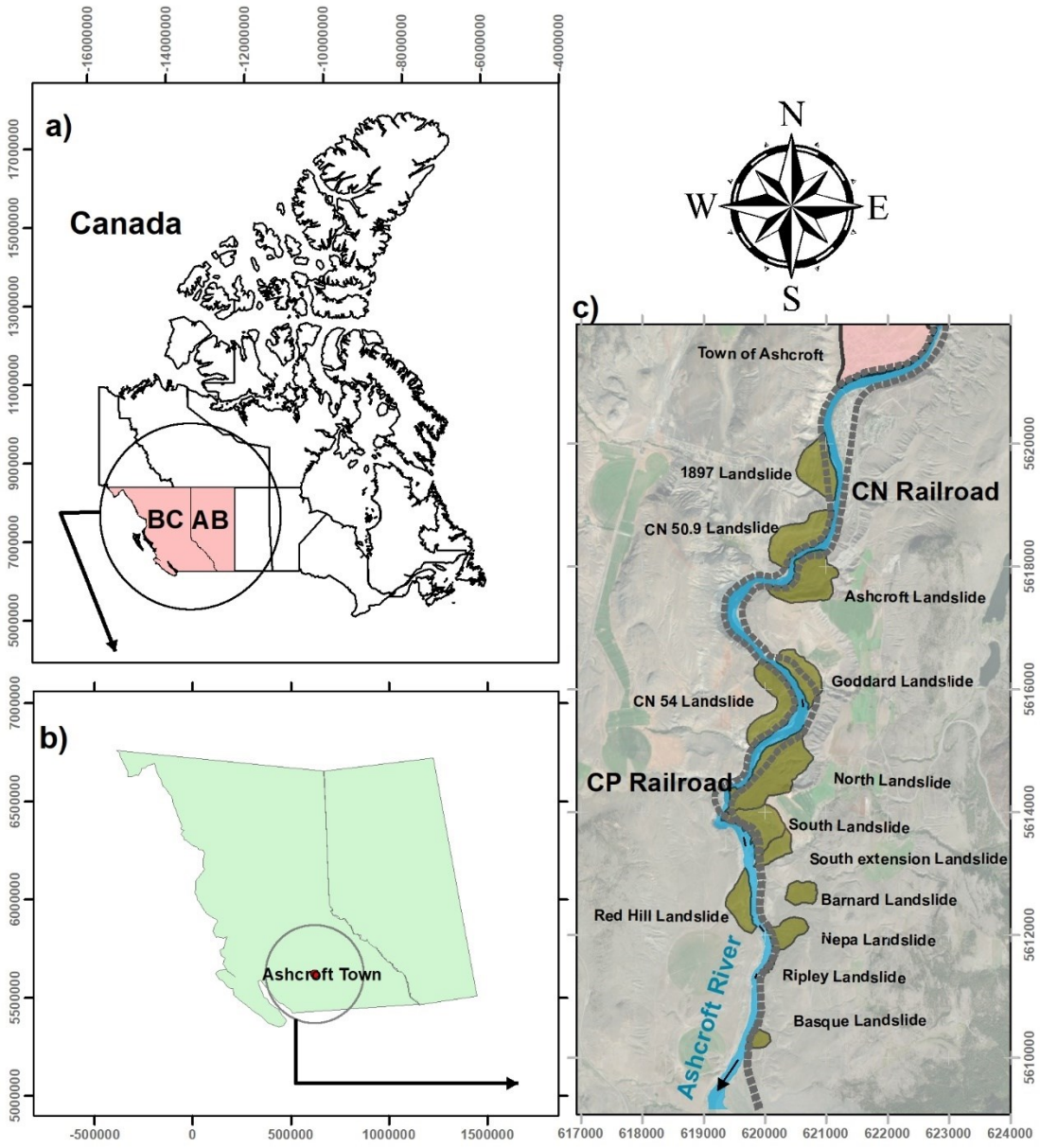

FIGURE 3-1. Thompson River Valley location (a,b) plan-view and active landslides across the valley (c). Coordinates in UTM (units in meters for scale purposes). BC and AB in (a) correspond to the provinces of British Columbia and Alberta, respectively.

Landslides in this valley have volumes between 0.75 million cubic meters (Ripley landslide – Figure 3-1) and 15 million cubic meters (North Slide – Figure 3-1), and their movement velocity range between 10 mm/year (Extremely Slow) and reported accelerated episodes of up to 50 mm/s historically (Very Rapid) (Journault et al., 2018)

The Ripley landslide is approximately 200 m long, 40 m high and 300 m wide. A front view of the landslide is shown in Figure 3-2 Macciotta et al. (2014). The Ripley landslide was recognized by Charles Ripley in the 19th Century by observation of an offset in a fence on the uphill side of CP railway tracks. Since then the landslide has been inactive or moved slow enough that regular maintenance of track allows for continued operations of CN and CP railways, which traverse this landslide. Shortly after construction of a section of track in 2005, the landslide showed some deformation and this movement was followed by the development of cracks and a scarp in 2007 (Hendry et al., 2015). Since then, the railway track and ballast has required adjustments at higher frequencies than for other sections of track (Huntley et al., 2019a). The Ripley landslide is the only landslide currently being monitored at almost real-time, as it has become a field laboratory for novel investigation technology (Hendry et al. 2015, Macciotta et al. 2016, Jornault et al. 2018, Huntley et al. 2019a, Schafer 2016, Huntley et al. 2019a, 2019b, 2020, Sattler et al. 2021). The other landslides in this area are being monitored with periodic slope inclinometer readings.

The Ripley Landslide's estimated volume of 750,000 m3 is relatively small in comparison to the other landslides in the Thompson River Valley, however it is one of the most active landslides with velocities between 25 and 180 mm/year (very slow according to the classification by Cruden and Varnes, 1996).

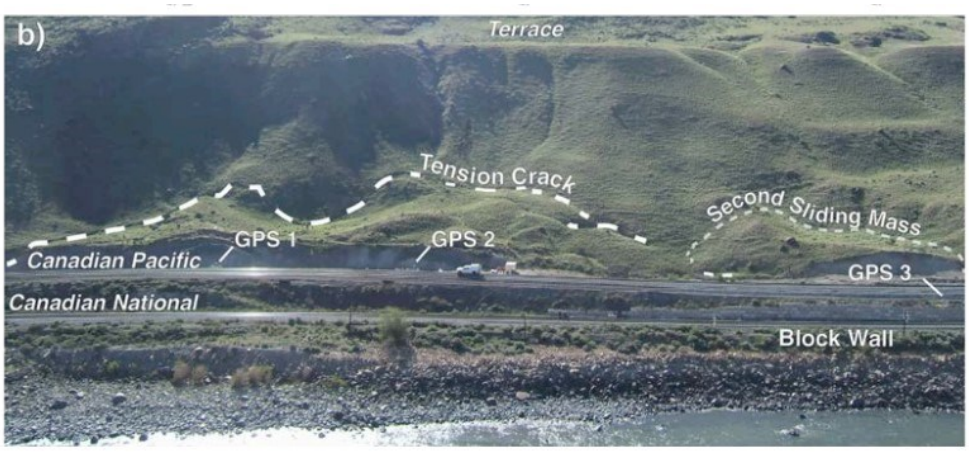

FIGURE 3-2. Ripley Slide Geometry including CN and CP railways and installed GPS on the site.

3.2. Materials and methods

3.2.1. Published displacement monitoring data at the Ripley Landslide

The GPS system monitoring data used in this paper was acquired through an installation by CP and analyzed by the University of Alberta under the Canadian Railway Hazard Research Program. The system consists of three GPS monitoring stations on the Ripley landslide, near the railway tracks, and one reference station located on stable bedrock outside the unstable area. GPS stations are Leica single-phase receivers in a differential GPS mode, able to detect 12.5 mm of cumulative ground movement with a variability of ± 1 mm (Macciotta et al., 2016). Lateral and vertical displacements are processed by the Leica GeoMOS software and information on the system's latitude, longitude and vertical coordinates is provided at an hourly frequency. Hourly readings are used to calculate daily positioning of the GPS stations. The GPS displacement data in this paper corresponds to that published by Macciotta et al., 2016 for the period between April 2008 and October 2014 (all 3 GPS start recording data in April 2008. GPS-1 and GPS-3 recorded data until 21st October 2014 while GPS-2 recorded data only until 29th April 2014. All three

systems showed some data gaps associated with repairs and maintenance of the system). These data are used to validate the landslide deformation trends (directionality) obtained by InSAR, assuming the landslide has not suffered changes in the direction of movement. Unfortunately, no displacement vector datasets coincide with the InSAR processing period in this paper. Positive values for horizontal movement show displacements in the downslope direction and negative vertical values show downward movement(Macciotta et al., 2016).Figure 3-3 shows the proximate locations of each installed GPS systems.

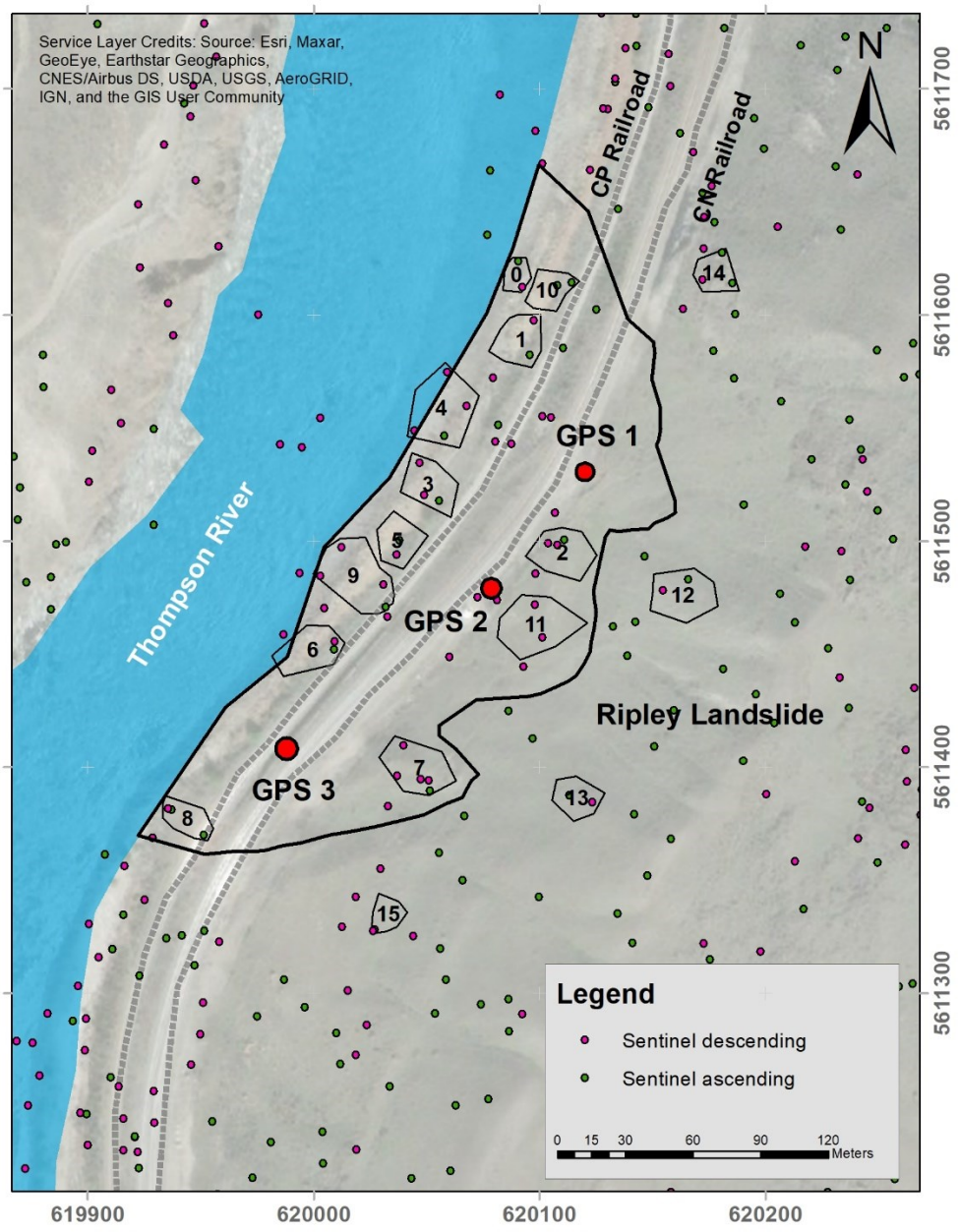

FIGURE 3-3. Location of Installed GPS systems on Ripley Landslide.

3.2.2. Satellite InSAR displacement data

Satellite InSAR displacement data used in this paper were collected from Sentinel 1 and processed by TRE ALTAMIRA CLS Group Company. Processed information included displacements in the line-of-sight (LOS) which is the visual line between the satellite sensor and

the points on the land being monitored between the end of 2014 to the Spring of 2018. The data with minimum gaps between May 2015 to May 2017 was selected to investigate the ground displacement of the Ripley landslide. The radar orbit is called ascending when a satellite moves from south to north and captures images, in our case, towards the east. The orbit is called descending when satellite travels from north to south and captures images, in our case, to the west. There are two important angles for each satellite LOS in order to interpret the calculated displacements. These are the angle between the LOS and the vertical plane, or theta (θ), and the angle between each satellite's orbit and the geographic north, or delta (δ). Figure 3-4 shows the typical angle layout for both ascending and descending satellites orbits.

Scatterers refer to data points that provide information for measuring the ground movement by LOS displacements. Permanent scatterers (PS) consist of some buildings, fences, and other man-made structures and also some natural features such as rocks or exposed ground which are likely Table. Distributed scatterers (DS) correspond to large areas (up to hundreds of square meters) and were identified from exposed ground or fields. Although each DS present an exact point for clarity of presentation, these points actually correspond to non-point features that are multiple pixel in size.

Table 3-1 illustrates a summary of properties of the data that were collected from each Sentinel orbit.

Both PS and DS data were provided by TRE using their SqueeSAR method which incorporates PSInSAR processing methods.

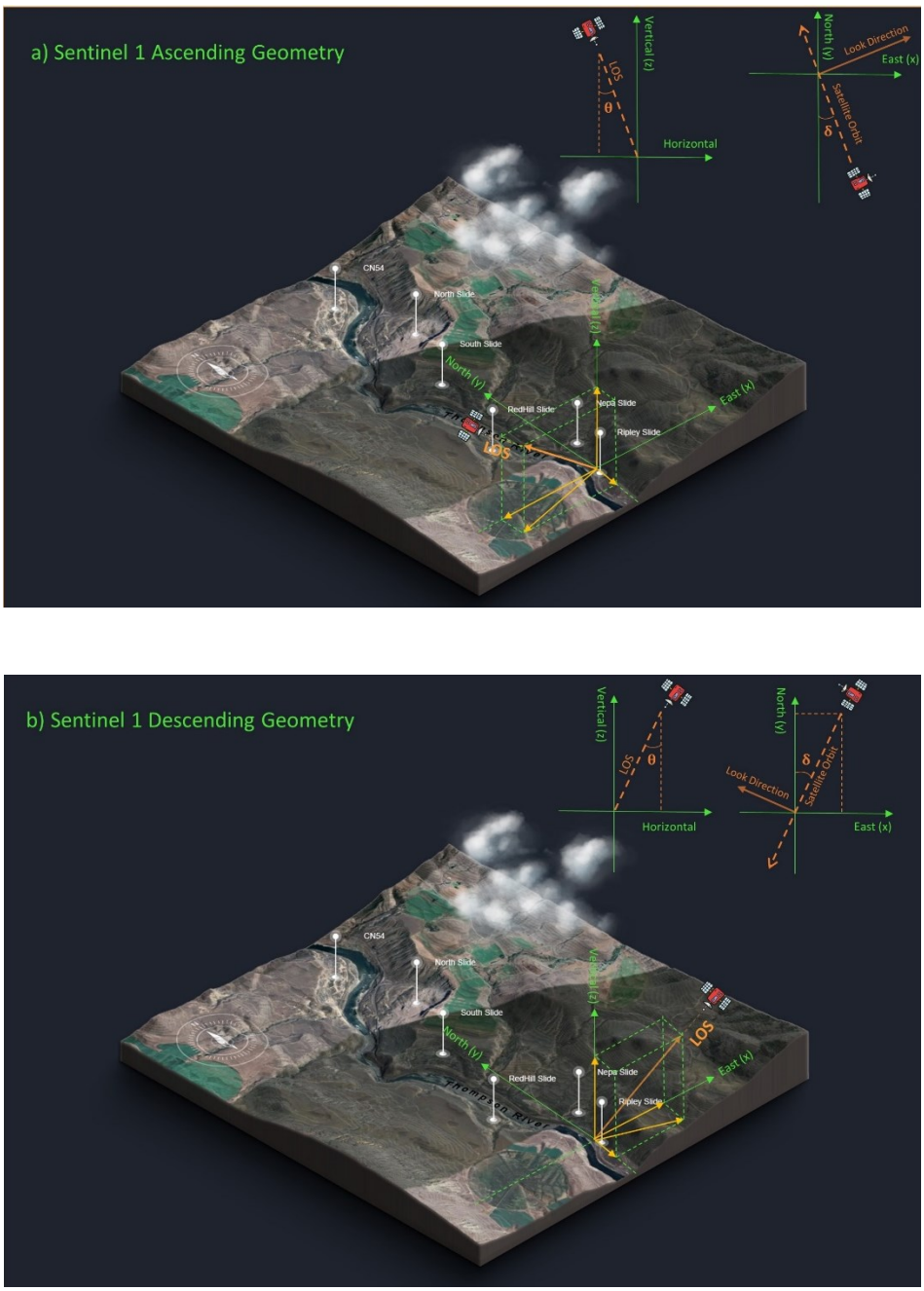

FIGURE 3-4. Geometry of the image acquisitions along the ascending(a) and descending(b) orbits (Inspired by Ground Deformation InSAR Analysis over the Thompson Canyon, British Columbia, Technical Details, August 2018, By TRE Group).

Table 3-1 Details of the processed satellite InSAR data

Radar Data Information		
Satellite	Sentinel 1	Sentinel 1
Acquisition Geometry	Ascending	Descending
Period Covered by Imagery	03-Nov-2014 to 17-Mar-2018	06-Nov-2014 to 01 Apr-2018
No. of Processed Images	51	59
Coordinate System	WGS 1984	WGS 1984
Area of Interest	869.2 Km^2	869.2 Km^2
Number of PS+DS	194083 (112343 PS, 81740 DS)	178396 (89510 PS, 88886 DS)
Sensor Mode	IW	IW
Image Resolution	20 m×5 m	20 m×5 m

Sentinel 1

Sentinel 1 was launched by the European Space Agency (ESA). Satellite images used in this study that cover the Ripley landslide were collected between November 3rd, 2014 and March 17th, 2018 for the ascending orbit, and between November 6th, 2014 and April 1st, 2018 for the descending orbit. LOS angles are shown in Table 3-2.

Table 3-2. Satellite viewing (LOS) angles for the Sentinel and Radarsat-2 imagery.

Satellite	Orbit Geometry	Track	Sensor Mode	Symbol	Angle (Degree)
Sentinel	Ascending	64	IW	θ	38.66
				δ	11.33
Sentinel	Descending	115	IW	θ	44.29
				δ	7.79

3.2.3. Displacement calculation at the surface of the Ripley landslide based on InSAR LOS displacements

In this paper we propose a method for interpreting the geometry of the deformation based on the satellite InSAR, noting this should be complimented with a classical evaluation of the line of sight (LOS) deformations and velocities.

The LOS InSAR displacement is a projection of the true landslide surface displacement on its axis. The procedure followed in the paper aims at calculating a close approximation to these real displacements, although a few assumptions are required. For simplification, the calculated displacements are referred to as the "Real" displacement vectors (R), where "bold" represents a vector. Given the orbits of the satellites are sub-parallel to the north-south direction, resolving north-south displacement component is not reliable. Therefore, a common assumption for landslide InSAR interpretation is to consider landslide motion in the downslope direction (azimuth and inclination) (Journault et al. 2018). The work presented in this paper does not assume the directionality of movement in the vertical plane, however it assumes that movement in the horizontal plane with an azimuth parallel to the slope azimuth in the area of measurement. Therefore, knowing the topography of the landslide provides the assumed unit vector of the horizontal component of R. This can be accomplished by calculating the unit vector of R in the horizontal plane, considering the vertical component as an unknown, and projecting R to the LOS unit vectors (based on the satellite geometry). Knowing the LOS displacement magnitude, the vertical component of R and its magnitude can be solved.

The unit vectors of LOS are denoted by $\boldsymbol{S_a}$ for Sentinel ascending and $\boldsymbol{S_d}$ for Sentinel descending. The projections of R on these directions would be the measured LOS displacements, and are denoted by vectors $\boldsymbol{P}_a \; and \; \boldsymbol{P}_d$, respectively, each with scalar magnitudes $M_a \; and \; M_d$.

Therefore, Equation 1 presents the expression for $\boldsymbol{P}_i$, where i represents the ascending or descending orbits.

$$\boldsymbol{P_i} = (\boldsymbol{R} \cdot \boldsymbol{S_i})\, \boldsymbol{S}_i = M_i\, \boldsymbol{S_i} \quad (1)$$

The components of R can be denoted as (x,y,z), and the components of the unit vectors of the LOS as $\boldsymbol{S}_i = (e, n, u)$. To finding the LOS unit vectors it is essential to use the angles between the LOS, the vertical plane, and azimuth from Table 3-2 (Equations 2, 3 and 4).

$$u = \cos\theta \quad (2)$$

$$e = \sin\theta \,.\, \sin\delta \quad (3)$$

$$n = \sin\theta \,.\, \cos\delta \quad (4)$$

The coordinate system used in this paper corresponds to (East, North, Up). The sign of u is positive and sign of n is negative for both orbits' LOS while the e sign is negative for the ascending orbit and it is positive for the descending orbit. The unit vectors are then calculated as:

$$\boldsymbol{S}_a = (-0.613, -0.123, 0.781) \quad (5)$$

$$\boldsymbol{S}_d = (0.692, -0.095, 0.716) \quad (6)$$

Replacing equations 5 and 6 into Equation 1, and solving for M_a and M_d provides the measured movements in the LOS in terms of the components of R (Equation 7 and Equation 8).

$$-0.613x - 0.123y + 0.781z = M_a \quad (7)$$

$$0.692x - 0.095y + 0.716z = M_d \quad (8)$$

The third equation to resolve the components of R follows the assumption that the total horizontal vector component of R is parallel to the slope's azimuth in the area of measurement (α) as follow:

$$\frac{x}{y} = \tan \alpha \qquad (9)$$

Equations 7, 8 and 9 provide a system of three equations three unknowns for estimating R. Scatterers locations for the different satellites and for different orbits are not the same. Therefore, this required selecting areas of the landslide where information from two orbits are available, and averaging all scatterers for each orbit within that area to calculate representative LOS displacements (Figure 3-5). The measurements are also not synchronous between orientations. Data from Sentinel ascending are gathered from November 2014 to March 2018 every 25 days while reported data is from November 2014 to April 2018 in 25 days intervals for Sentinel descending. This required the selection of relatively long periods of time for calculating average R (annual basis), such that differences of a few days wouldn't have a meaningful impact in the results. The slope displacement rate of the Ripley landslide had been reported up to 150 mm/year (or 0.4 mm/day), suggesting that asynchronous measurements by less than two weeks for a total period of analysis of two years could represent approximately 2% error. A best fit line allowed estimating the deformation trend, and that was used to calculate the total displacements for the different sectors.

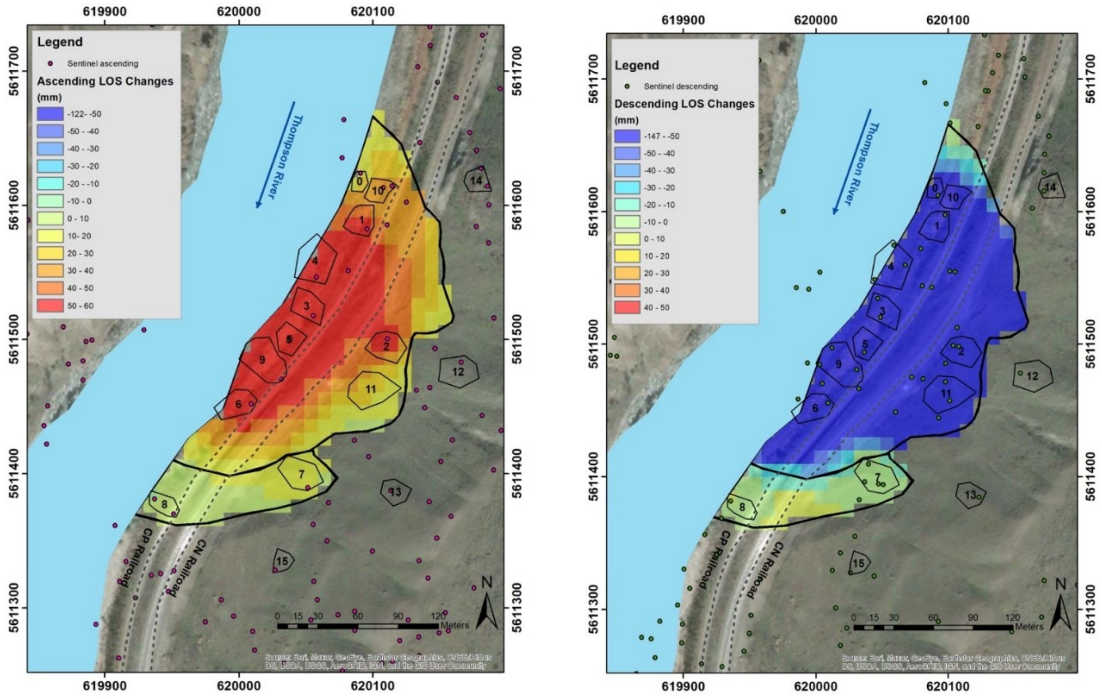

FIGURE 3-5. InSAR data coverage for both Sentinel Ascending and Descending orbit on the Ripley landslide and areas selected for analysis (containing LOS Changes during the selected time frame).

3.3. Results

3.3.1. *Satellite InSAR results at the Ripley landslide*

The LOS vectors in the horizontal plane for each area of analysis are shown in figure 3-6. The magnitude and direction of LOS vectors for each area are located on the center of the area while it is representative of the average values for all captured points within the area. LOS directions for the same orbit are all parallel, given that LOS direction is defined by the orbit geometry. This figure also shows the direction of the average slope azimuth. It is observed that LOS magnitudes are large and of similar magnitude near the river, and significantly decrease near the back scarp of the landslide. Figure 3-7 shows the cumulative LOS deformations for each

area for both Sentinel ascending and Sentinel descending orbits. Acceleration periods tend to start in the fall and deacceleration tend to start in the spring. These show clear episodes of acceleration and deceleration, consistent with previous observations (Hendry et al. 2015, Macciotta et al. 2016, Jornault et al. 2018). In this published study the acceleration corresponds to the drawdown effect of the Thompson River on the Ripley landslide.

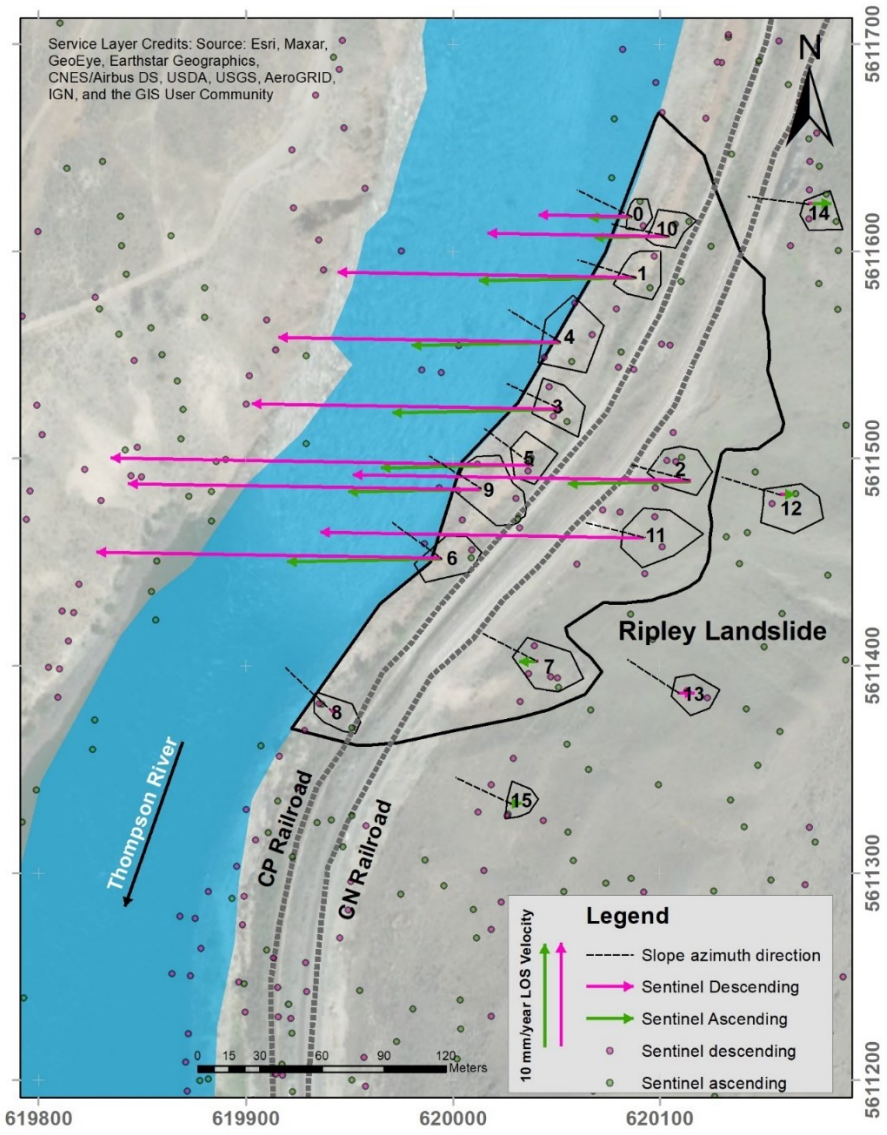

FIGURE 3-6. LOS vectors projected on the horizontal plane for both Sentinel ascending and Sentinel descending orbits. The average direction of the slope azimuth is also shown.

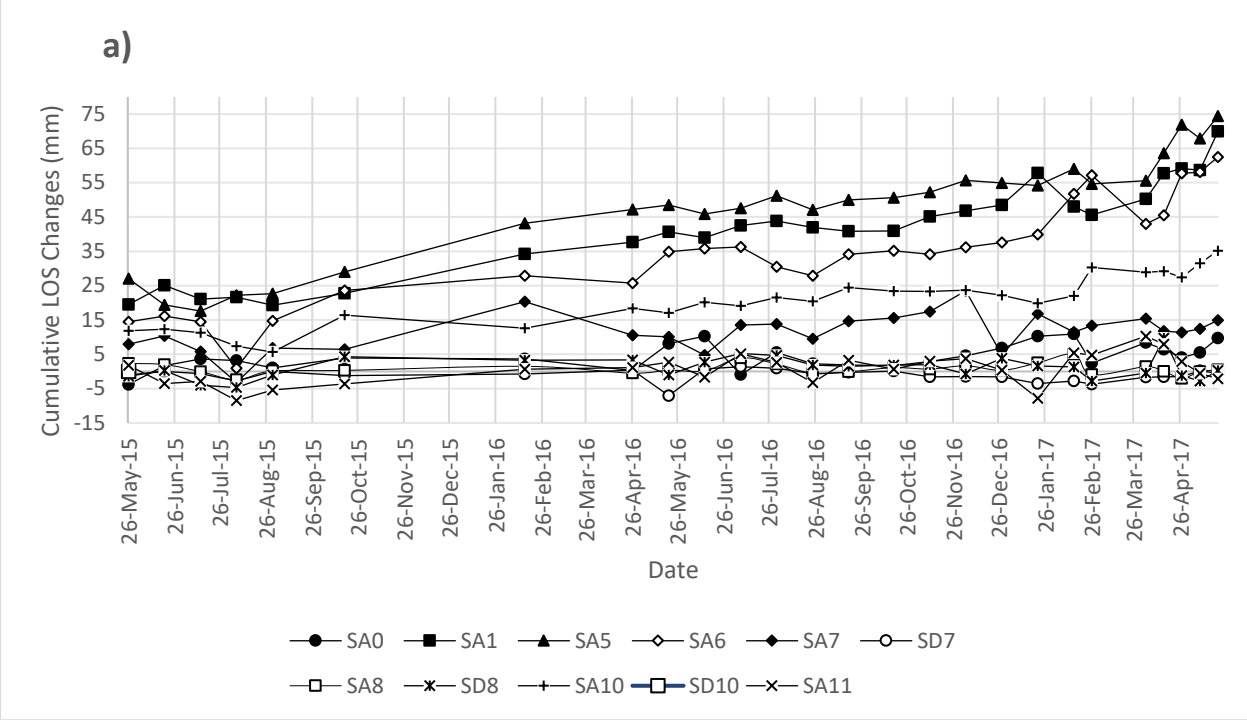
a)
Cumulative LOS Changes (mm)
75
65
55
45
35
25
15
5
-5
-15
26-May-15
26-Jun-15
26-Jul-15
26-Aug-15
26-Sep-15
26-Oct-15
26-Nov-15
26-Dec-15
26-Jan-16
26-Feb-16
26-Mar-16
26-Apr-16
26-May-16
26-Jun-16
26-Jul-16
26-Aug-16
26-Sep-16
26-Oct-16
26-Nov-16
26-Dec-16
26-Jan-17
26-Feb-17
26-Mar-17
26-Apr-17
Date
SA0
SA1
SA5
SA6
SA7
SD7
SA8
SD8
SA10
SD10
SA11

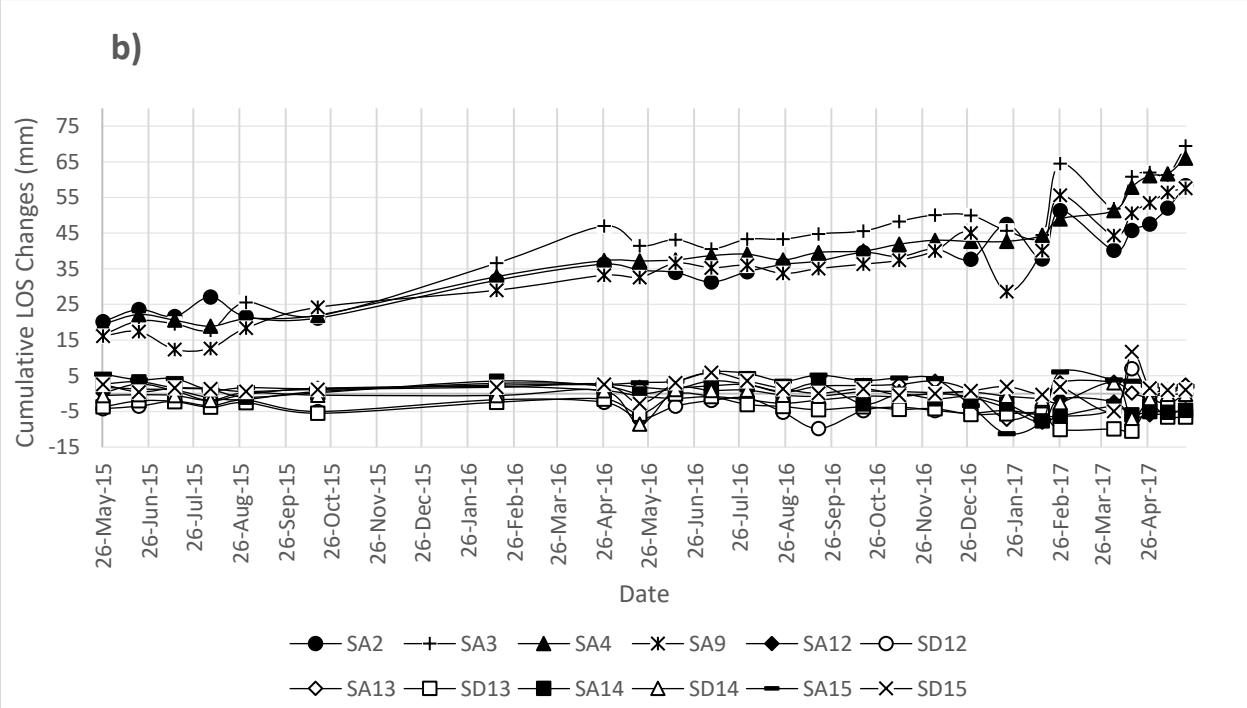
b)
Cumulative LOS Changes (mm)
75
65
55
45
35
25
15
5
-5
-15
26-May-15
26-Jun-15
26-Jul-15
26-Aug-15
26-Sep-15
26-Oct-15
26-Nov-15
26-Dec-15
26-Jan-16
26-Feb-16
26-Mar-16
26-Apr-16
26-May-16
26-Jun-16
26-Jul-16
26-Aug-16
26-Sep-16
26-Oct-16
26-Nov-16
26-Dec-16
26-Jan-17
26-Feb-17
26-Mar-17
26-Apr-17
Date
SA2
SA3
SA4
SA9
SA12
SD12
SA13
SD13
SA14
SD14
SA15
SD15

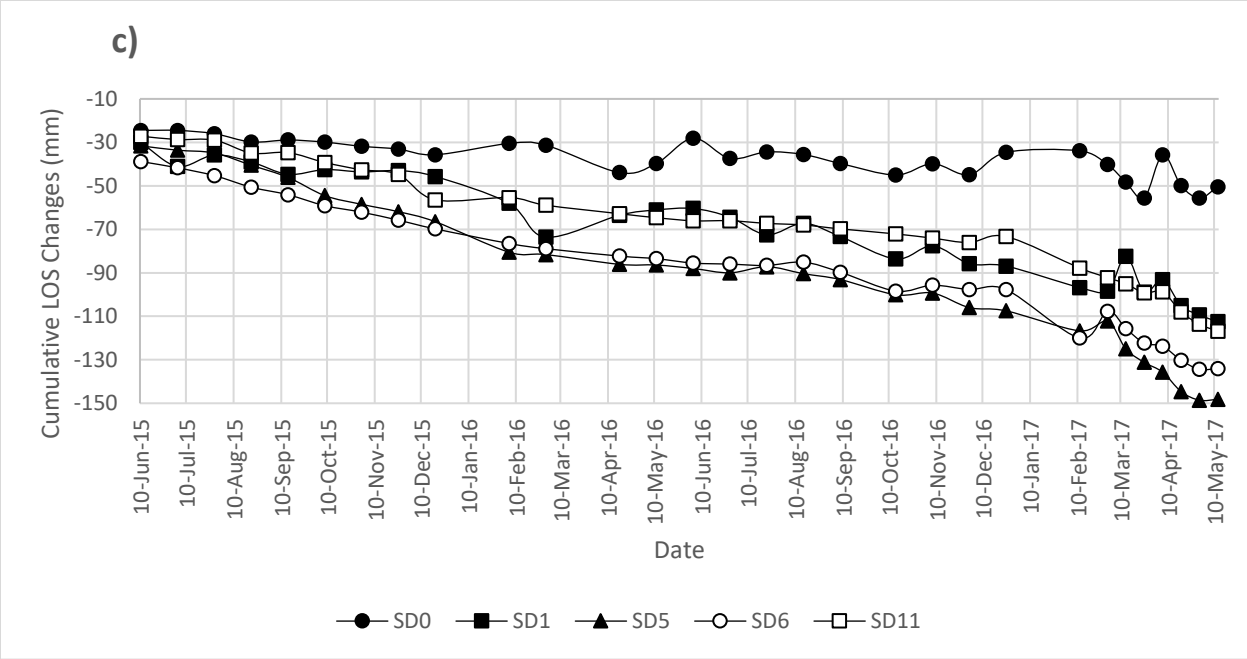

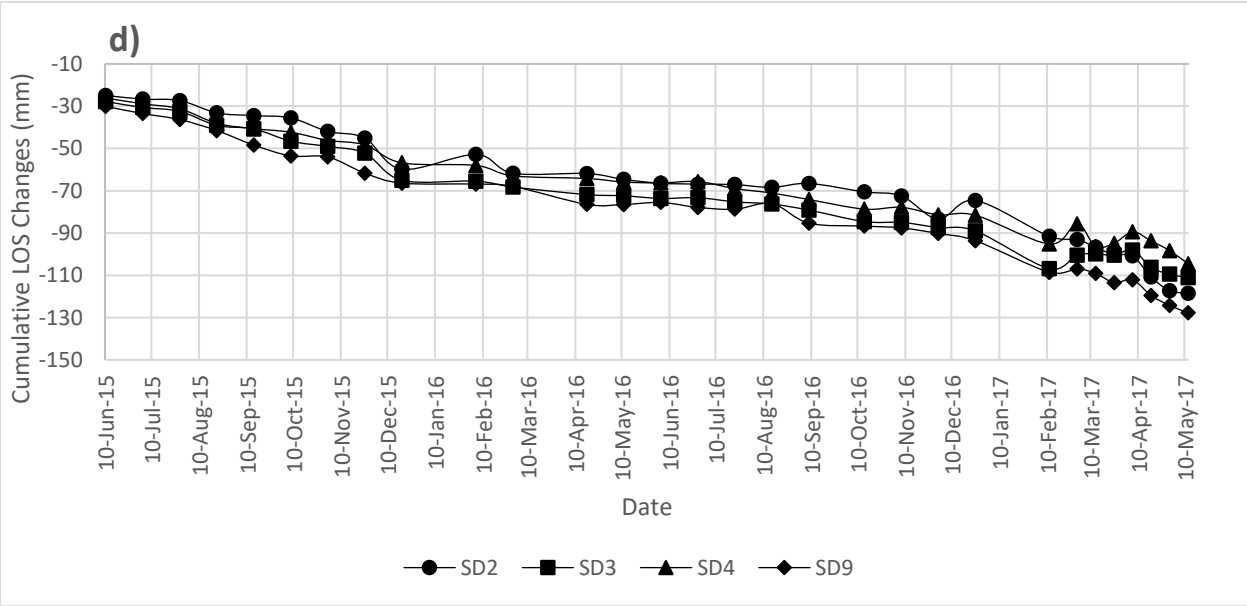

FIGURE 3-7. Average cumulative LOS displacement for both Sentinel ascending and Sentinel descending orbits for specific areas within the Ripley landslide (SA for Sentinel Ascending and SD for Sentinel Descending).

Figure 3-8 shows the plan view of the total horizontal component of the calculated R for the selected areas on the Ripley landslide. The Satellite data used for calculating R correspond to the period between May 26th 2015 and May 21th 2017 for Ascending orbit data and between June 10th 2015 and May 12th 2017 for Descending orbit data to estimate annual displacement. The results are shown as average velocity of the real displacement vectors for each selected area in mm/year. Velocities are less than 3 mm/year behind the known back scarp and ranged between12 to53 mm/year at the back scarp within the landslide body, and up to 81 mm/year close to the river, which shows very slow to slow ground movement according to velocity classification by Curden and Varnes (1996) (Hungr et al., 2014). These results agree the reported results by Huntely et al 2021 both in magnitudes and directions, which report displacements between 68 to 82 mm/year for different locations within the Ripley landslide body with the maximum ground movement occurs in the middle of the toe slide (D. Huntley, 2021).

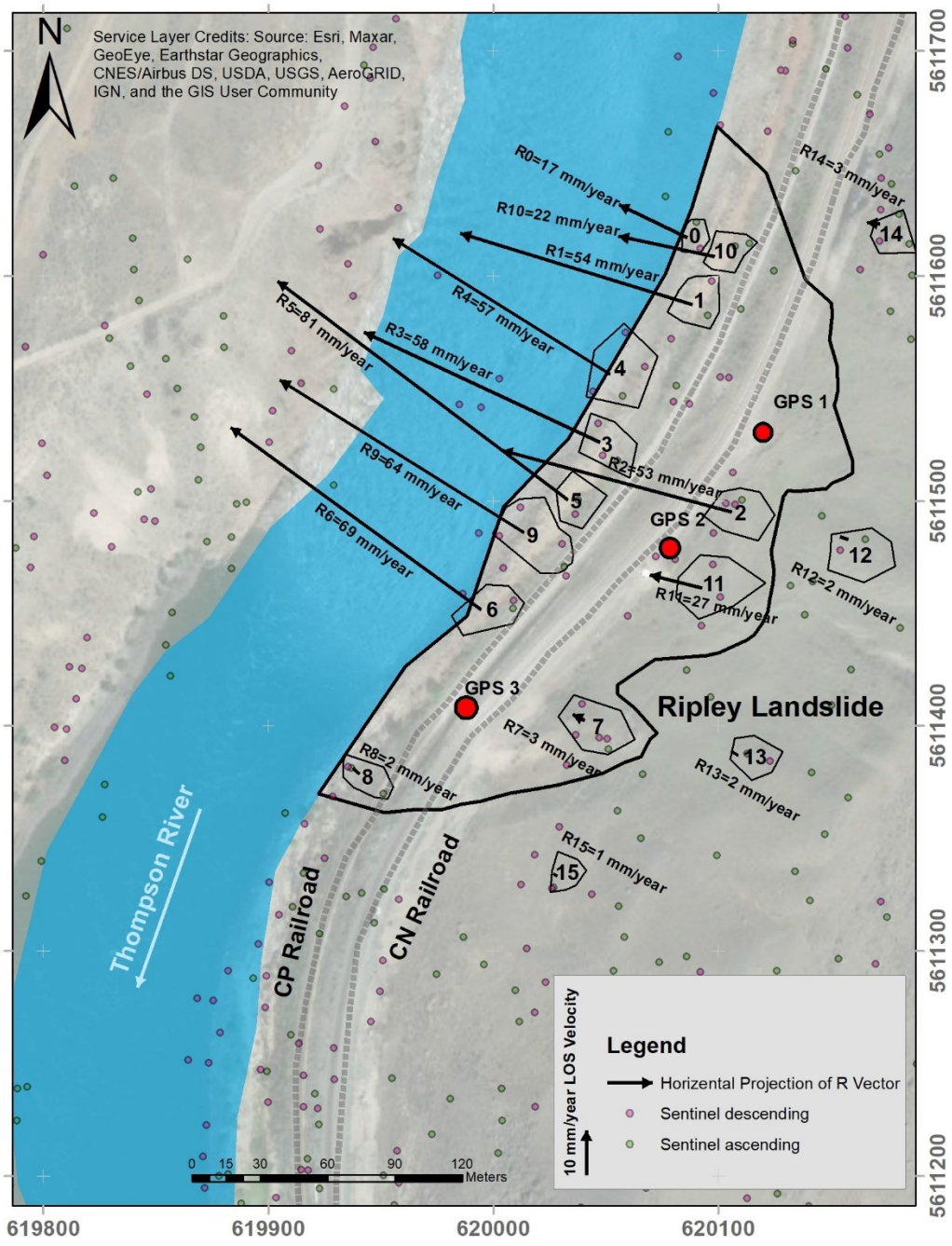

FIGURE 3-8. Calculated total horizontal component of deformation (R) in plan-view on Ripley landslide.

Figure 3-9 illustrates the ground movement velocities in section-view on different cross sections defined on the Ripley landslide. These sketched section views inspired by previous

researches (Hendry et al., 2015; M.B.Schafer 2016). GPS average annual velocity vectors are also shown in the cross sections intersecting the location of the GPS units. Table 3-3 presents the magnitudes of R, Azimuth and Horizontal angles (angle between R and the Horizontal plane).

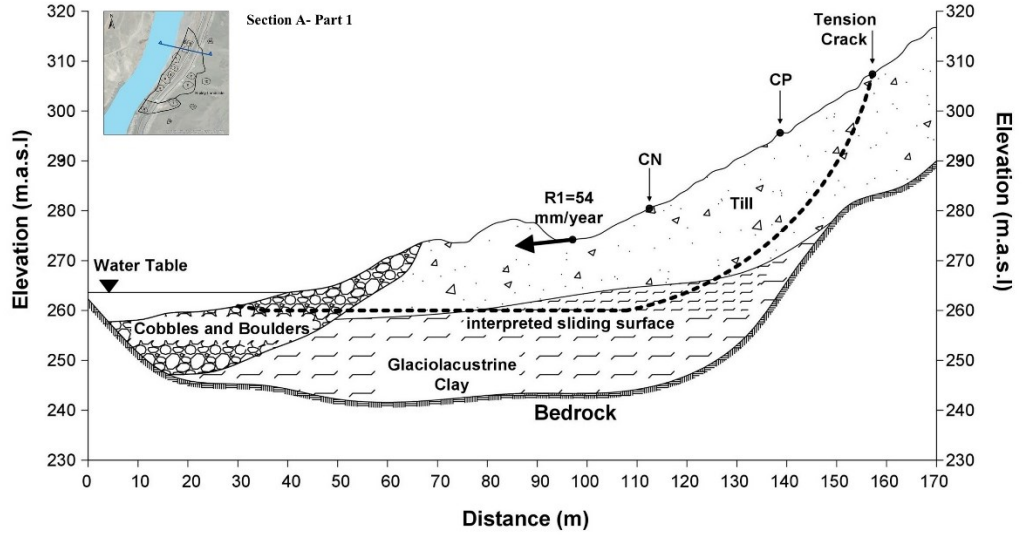
Section A- Part 1
Tension Crack
CP
CN
R1=54 mm/year
Till
Water Table
Cobbles and Boulders
interpreted sliding surface
Glaciolacustrine Clay
Bedrock
Elevation (m.a.s.l)
Distance (m)

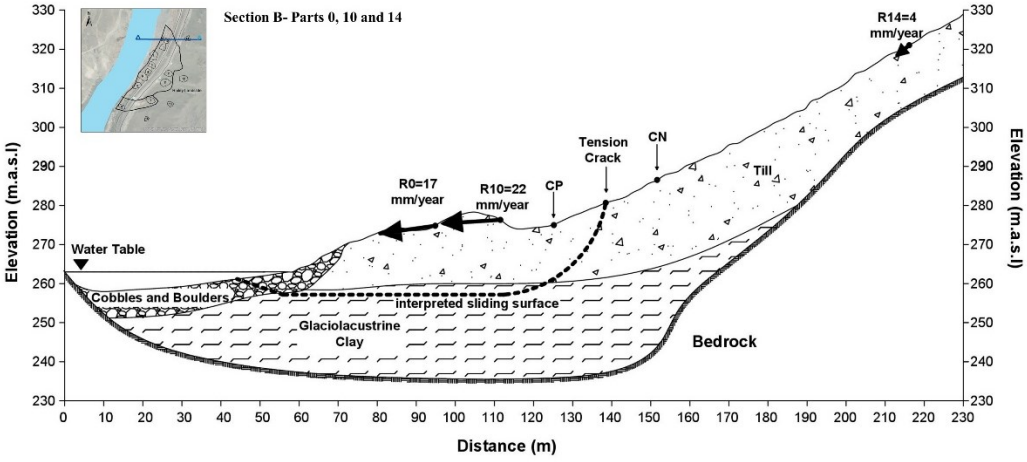
Section B- Parts 0, 10 and 14
R14=4 mm/year
Tension Crack
CN
Till
R0=17 mm/year
R10=22 mm/year
CP
Water Table
Cobbles and Boulders
interpreted sliding surface
Glaciolacustrine Clay
Bedrock
Elevation (m.a.s.l)
Distance (m)

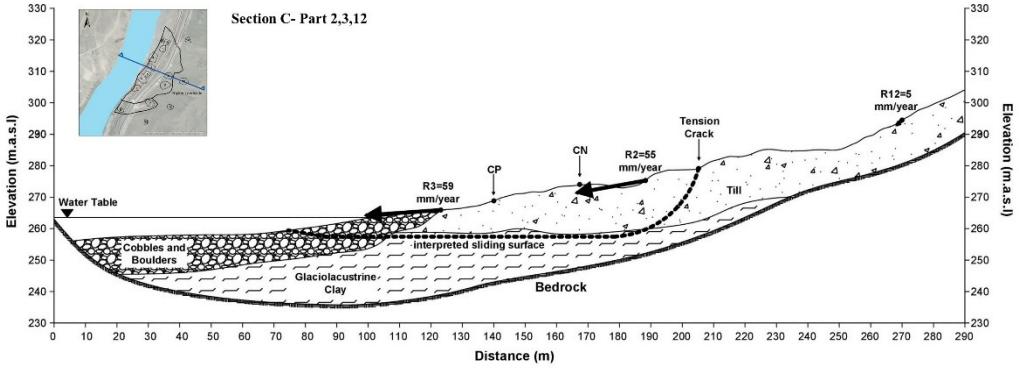
Section C- Part 2,3,12
R12=5 mm/year
Tension Crack
CN
R2=55 mm/year
CP
R3=59 mm/year
Till
Water Table
Cobbles and Boulders
interpreted sliding surface
Glaciolacustrine Clay
Bedrock
Elevation (m.a.s.l)
Distance (m)

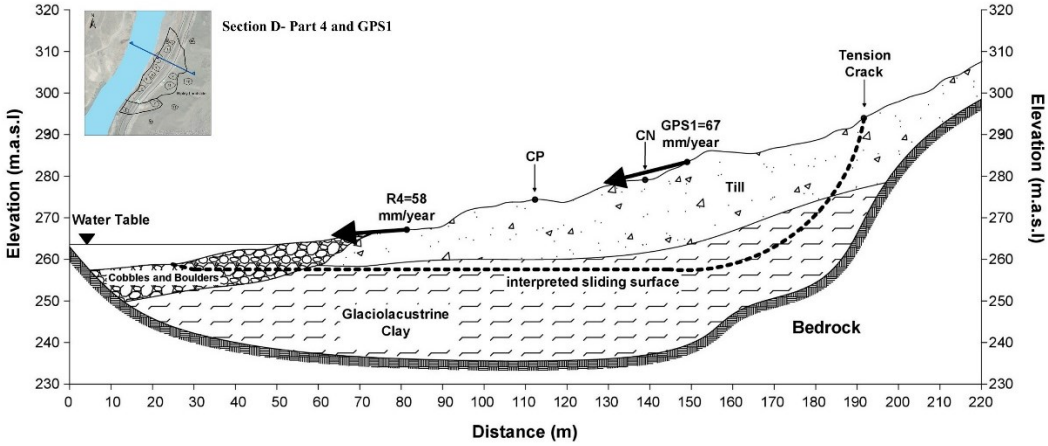
Section D- Part 4 and GPS1
Tension Crack
GPS1=67 mm/year
CN
CP
Till
R4=58 mm/year
Water Table
Cobbles and Boulders
interpreted sliding surface
Glaciolacustrine Clay
Bedrock
Elevation (m.a.s.l)
Distance (m)

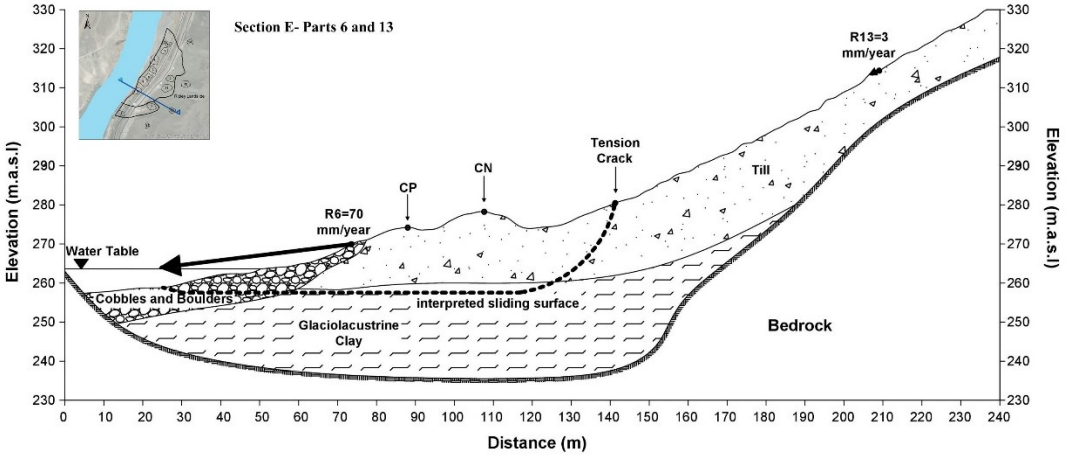
Section E- Parts 6 and 13
R13=3 mm/year
Tension Crack
CN
CP
Till
R6=70 mm/year
Water Table
Cobbles and Boulders
interpreted sliding surface
Glaciolacustrine Clay
Bedrock
Elevation (m.a.s.l)
Distance (m)

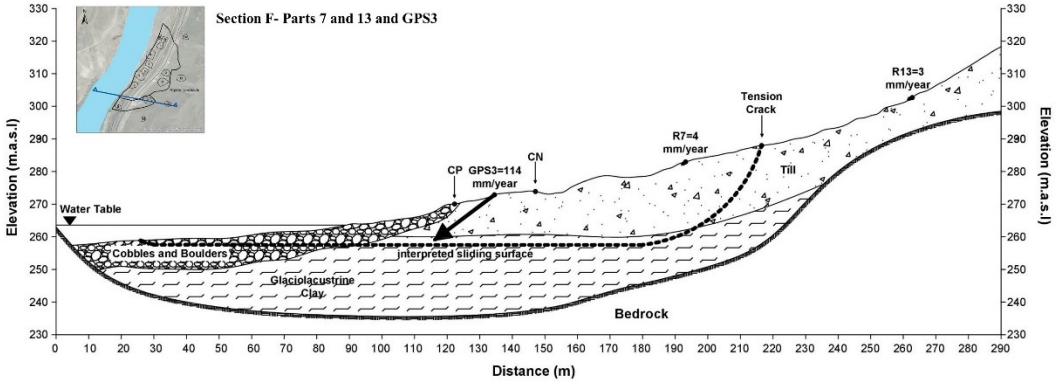
Section F- Parts 7 and 13 and GPS3
R13=3 mm/year
Tension Crack
R7=4 mm/year
CP
GPS3=114 mm/year
CN
Till
Water Table
Cobbles and Boulders
interpreted sliding surface
Glaciolacustrine Clay
Bedrock
Elevation (m.a.s.l)
Distance (m)

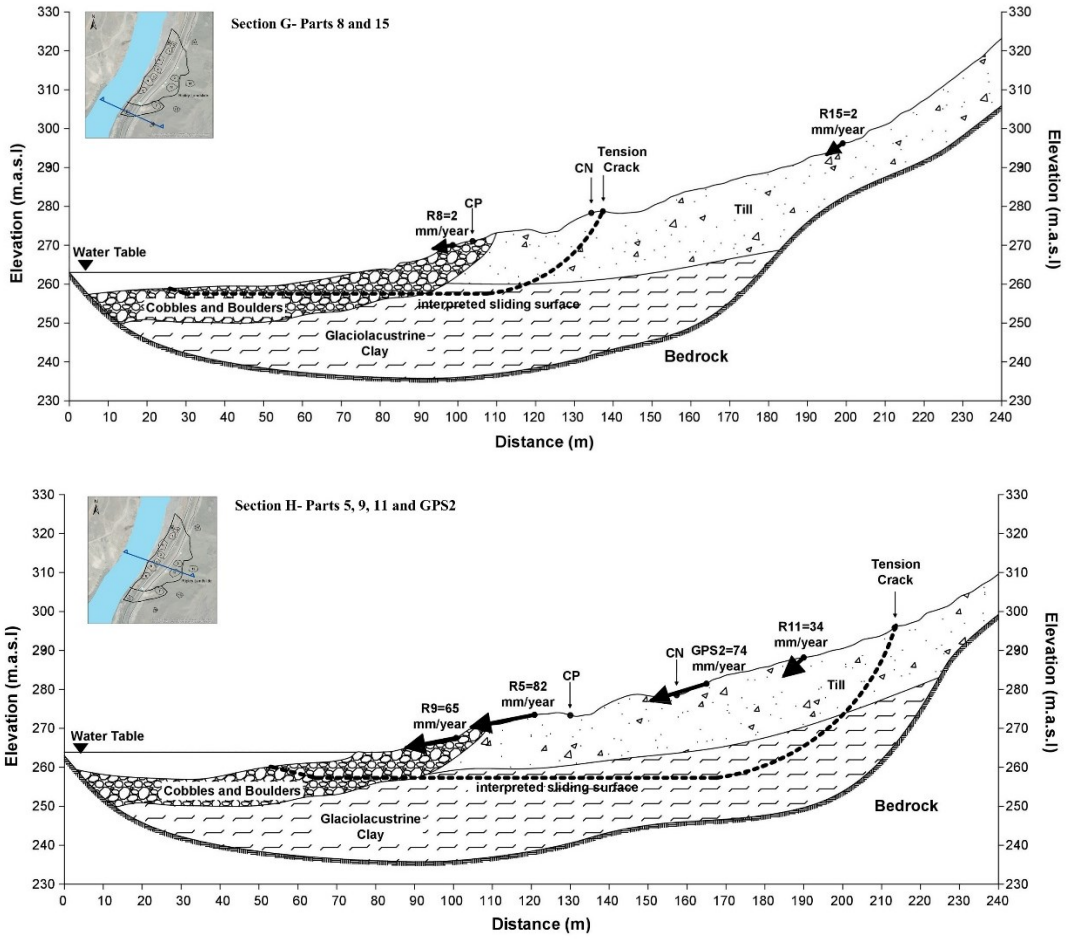

FIGURE 3-9. Real Vectors (Ground movement) in section- view on Ripley Landslide (Sliding surfaces are drawn based on the position of tension tracks and interpreted shear surface by Hendry et al. 2015 based on previous BH and SAA installation).

Table 3-3. Magnitudes of R and direction.

Area	Recorded date	Total Magnitude (mm/year)	Horizontal component (mm/year)	Westward Magnitude (mm/year)	Northward Magnitude (mm/year)	Downward Magnitude (mm/year)	Azimuth Angle (degree)	Angle with Horizontal plane (degree)
R0	May 2015 to May 2017	17	17	15	7	2	296	8
R1	May 2015 to May 2017	54	54	52	16	6	287	6
R2	May 2015 to May 2017	55	53	51	14	14	285	15
R3	May 2015 to May 2017	59	58	53	25	4	295	4
R4	May 2015 to May 2017	58	57	49	30	4	302	4
R5	May 2015 to May 2017	82	81	65	49	13	307	11
R6	May 2015 to May 2017	70	69	56	41	7	306	7
R7	May 2015 to May 2017	4	3	2	1	3	297	37
R8	May 2015 to May 2017	2	2	1	1	0	313	10
R9	May 2015 to May 2017	65	64	55	34	11	302	11
R10	May 2015 to	22	22	22	5	1	282	4

	May 2017							
R11	May 2015 to May 2017	34	12	11	3	32	284	43
R12	May 2015 to May 2017	5	2	2	1	4	287	43
R13	May 2015 to May 2017	3	2	2	1	1	303	24
R14	May 2015 to May 2017	4	3	3	0	2	277	30
R15	May 2015 to May 2017	2	1	1	1	1	295	35

3.3.2. Comparison with in-place displacement monitoring instrumentation

Published GPS displacement results at the Ripley landslide were used to evaluate the validity of the estimated R.

GPS data was selected between the installation day on April 11th, 2008 and April 11th, 2014. Annual results for the 6 years are averaged to get an estimated characteristic annual ground movement. In this regard, Macciotta et al. (2016) showed that in general, the acceleration and deceleration trend of the Ripley landslide measured by the GPS system was consistent for this period. The time series of GPS cumulative displacements in this period are presented as vertical and total horizontal components in Figure 3-10. Figure 3-11 shows each GPS horizontal displacement in Plan-view together with the calculated R vectors. The summary of recorded displacement by each GPS is shown in Table 3-4. The GPS velocities in Table 3-4 are consistent with the calculated velocities for the R displacement vectors near the toe of the landslide.

Vertical displacements and horizontal direction (Figure 3-11) are also generally consistent, with support the results of R calculations.

Table 3-4. Movement Records of Installed GPS on Ripley Slide.

GPS Name	Recorded Dates	Westward Movement (mm)	Northward Movement (mm)	Downward Movement (mm)	Total Movement (mm)	Horizontal Movement (mm)	Angle with Horizontal Plane (Degree)	Azimuth Angle (Degree)	Average Velocity (mm/year)
GPS1	11-Apr-08 to 11-Apr-14	355	154	97	399	387	14	293	67
GPS2	11-Apr 08 to 11-Apr-14	377	199	127	445	426	17	298	74
GPS3	11-Apr-08 to 11-Apr-14	443	319	410	683	546	37	306	114

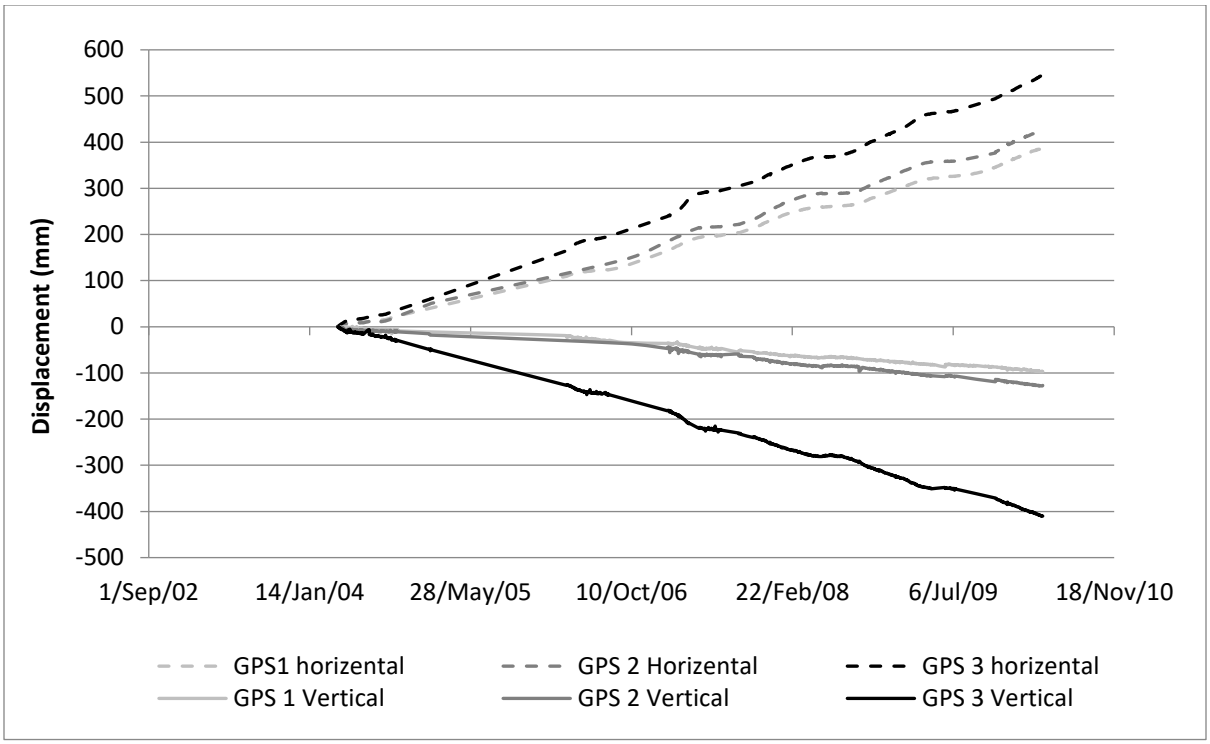

FIGURE 3-10. Cumulative Horizental and Vertical displacements of installed GPS systems on Ripley landslide.

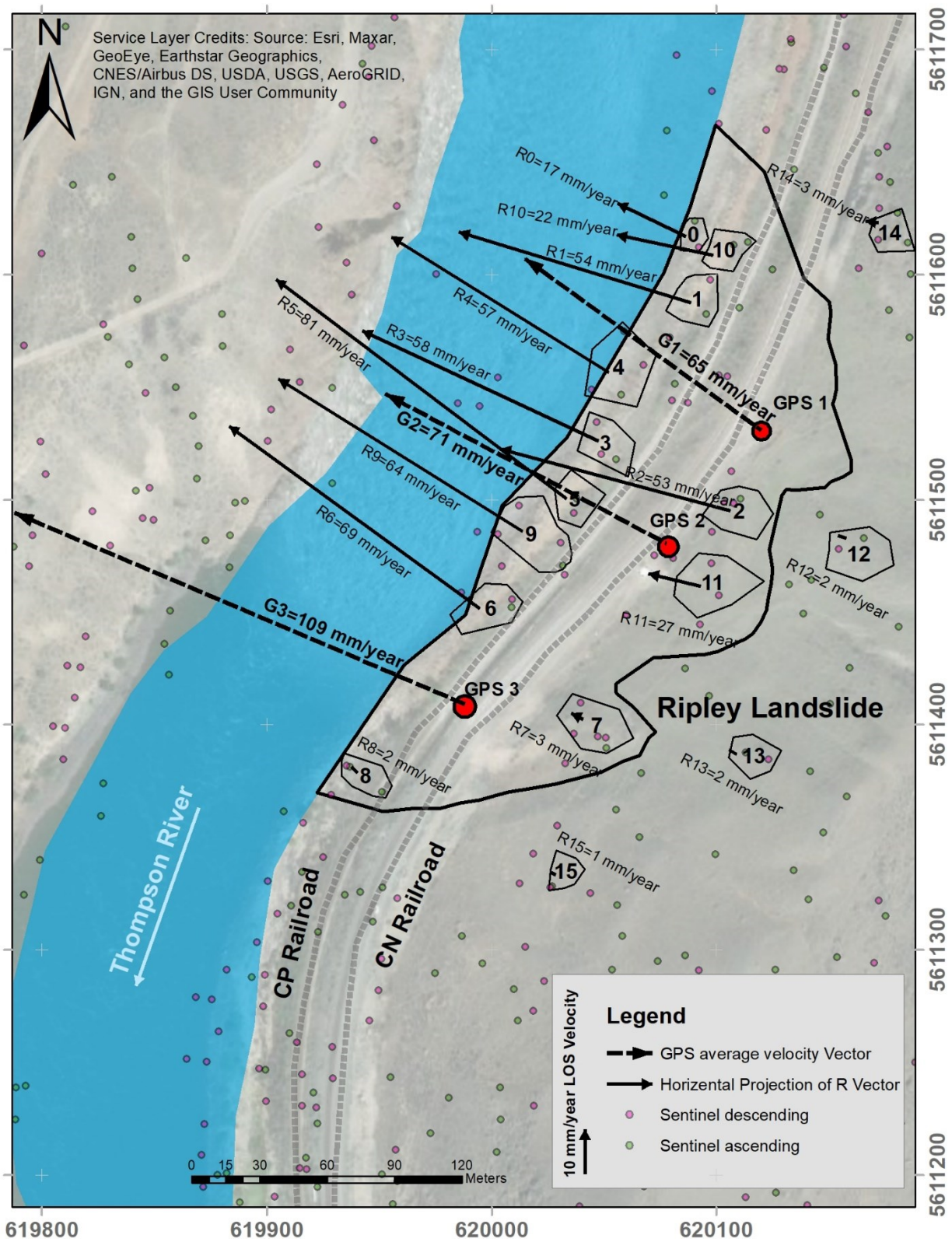

FIGURE 3-11. R Vectors and GPS average velocity vectors (mm/y) in plan-view.

3.4. Discussion

Figure 3-5 illustrated the scarcity of PS on the Ripley landslide from Sentinel ascending and descending orbits. Despite this low scatterers' density, selected regions on the landslide did include scatterers for both satellite orientations such that an average R vector could be calculated. LOS results show faster deformations at the landslide's toe and slowing towards the upper areas of the landslide. The LOS displacement for both satellite orientations is significantly lower outside the landslide extents to the North and South.

The fastest velocity was calculated in region 5 with 82 mm/year. This region is located near railway tracks on the center of the Ripley landslide as it is shown in Figure 3-8. The Ripley landslide is a very slow to slow moving landslide based on the velocity classification by Curden and Varnes (1996) and (Hungr et al., 2014). Figure 3-7 indicates there are episodes in which the landslide is showing an accelerated rate of deformation as opposed to episodes in which the landslide moves slower. Although it is not as explicit as the seasonal trend of cumulative displacement of GPS data which is shown in figure 3-10, the cumulative LOS changes for both Sentinel ascending and descending satellites in figure 3-7 introduces a faint trend in LOS changes which shows two acceleration seasons between October 2015 to May 2016 and Nov 2016 to the end of data, while they show deceleration between May 2016 and Nov 2016. This agrees with previous research which showed a correlation between ground movement and river water table fluctuation. Reductions in river flows (and drop in water head) has been associated with episodes on landslide acceleration (Hendry et al., 2015)(D. Huntley, 2021). The seasonal movement is more obvious for areas near river which showed more movement than other areas near the back scarp on the landslide body and also outside landslide boundaries. The inability of data to perform a strong trend can be referred to the relatively longer time intervals between

InSAR readings for both satellites and seasonal impacts on InSAR results (e.g. vegetation growth, weather changes, ground moisture).

Calculated R vectors are in general good agreement with displacement measurements from GPS-1 and GPS-2 (Figure 3-10). The velocity for R4 is 58 mm/year with an azimuth of 302 degrees (Table 3-3) while the average velocity and azimuth angle are reported as 67 mm/year and 293 degrees respectively for GPS-1 in Table 3-4. For R5 the azimuth angle is 307 degrees (Table 3-3), which is consistent with GPS-2 in Table 3-4 (298 degrees), and the recorded ground displacement velocity by GPS-2 is 74 mm/year, compared to 82 mm/year for R5.

However, GPS-3 shows a faster landslide velocity and a larger vertical component as opposed to other locations near the track. Although there are no InSAR regions coincidental with GPS-3, this unit shows different displacement vector characteristics than InSAR regions in the vicinity. It has been interpreted that the vertical movement of GPS 3 may be exaggerated because it is installed on a retaining structure that was built as part of track construction in 2005, and the weight of the structure over materials loosened by landslide deformations could lead to increased ground settlement (Macciotta et al., 2014).

Figure 3-8 shows that the magnitude of landslide displacements near the railway tracks and towards the river is significantly larger than deformations upslope, closer to the back scarp. It is illustrated in the cross sections in Figure 3-9 that the magnitude of R vectors tends to decrease with distance from the river, however the vertical components of ground movement are greater at locations near the back scarp. Displacements near the railway tracks and closer to the river are predominantly sub-horizontal while the vertical component of calculated R vectors near the back scarp slightly increases in proportion to the total R magnitude. The magnitude of R vector velocities in Table 3-3 is between 17 and 82 mm/year and the angle with vertical plane is from

75 to 86 degrees near the landslide's toe while this angle is less than 60 degrees for section near the back scarp. This would be consistent with the interpretation of the kinematics corresponding to a compound landslide, where a driving wedge in the upper section of the slope moves downslope pushing a passive wedge sliding over sub-horizontal shear surfaces. The vertical component of GPS displacements are also more notable than the vertical components of calculated R located on landslide's toe. The differences between displacement direction in section-view for GPS and InSAR results can be assigned to their different distance from landslide back scarp.

Calculated R velocities were very small behind the back scarp of the landslide (between 2 and 5 mm/year). These values could suggest some initiation of movement behind the interpreted back scarp of the Ripley landslide, however these small magnitudes could be within the limits of detection of the approach used, particularly when considering the assumptions required for the calculation of R. any initiation of movement upslope from the known extents of the landslide could represent landslide retrogression, which is a common feature of most other landslides in the area. However, further monitoring would be required upslope from the known active area of the landslide to identify if retrogression of the landslide has initiated.

3.5. Conclusion

The Ripley landslide is a very-slow moving landslide moving on a sub-horizontal weak clay layer. The landslide is located on an important transportation corridor in Canada along the Thompson River valley, and the two largest railway main lines traverse this landslide. This paper presents an update on the Ripley Landslide displacement trends and kinematics using InSAR monitoring data. To obtain an improved understanding of InSAR displacement measurements, the landslide is divided into 12 areas that correspond to coverage from both Sentinel ascending

and Sentinel descending orbits. A method is utilized where the horizontal component of movement is considered parallel to the slope azimuth in order to calculate the three-dimensional ground displacement vector. Ground displacement monitored with three GPS units on the landslide generally support the results from the method adopted.

Total InSAR LOS displacement velocities ranged between 2 mm/year and 82 mm/year, with faster sections near railroad tracks and the toe of the landslide, and slower sections at the back scarp of the landslide and upslope from the known active area. It is observed that landslide movement has a larger relative vertical component near the back scarp and becomes closer to horizontal direction near the railway tracks and near the toe. This would be consistent with the interpretation of the kinematics corresponding to a compound landslide, where a driving wedge in the upper section of the slope moves downslope pushing a passive wedge sliding over sub-horizontal shear surfaces.

Calculated ground velocities were very small behind the back scarp of the landslide (between 2 and 5 mm/year). These values could suggest some initiation of movement behind the interpreted back scarp of the Ripley landslide, however these small magnitudes could be within the limits of detection of this approach, and further monitoring with in-situ instruments such as GPS, robotic total station and prisms, to complement remote sensing techniques, e.g., satellite or ground based InSAR, would be required upslope from the known active area of the landslide for identifying any potential landslide retrogression.

Acknowledgments:

The authors would like to acknowledge Canadian Pacific Railway (CP) and TRE Altamira for providing the InSAR monitoring results used in this study. This research was performed within the umbrella of the Railway Ground Hazards Research Program (RGHRP), which is funded by

the Natural Sciences and Engineering Research Council of Canada (NSERC), Canadian Pacific Railway, Canadian National Railway, and Transport Canada; and is a collaboration that incudes Queen's University, the Canadian Geological Survey and the University of Alberta.

4. Updated understanding of the Thompson River Valley landslides kinematics using satellite InSAR

A Version of this chapter is under review for publication in Geosciences Journal.

Abstract:

The Thompson River valley is one of the most important transportation corridors in western Canada as it hosts two important railways. This valley has experienced several historical landslide events, many of them along a 10 km section south of the town of Ashcroft. Six of these landslides, showing varying states of activity, were selected for analysis in this paper, as these have the potential for most impact on the railways. The stratigraphic interpretation of these landslides is combined with satellite InSAR data from May 2015 to May 2017 to enhance the current understanding of the landslide kinematics. Two InSAR orientations are combined geometrically with the assumption that the horizontal component of landslide movement is parallel to the slope azimuth, which provides a practicable approach to approximate landslide displacement vectors. The results classify these landslides as very slow-moving. The maximum velocities recorded are 29, 35, 26, 64, 18 and 52 mm/year for the Goddard, North, South, South extension, Barnard and Redhill landslides, respectively. All landslides except the Redhill landslide show near-horizontal movements near the toe, with increasing vertical component as measurements approach the back scarp. This confirms the kinematics include rotational and compound mechanisms.

Keywords: InSAR, landslides, kinematics, remote sensing

4.1. Introduction

Landslides are known as a natural phenomenon which pose risks to infrastructure and lives all around the world. Many cases of landslides have been reported in Canada which caused many

life losses and damage to infrastructure (Charrière et al., 2015; Cruden & Martin, 2007; Mei et al., 2008; Vallee, 2019). Hundreds of fatalities and millions of dollars in costs caused by landslides have been recorded in Canada since 1771 (Choe et al., 2021a). A recent report confirmed four fatalities as a consequence of a landslide in British Columbia's Highway 99 in November 2021 (Simon Little, Global News, November 20, 2021).

Technical and economic challenges of stabilization or avoidance of landslides in susceptible areas means that identification of landslides and monitoring terrain's movement is the most efficient risk management tool when combined with warning and action plans. Furthermore, it can inform maintenance requirements for key infrastructure such as roads and railway tracks. Monitoring is commonly employed as part of early warning systems (Huntley et al., 2019a; Journault et al., 2018; Macciotta et al., 2016). Also, monitoring and understanding of landslides become even more important because of climate change effects on landslide activity, for example due to acceleration of glacier melting that is expected to increase landslide activity in northern regions in Canada. (Choe et al., 2021). Remote landslide monitoring can be used for specific landslides or on large areas to increase understanding of landslide kinematics and triggers, and to improve landslide risk management strategies (Dean et al. 2020, Macciotta et al. 2020, Woods et al. 2020, Lan et al. 2021, Rodriguez et al. 2021, Macciotta and Hendry 2021).

This paper presents an updated understanding of landslide kinematics using satellite InSAR for six active landslides along the Thompson River Valley in British Columbia, Canada. These landslides are located along a 10 km section south of the town of Ashcroft. Some of these landslides have been studied by a number of researchers (Hendry et al. 2015, Macciotta et al. 2016, Jornault et al. 2018, Huntley et al. 2019a, D. Huntley, 2021; Eshraghian et al., n.d., 2008; Huntley et al., 2021) and this paper provides an update on their kinematics based on the

interpreted stratigraphy in the area (Schafer 2016, Huntley et al. 2019a, 2019b, 2020, Sattler et al. 2021, Huntley et al 2021) and InSAR monitoring between May 2015 and May 2017 (These correspond to InSAR processed datasets that were made available).

Two InSAR orientations are combined geometrically with the assumption that the horizontal component of landslide movement is parallel to the slope azimuth, which provides a practicable approach to approximate landslide displacement vectors. This approach was validated for the area matter of this paper in Soltanieh and Macciotta (in press) on the Ripley landslide, which has a long history of monitoring (Macciotta et al., 2016).

4.1.1 Landslide remote sensing and satellite InSAR

New observation technologies help geotechnical engineers to investigate the terrain's movement continuously. Many tools such as remote sensing, GPS monitoring, geophysical imaging and geotechnical surveys are employed for landslide characterization (Xu et al., 2016). Interferometric Synthetic Aperture Radar (InSAR), Light Detection and Ranging (LiDAR), and Unmanned Aerial Vehicle (UAV) photogrammetry are some examples of remote sensing techniques which are employed to monitor cut slopes or natural slopes in routine geohazard monitoring programs. Using these remote sensing methods, engineers and researchers are able to investigate landslide kinematics on large areas with high spatial resolution, when compared with in-place instruments such as slope inclinometers or survey monuments (Rodriguez et al., 2020).

Radar satellites can carry sensors for Interferometric Synthetic Aperture Radar (InSAR) monitoring, where the relative change in the distance between the radar and ground surface can be calculated by using wavelength information. These abilities make InSAR a robust method in many applications to detect surface displacements of crustal deformation, glacier motion and landslides (Abe et al., 2020).

The accuracy of satellite InSAR gives many advantages for monitoring landslide activity, particularly in remote areas where installation and using in-place ground monitoring instruments is challenging both economically and technically. Despite extensive application of satellite InSAR for monitoring landslides in the recent 30 years, using this method is still challenging for rapid landslides due to gaps between two consecutive data acquisitions and the potential high acceleration of some landslides. There are also other challenges in this technique, such as atmospheric noise, vegetation cover, and seasonal effects like rainfall or snow cover (Choe et al.,

2021b). Even with these limitations, satellite InSAR has become an effective and reliable method for many applications (Mancini et al., 2021).

Using satellite InSAR data together with other monitoring information like precipitation or ground water fluctuation data can allow for a robust understanding of landslide mechanisms and possible triggers, and this method can be employed effectively to measure displacement of slow or extremely slow-moving slopes as well as capturing the initiation of acceleration. Although satellite revisiting times (now approximately 3 days to 1 week) limit the temporal resolution of InSAR monitoring, good resolution of InSAR monitoring systems (sub-cm/year) makes it a very useful tool for monitoring landslides (Huntley, 2021).

4.1.2 The Thompson River valley landslides south of Ashcroft

The Thompson River valley, south of town of Ashcroft in British Colombia Canada; is host to Canadian Pacific Railway (CP) and Canadian National Railway (CN) main lines connecting the port of Vancouver and the rest of Canada. This corridor is therefore very important for the Canadian economy (Clague & Evans, n.d.). The importance of this corridor led Natural Resources Canada (NRCAN), the Geological Survey of Canada (GSC), and Transport Canada (TC), in partnership with both CNR and CP, the University of Alberta, and Queen's University; to monitor the Thompson River valley along a 10km section south of the town of Ashcroft, where up to 14 landslides have been identified (Huntley et al., 2021; Porter et al., n.d.). A collaboration with TRE ALTAMIRA CLS Group (TRE) provided the satellite InSAR data in used in this study.

River erosion cut the Thompson River valley, which was formed by a series of glaciations. Valley slopes in the glacial sediments are between 75 and 125 m high and its angle from toe to

valley crest vary between 15 and 30 degrees. Multiple glacial advance and retreat intervals in the Pleistocene period filled the valley with a complex sequence of a wide range of deposits, from poorly sorted sand and gravel to rhythmically interbedded silt and clay. Triassic and Jurassic volcanic and sedimentary rocks formed the local bedrock in this area (Clague and Evans 2003; Huntley and Bobrowsky 2014; Journault 2018; Porter et al., 2000). The southward flowing Thompson River cut 150 meters of glacial deposited sediments leading to the formation of several landslides (Porter et al. 2002; Journault 2018). The presence of a weak silt and clay layer has been identified as the main geomorphological feature for the formation of these landslides, which are characterized by multiple graben and horst features as well as steep internal shear and basal through-going surfaces along these weak materials (Clague and Evans 2003; Eshraghian et al. 2007; Journault 2018). The residual shear strengths in these weak silt and clay layers are characterized by friction angles between 9 and 16 degrees (Hendry et al., 2015; Stark and Eid, 1994; Porter et al.,2000). Figure 4-1 shows the location of Thompson River valley and the extents of 12 of the 14 landslides identified in this valley. The volumes of the landslides in Thompson River valley vary between 0.75 million cubic meters for Ripley landslide and more than 15 million cubic meters for North Landslide. Displacement rates range between 10 mm/year (extremely Slow) and up to 50 mm/s (very rapid) historically in some areas (Journault et al., 2018).

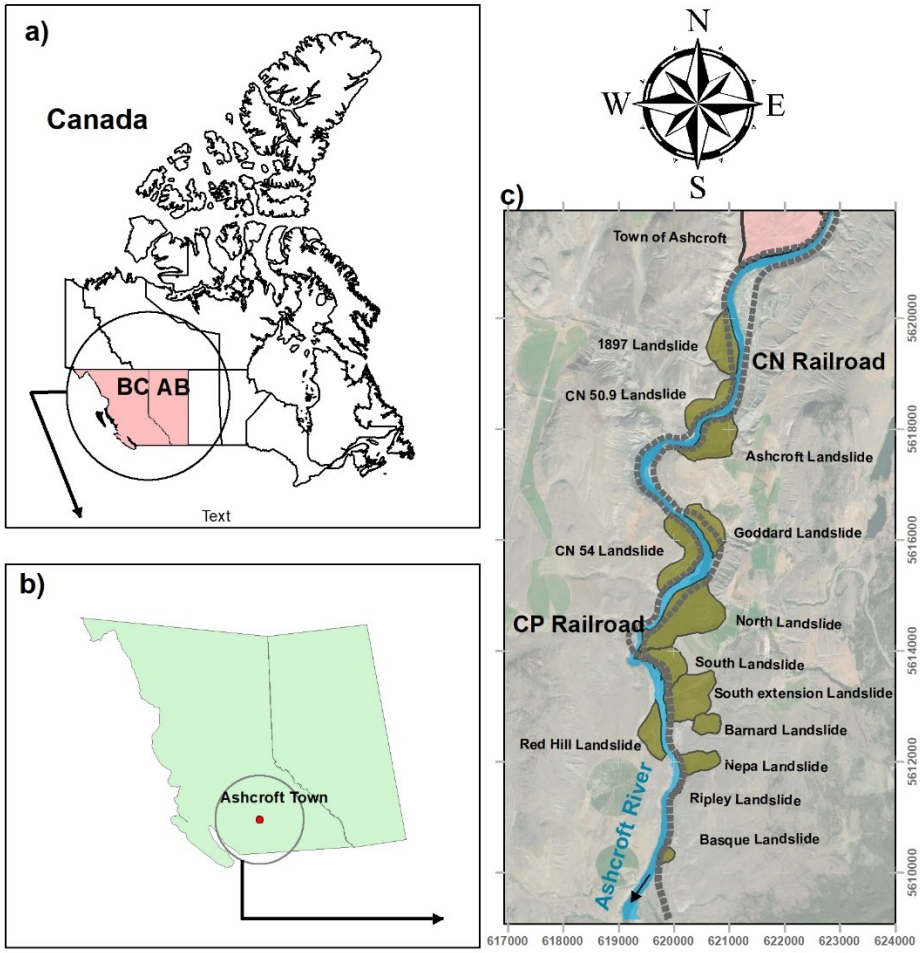

FIGURE 4-1: Location of the Thompson River Valley (a,b) plan-view and active landslides across the valley (c). Coordinates in UTM. BC and AB in (a) correspond to the provinces of British Columbia and Alberta, respectively.

4.2. Materials and methods

4.2.1 Satellite InSAR displacement data

The satellite InSAR data were captured by the Sentinel 1 project and processed by TRE. Satellite images used in this study were collected between November 3rd, 2014 and March 17th, 2018 for the ascending orbit, and between November 6th, 2014 and April 1st, 2018 for the descending

orbit. The line of sight (LOS) displacement, which is the projection of the real surface displacement on the visual line between radar's sensor installed on satellite and the area monitored, correspond to overlapping timelines for each geometry (ascending and descending). The ascending geometry data correspond to data captured when the satellite moves from south to north and, given the satellite sensor positioning, captured images look towards the east. The descending geometry corresponds to data captured when the satellite travels from north to south and looks west. These geometries are defined by the angle between the LOS and the vertical plane -theta (θ)- and the angle between the satellite's orbit and the geographic north -delta (δ). LOS angles are shown in Table 4-1. Figure 4-2 shows a schematic of the geometry for both Sentinel ascending and descending orbits.

Radar Data Information		
Satellite	Sentinel 1	Sentinel 1
Acquisition Geometry	Ascending	Descending
Period Covered by Imagery	03-Nov-2014 to 17-Mar-2018	06-Nov-2014 to 01 Apr-2018
No. of Processed Images	51	59
Coordinate System	WGS 1984	WGS 1984
Area of Interest	869.2 Km^2	869.2 Km^2
Number of PS+DS	194083 (112343 PS, 81740 DS)	178396 (89510 PS, 88886 DS)
Sensor Mode	IW	IW
Image Resolution	20 m×5 m	20 m×5 m

Table 4-1 Details of the processed satellite InSAR data

InSAR displacement data correspond to Scaterers, including those on structures and natural features such as rock outcrops or exposed ground which are likely sTable (permanent scatterers or PS) and distributed scatterers (DS) on large areas (up to hundreds of square meters) identified from exposed ground. Although each DS is represented by a point (location), these points actually correspond to non-point features (areas). A summary of the data properties collected by the Sentinel satellite are presented in Table 4-2. The processing technique for InSAR ground displacement calculations used by TRE correspond to the SqueeSAR method and it incorporates PSInSAR processing (Ferretti et al., 2011) .

Satellite	Orbit Geometry	Track	Sensor Mode	Symbol	Angle (Degree)
Sentinel	Ascending	64	IW	θ	38.66
				δ	11.33
Sentinel	Descending	115	IW	θ	44.29
				δ	7.79

Table 4-2 Satellite viewing (LOS) angles for the Sentinel and Radarsat-2 imagery

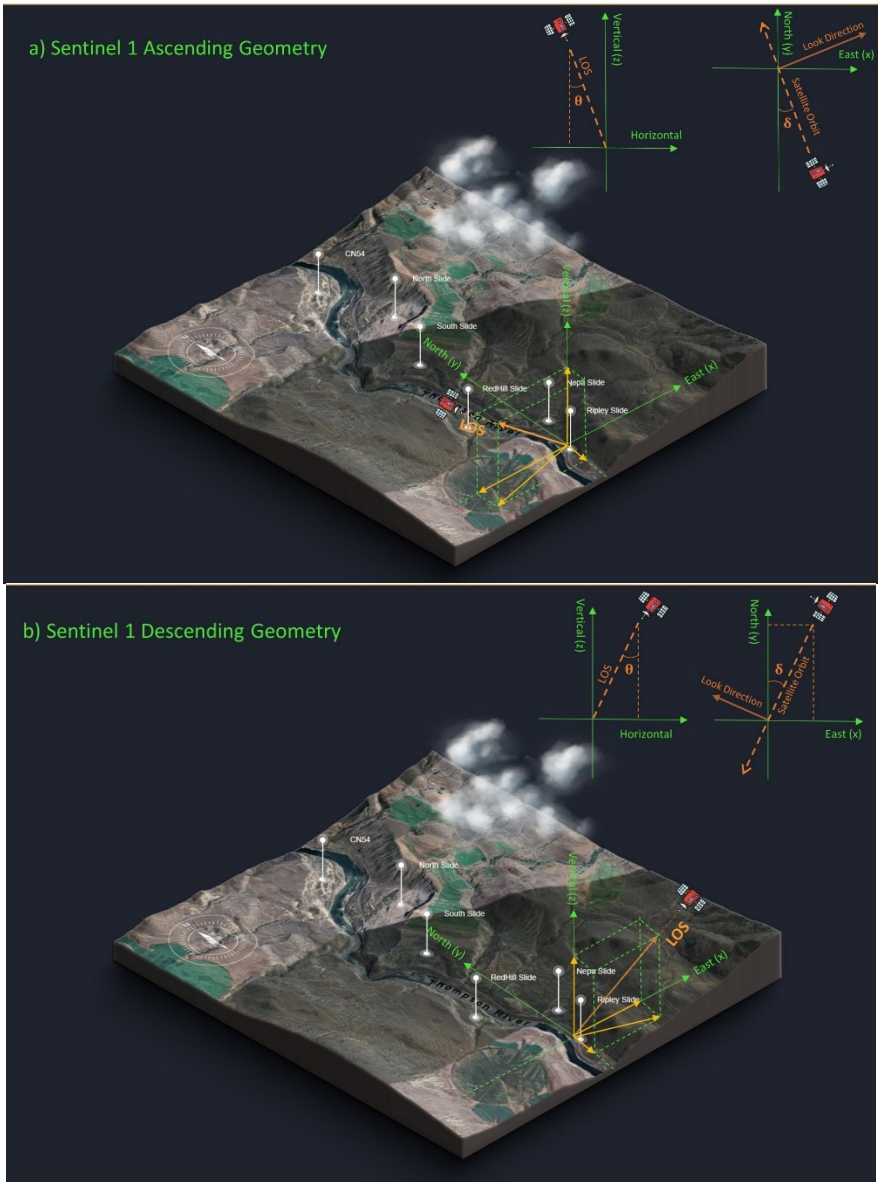

FIGURE 4-2: Geometry of the image acquisitions along the ascending(a) and descending(b) orbits (Inspired by Ground Deformation InSAR Analysis over the Thompson Canyon, British Columbia, Technical Details, August 2018, By TRE Group)

4.2.2 Surface ground displacement calculations based on InSAR LOS displacements

The projection of true landslide surface displacement on each LOS direction is equal to the change in LOS distance between two different readings. In theory, three LOS displacements are needed to fully resolve the true landslide surface displacement. However, LOS displacements correspond to different acquisition times and different data point locations between the ascending and descending geometries. Therefore, the solution requires adopting some spatial and temporal averaging of data. Furthermore, the predominantly north-south direction of the satellite orbit precludes optimal use of the north component of LOS displacements. The processes followed in this paper is presented and validated for a landslide in this area by Soltanieh and Macciotta (in-press).

The true ground displacement is called "Real vector" and is represented by bold **R** to show it is a vector. The north-south displacement components are not considered reliable given the orbits are sub-parallel to the north-south direction. Assuming **R** parallel to the downslope direction (both azimuth and inclination) is a common assumption for landslide InSAR interpretation (Journault et al., 2018). In this paper, it is assumed that the projection of **R** in the horizontal plane is parallel to the slope azimuth (average slope azimuth in the area of analysis). Therefore, the unit vector of the horizontal component of **R** can be calculated using the topography of the area. A digital elevation model (DEM) of the Thompson River valley was used in ArcMap (ArcGIS, ArcMAP 10.7.1 ESRI) to calculate the average azimuth of the vector normal to the slope. Considering the vertical component of **R** as an unknown, the assumption of the horizontal component direction, and projecting **R** to the LOS unit vectors based on the satellite geometries for both satellite

orbits; allows to calculate an approximation for all components of **R**. The following process is presented in Soltanieh and Macciotta (in-press):

Unit vectors of LOS are denoted as $\boldsymbol{S_a}$ for Sentinel ascending and $\boldsymbol{S_d}$ for Sentinel descending. The projections of **R** on these directions are the measured LOS displacements, denoted by vectors $\boldsymbol{P}_a \; and \; \boldsymbol{P}_d$, respectively. Each of these vectors have a scalar magnitude $M_a \; and \; M_d$, respectively. Equation 1 presents the expression for $\boldsymbol{P}_i$, where i represents the ascending or descending orbit.

$$\boldsymbol{P_i} = (\boldsymbol{R} \cdot \boldsymbol{S_i})\, \boldsymbol{S}_i = M_i\, \boldsymbol{S_i} \tag{1}$$

The components of the vector **R** are denoted as (x,y,z), where the components of the unit vectors of the LOS are denoted as $\boldsymbol{S}_i = (e, n, u)$. Calculating the LOS unit vectors requires the angles between the LOS, the vertical plane, and azimuth from Table 2 (Equations 2, 3 and 4).

$$u = \cos\theta \tag{2}$$

$$e = \sin\theta \,.\, \sin\delta \tag{3}$$

$$n = \sin\theta \,.\, \cos\delta \tag{4}$$

The coordinate system adopted corresponds to (East, North, Up). The sign of u is positive and the sign of n is negative for both orbits' LOS. the sign of e is negative for the ascending orbit and it is positive for the descending orbit. The unit vectors are calculated following:

$$\boldsymbol{S}_a = (-0.613, -0.123, 0.781) \tag{5}$$

$$\boldsymbol{S}_d = (0.692, -0.095, 0.716) \tag{6}$$

Replacing equations 5 and 6 into Equation 1, and solving for $M_a \; and \; M_d$ result in the measured LOS displacements in terms of the components of **R** (Equation 7 and Equation 8).

$$-0.613x-0.123y+0.781z=M_a \quad (7)$$

$$0.692x-0.095y+0.716z=M_d \quad (8)$$

The third equation required to calculate the components of **R** corresponds to the assumption that the total horizontal vector component of **R** is parallel to the slope's azimuth in the area of measurement (α):

$$\frac{x}{y} = \tan\alpha \quad (9)$$

Equations 7, 8 and 9 are a system of three equations and three unknowns for estimating **R**.

It was mentioned that the spatial and temporal inconsistency between ascending and descending InSAR data required spatial and temporal averaging. Spatial averaging considered segmentation of the landslides that balanced data density (e.g. availability of data) and covering different portions of the landslide to allow kinematic interpretation. This decision-making process was done qualitatively and based on the experience of the authors. Figure 4-3 shows the data density for all investigated landslides. It is shown that almost all these areas contain more than one scatterer of each orbit and the average of these scatterers are used as representative of LOS displacements for the area.

To minimize the influence of asynchronous data points between orbits, relatively long periods of time for calculating average **R** (annual basis) were adopted, which led to differences of only a few days in the data for both orbits. This was considered adequate and was tested for the Ripley landslide (Soltanieh and Macciotta, in-press). The movement rate of Ripley landslide had been reported at approximately 150 mm/year (0.4 mm/day), suggesting that asynchronous measurements by less than two weeks for a total period of analysis of two years (May 26th 2015

to May 21st 2017 for ascending orbit and June 10th 2015 to May 12th 2017 for descending orbit, time span used in this paper) would represent approximately 2% error.

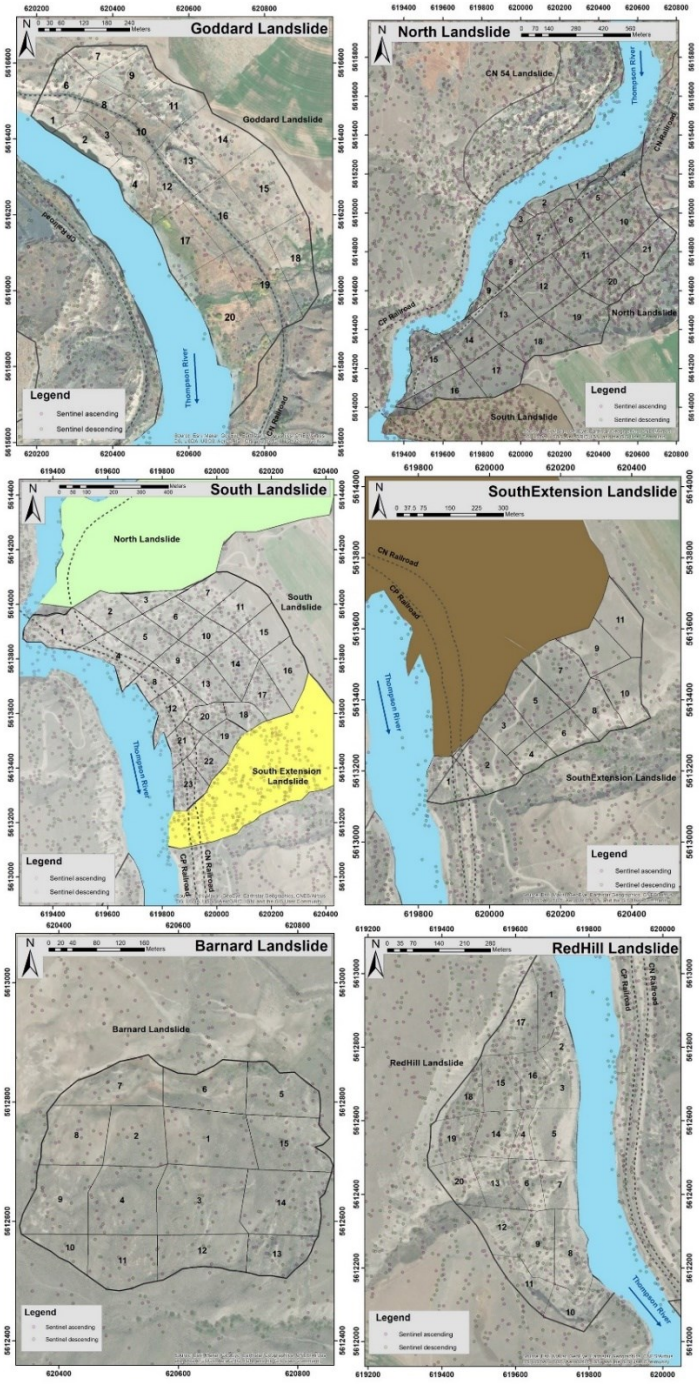

FIGURE 4-3- InSAR data density for different landslides along the Thompson River valley for both Ascending and Descending orbits.

4.3 Results

This section presents the LOS ground displacements measured by Sentinel 1 in both orientations, and the calculated **R** for each landslide sector. **R** is presented as the horizontal component on plan view, and as the resultant vector of vertical and horizontal components in section views. The cross sections were developed based on the topography of the area and the stratigraphy for the landslides in Eshgahrian (Eshraghian 2007, Eshraghian 2007). The stratigraphy for the Redhill landslide was estimated based on information about adjacent landslides.

4.3.1 Goddard Landslide

The magnitudes of recorded cumulative LOS displacement at the end of the selected timelines for both orbits (May 26th 2017 and for ascending orbit and May 12th 2017 for descending orbit) are shown in figure 4-4 for each sector of the landslide. Landslide displacement is minor in most places on the Goddard landslide. The LOS displacement rates are less than 10 mm/year in most sectors of the landslide during the period of analysis.

Figure 4-5 shows the cumulative average LOS for each sector of the landslide. The average cumulative LOS displacement does not exceed 20 mm. The activity of the landslide is low and no specific seasonal acceleration was identified in this landslide.

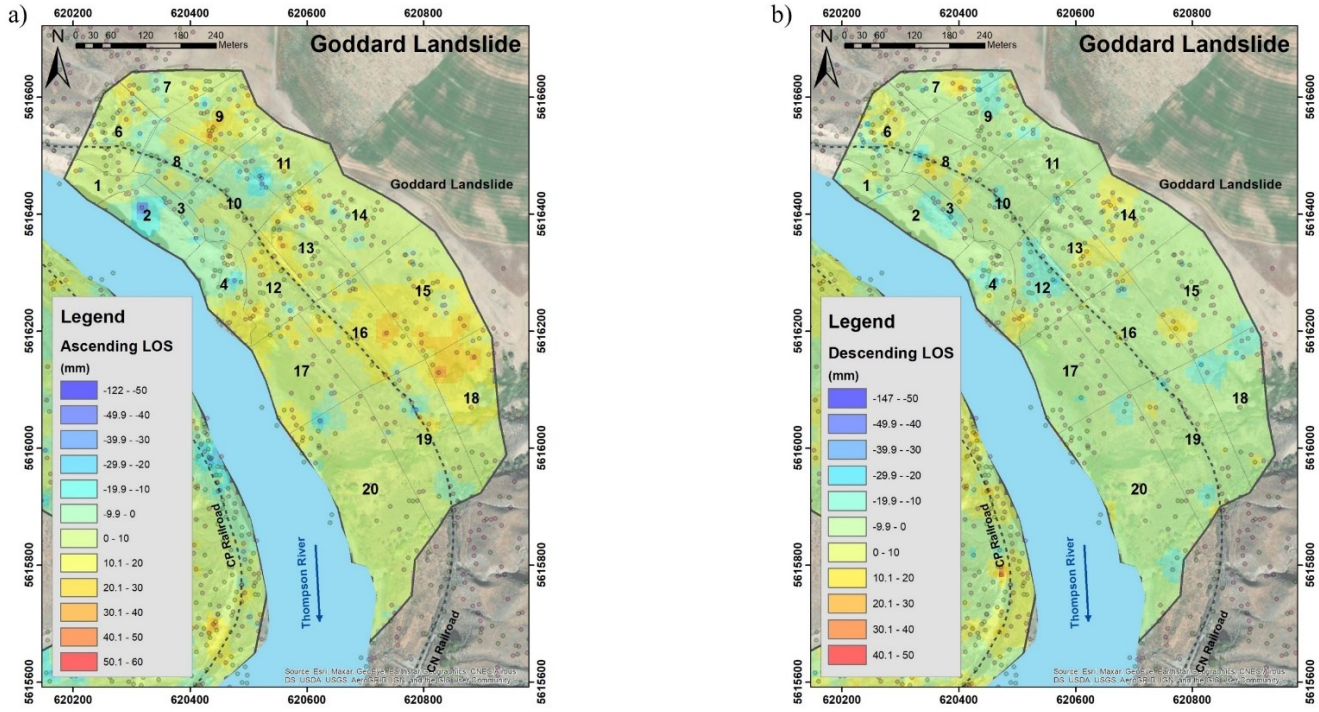

FIGURE 4-4-The cumulative LOS changes at the end of the selected timeline for Goddard landslide for a) Sentinel ascending and b) Sentinel descending orbits.

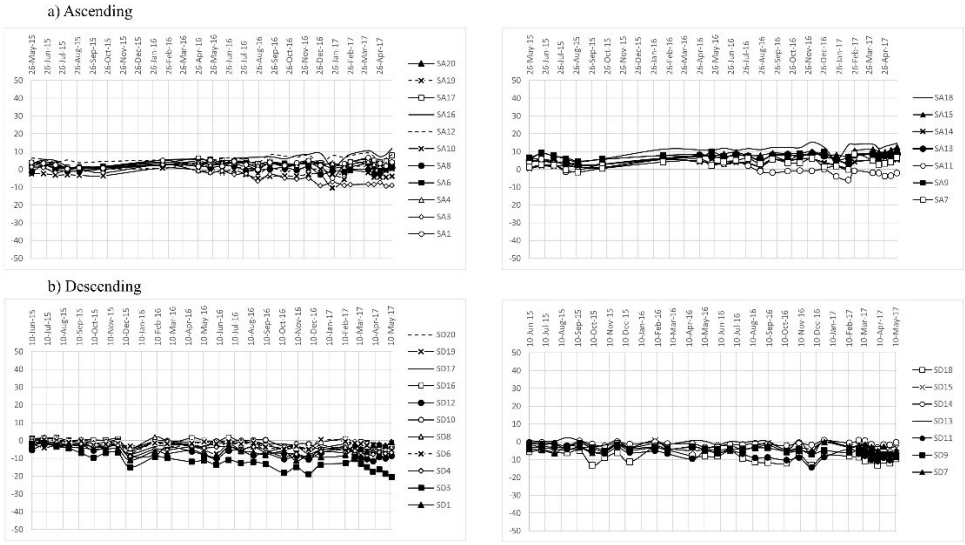

FIGURE 4-5- Cumulative LOS changes between May 2015 to May 2017 gathered by Sentinel ascending and descending within Goddard landslide extent.

Figure 4-6 shows the horizontal component of **R** for each sector of the Goddard landslide in plan-view. The horizontal component of **R** is near zero for most sectors of the landslide except for part 7. Figure 4-7 presents the vertical component of **R** on selected cross sections for the Goddard landslide. The vertical components also support the low activity of landslide. Steep vertical components would correspond to graven blocks. One upward vertical component is likely due to the small amount of displacement which is likely within the limits of detection of the technology and the assumptions adopted in this paper. Table 4-3 presents a summary of calculated magnitudes of **R** and their components. Note that the slow movements calculated make interpretation of the kinematics uncertain based on movement only. Internal steep shear surfaces in Figure 4-7a are interpreted based on topographic characteristics and displacement vectors. Displacement vectors in Figure 4-7b did not allow for kinematic interpretation without significant uncertainty.

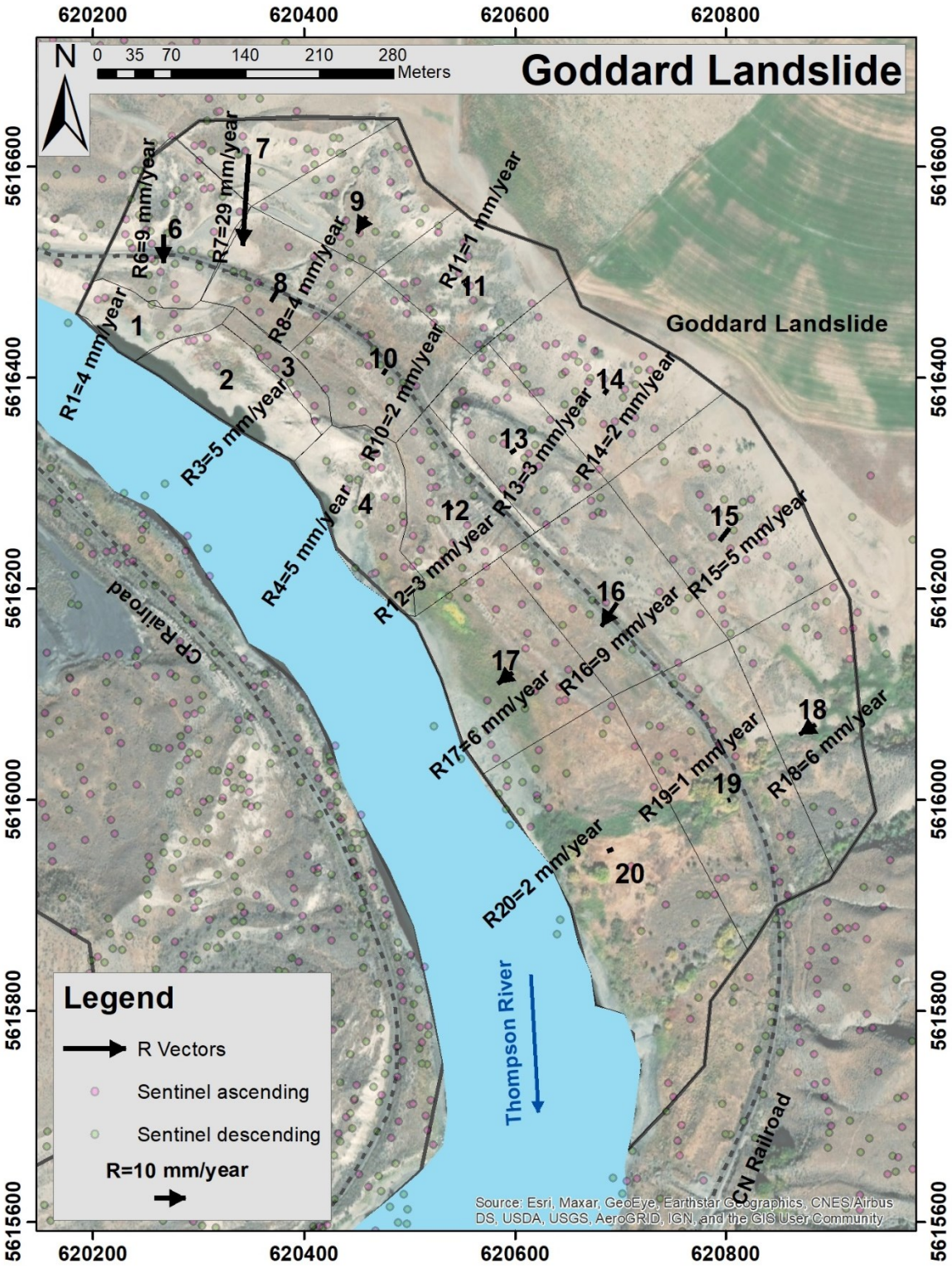

FIGURE 4-6- Calculated horizontal component of **R** vectors for divided parts within the Goddard landslide extent in plan-view

- Goddard Landslide Section A

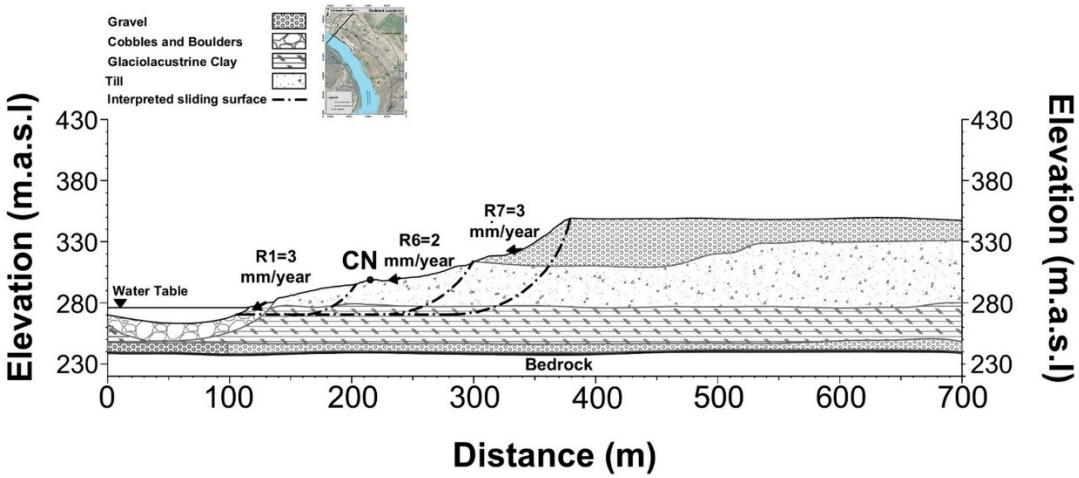

- Goddard Landslide Section B

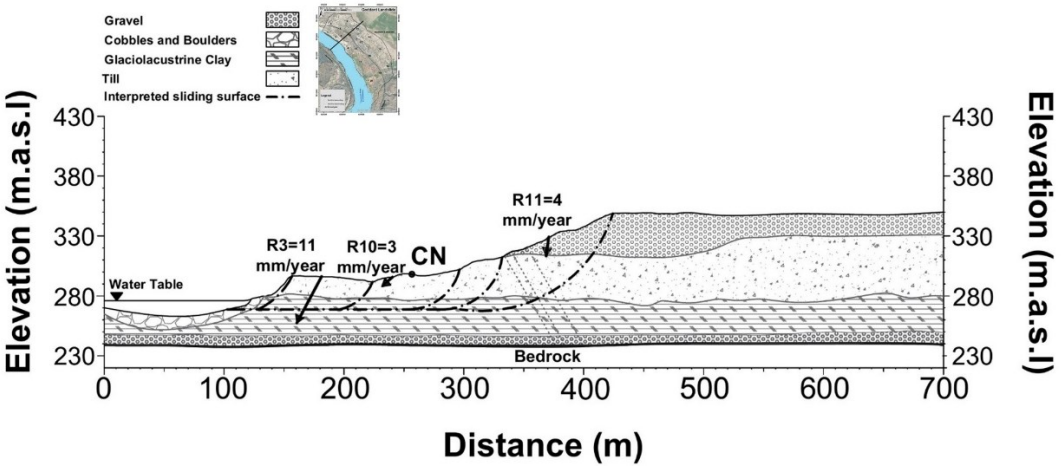

- Goddard Landslide Section C

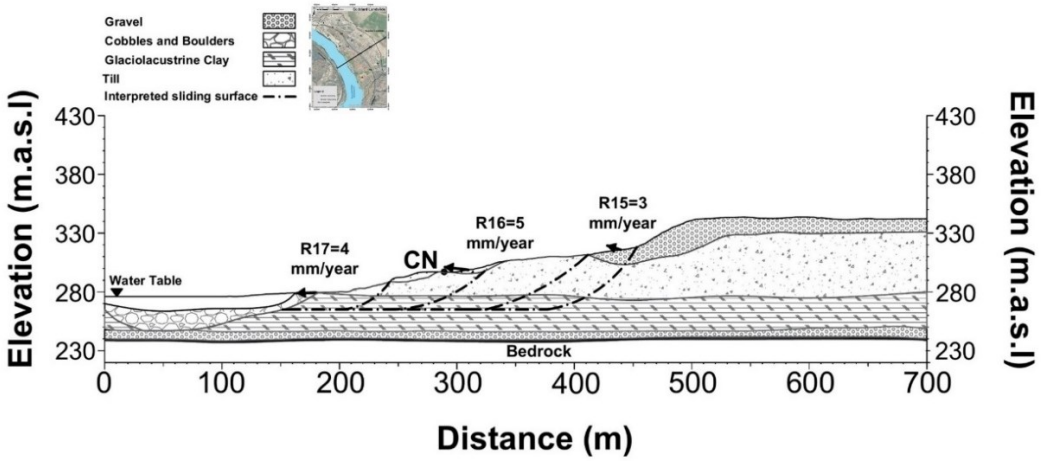

FIGURE 4-7- Calculated Vertical component of **R** for selected cross sections of the Goddard landslide

Area	Recorded date	Total Magnitude (mm/year)	Horizontal Magnitude (mm/year)	X direction component (mm/year)	Y direction component (mm/year)	Z direction component (mm/year)	Azimuth Angle (Degree)	Angle with Horizontal plane (Degree)
R1	May 2015 to May 2017	4	4	-2	-3	-2	208	27
R2	May 2015 to May 2017	Insufficient data						
R3	May 2015 to May 2017	11	5	-4	-4	-10	222	62
R4	May 2015 to May 2017	6	5	-3	-4	-2	213	27
R6	May 2015 to May 2017	9	9	0	-9	-2	182	11
R7	May 2015 to May 2017	29	29	-2	-29	-3	184	5
R8	May 2015 To May 2017	4	4	-2	-4	-1	210	8
R9	May 2015 to May 2017	6	6	-3	-5	-1	210	13
R10	May 2015 to May 2017	3	2	-1	-2	-2	212	42
R11	May 2015 to May 2017	4	1	0	0	-4	223	82
R12	May 2015 to May 2017	3	3	-2	-2	-1	226	13
R13	May 2015 to May 2017	3	3	-2	-2	0	234	2
R14	May 2015 to May 2017	2	2	-1	-2	1	217	25
R15	May 2015 to May 2017	5	5	-3	-4	1	217	11
R16	May 2015 to May 2017	9	9	-5	-7	1	213	4
R17	May 2015 to May 2017	6	6	-4	-3	0	233	0
R18	May 2015 to May 2017	6	6	-5	-3	2	239	16
R19	May 2015 to May 2017	2	1	-1	0	-2	246	65
R20	May 2015 to May 2017	3	2	-2	-1	-1	250	21

Table 4-3- Summary of calculated **R** magnitude and geometry for the Goddard landslide

4.3.2 North Landslide

The recorded 2-year cumulative LOS displacements are presented in Figure 4-8. Ground movement in these 2 years is very limited in the North landslide (less than 10 mm/year) for most sectors except for sectors 2 and 3, and some parts of sector 1 for the descending orbit, which are located on the toe of the North landslide. Figure 9 shows the cumulative LOS displacements in these 2 years.

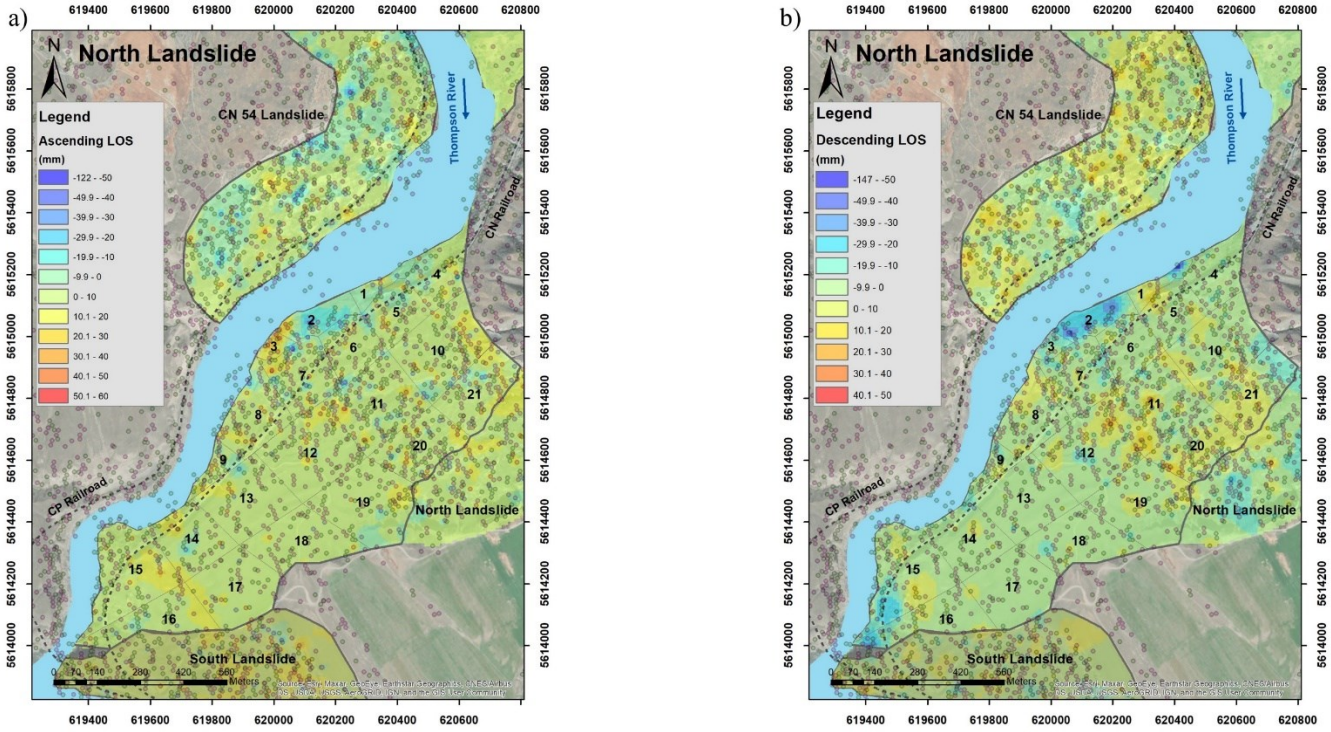

FIGURE 4-8- The cumulative LOS changes at the end of the selected timeline for the North landslide for a) Sentinel ascending and b) Sentinel descending orbits.

All sectors except for sector 3, LOS displacements are in the range of ±10 mm (ascending) and up to 25 mm at the end of the time period. The cumulative LOS displacements are ±10 mm (descending) for all sectors except sectors 1, 2 and 3. The maximum displacement occurred in sector 1 (approximately 50 mm in 2 years).

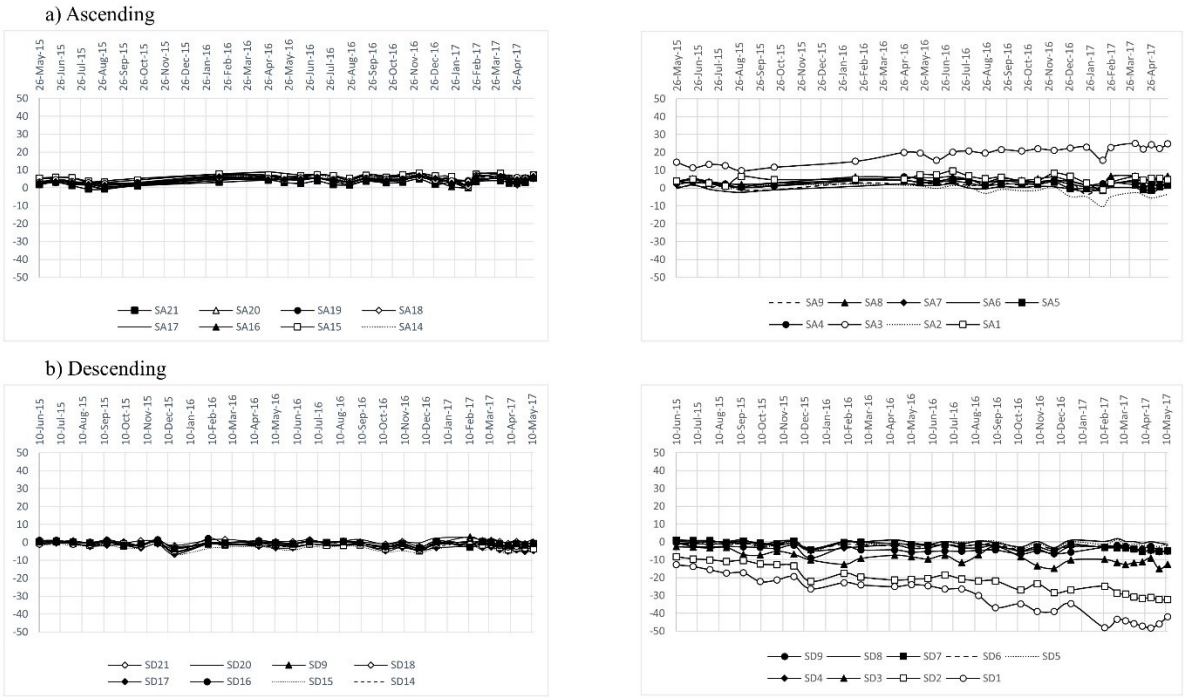

FIGURE 4-9- Cumulative LOS changes between May 2015 to May 2017 gathered by Sentinel ascending and descending within the North landslide extent

The horizontal components of **R** are shown in Figure 4-10. The maximum calculated horizontal component is 35 mm/year (sector 1). This magnitude is between 2 and 24 mm/year for other sectors, and the higher activity is observed on the toe of the landslide (sectors 1, 2 and 3). Figure 4-11 shows calculated **R** in selected sections on the North landslide. The vertical component of ground movement is negligible for most sectors except sectors 1 and 2 on the landslide' toe. Some vertical components show upward movement, likely due to displacement magnitudes within the limits of detection of the technology and method adopted in this paper, and it is clear that most of the landslide is showing minimum to no activity with the exception of some locations at the toe. Table 4-4 summarizes the calculated components of **R** for all sectors of the North landslide.

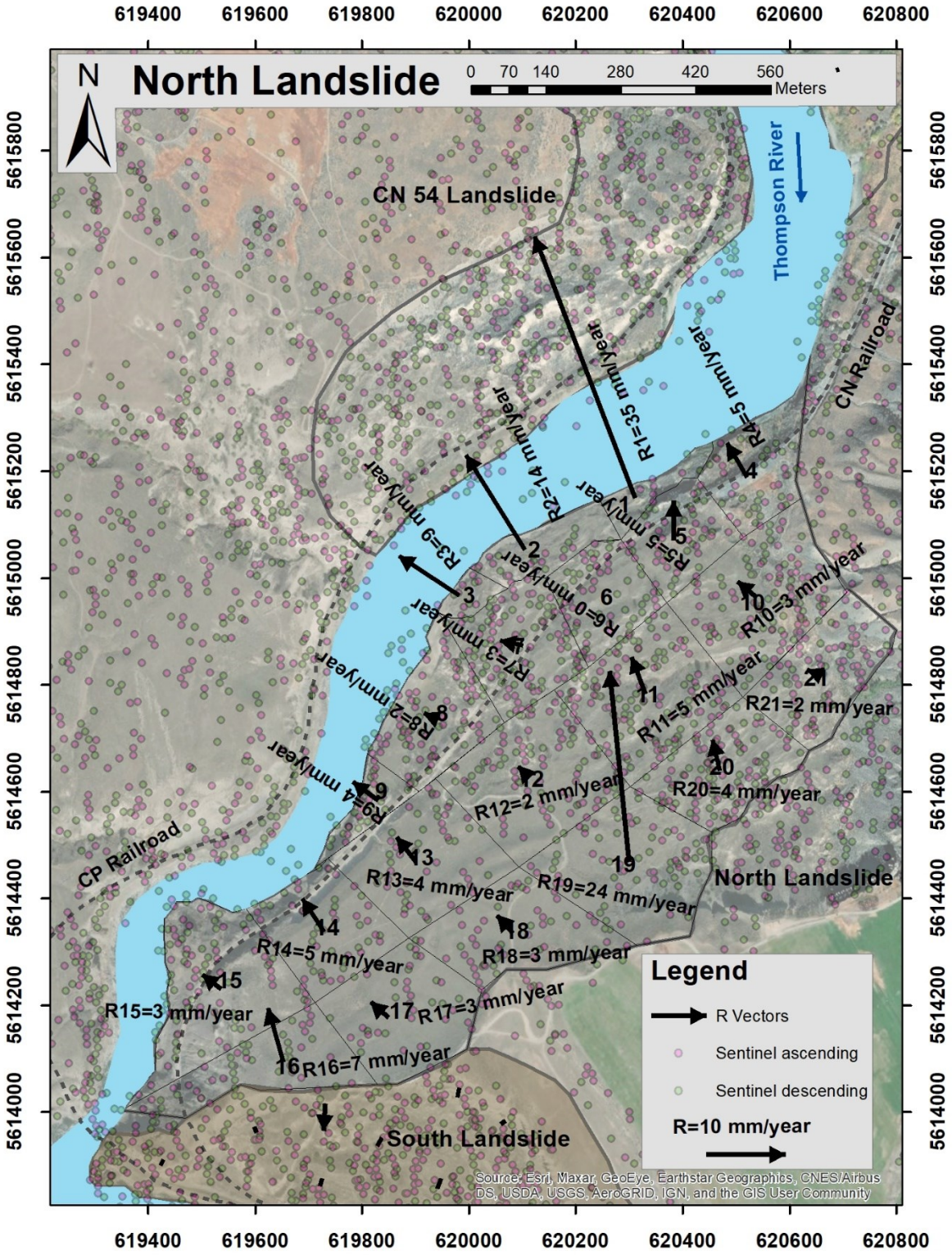

FIGURE 4-10- Calculated horizontal component of **R** for all sectors if the North landslide

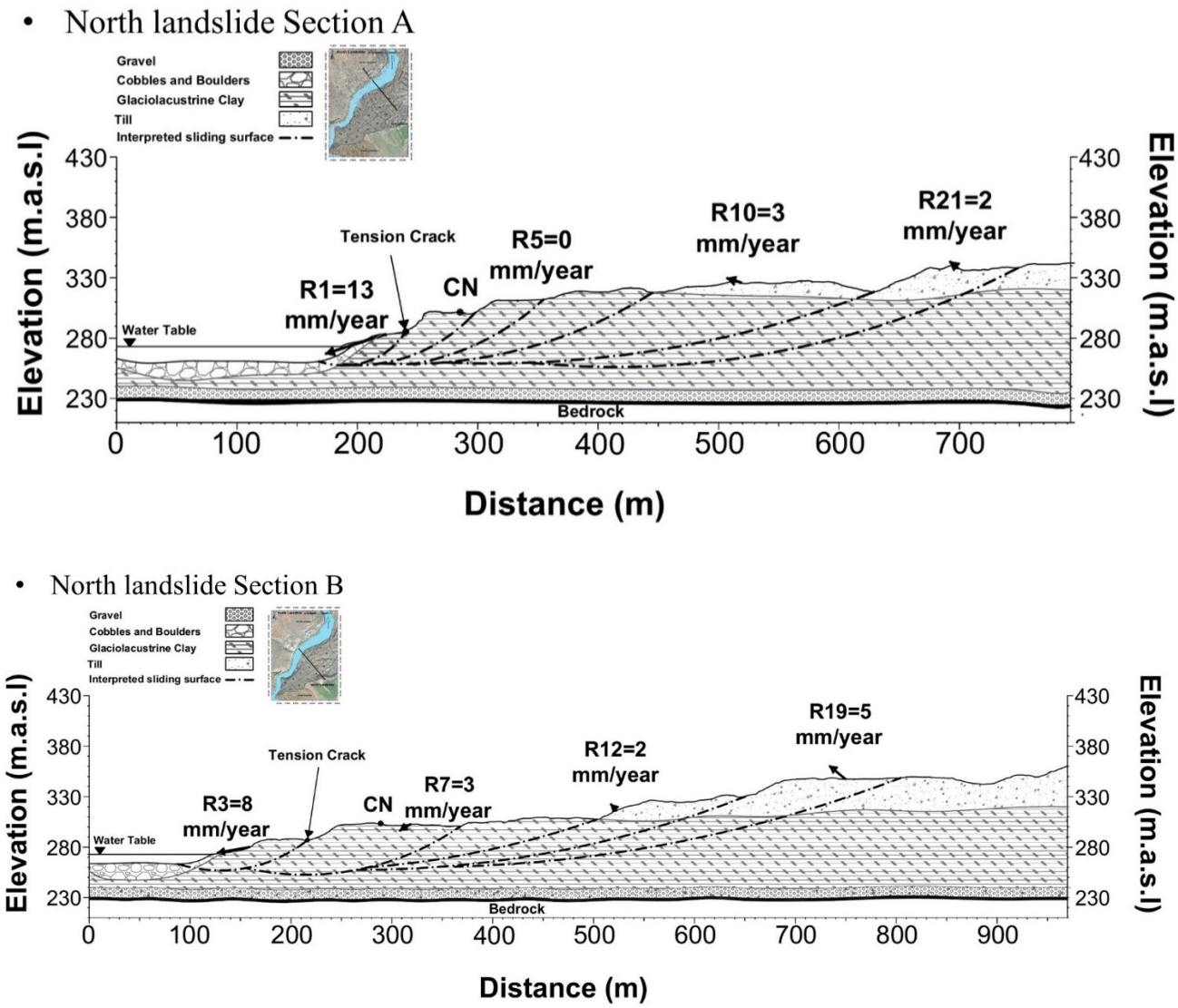

FIGURE 4-11- Figure 7- Calculated Vertical component of **R** for selected sectors of the North landslide

Area	Recorded date	Total Magnitude (mm/year)	Horizontal Magnitude (mm/year)	X direction component (mm/year)	Y direction component (mm/year)	Z direction component (mm/year)	Azimuth Angle (Degree)	Angle with Horizontal plane (Degree)
R1	May 2015 to May 2017	35	35	-12	32	-4	339	7
R2	May 2015 to May 2017	16	14	-8	12	-8	328	28
R3	May 2015 to May 2017	9	9	-8	5	1	303	8
R4	May 2015 to May 2017	5	5	-2	4	0	330	3
R5	May 2015 to May 2017	5	5	0	5	0	0	3
R6	May 2015 to May 2017	0	0	0	0	0	-	-
R7	May 2015 to May 2017	3	3	-3	1	-2	282	30
R8	May 2015 To May 2017	2	2	-2	1	1	295	18
R9	May 2015 to May 2017	4	4	-3	1	-2	282	3
R10	May 2015 to May 2017	4	3	-3	2	0	306	3
R11	May 2015 to May 2017	5	5	-2	4	2	339	18
R12	May 2015 to May 2017	3	2	-1	2	2	318	39
R13	May 2015 to May 2017	4	4	-2	3	0	322	2
R14	May 2015 to May 2017	5	5	-3	5	0	327	1
R15	May 2015 to May 2017	3	3	-2	2	0	307	4
R16	May 2015 to May 2017	7	7	-2	7	0	344	3
R17	May 2015 to May 2017	3	3	-2	2	0	311	4
R18	May 2015 to May 2017	3	3	-2	2	1	318	12
R19	May 2015 to May 2017	24	24	-2	23	4	354	9
R20	May 2015 to May 2017	4	4	-1	3	2	346	29
R21	May 2015 to May 2017	2	2	-2	1	1	292	38

Table 4-4- Summary of calculated **R** magnitude and geometry for the North landslide

4.3.3 South Landslide

The cumulative 2-year LOS displacement is shown in Figure 4-12. The LOS displacements for different sectors are low on this landslide except for sectors 18 to 23, which are located on the landslide's toe and upwards, at the south portion of the landslide. Figure 4-13 shows the cumulative LOS displacements of each sector. The 2-year displacements are in the range of ±10 mm for almost all sectors except for sectors 18 to 23. The maximum displacements are over 40 mm in sector 23 (ascending) and approximately -50 mm on sector 18 (descending). Movements appear to accelerate in late summer and decelerate in spring, corresponding to river fluctuation (acceleration corresponds to river lows and a drawdown effect as identified for the Ripley Landslide in Hendry et al. 2015).

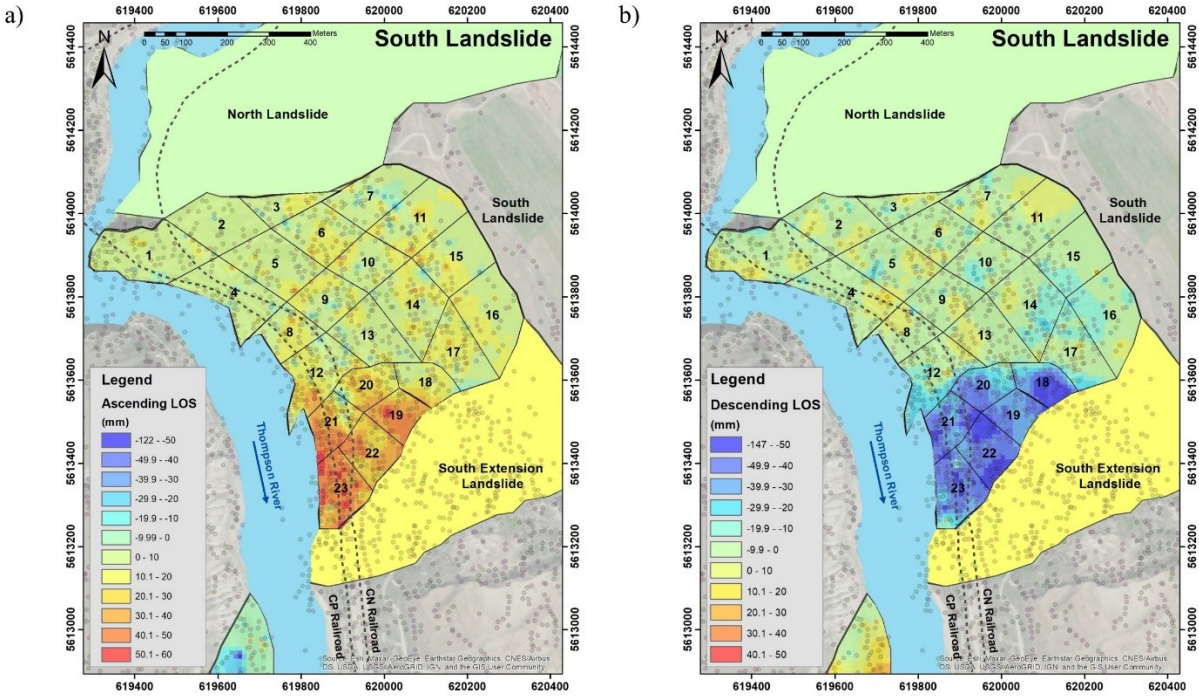

FIGURE 4-12- Cumulative 2-year LOS displacement for the South landslide. a) Sentinel ascending and b) Sentinel descending orbits.

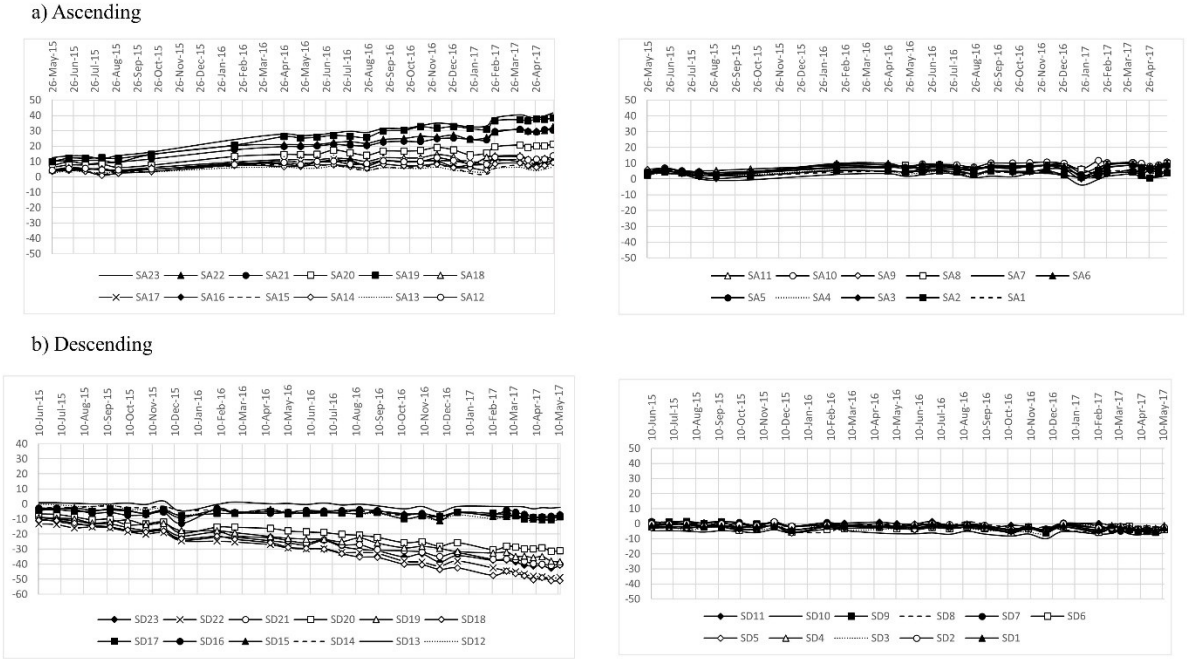

FIGURE 4-13- Cumulative 2-year LOS displacements for the South landslide

Figure 4-14 shows the results of calculated **R**. This figure shows the horizontal component, which varies between 2 and 26 mm/ year for different sectors on the landslide. The landslide appears inactive on all sectors except on the south region. Figure 4-15 shows calculated **R** on selected cross sections. The vertical component of movement is larger in sector 18 further upslope than river elevation in comparison to other sectors at the toe. Table 4-5 shows the different components of **R** and their geometric characteristics.

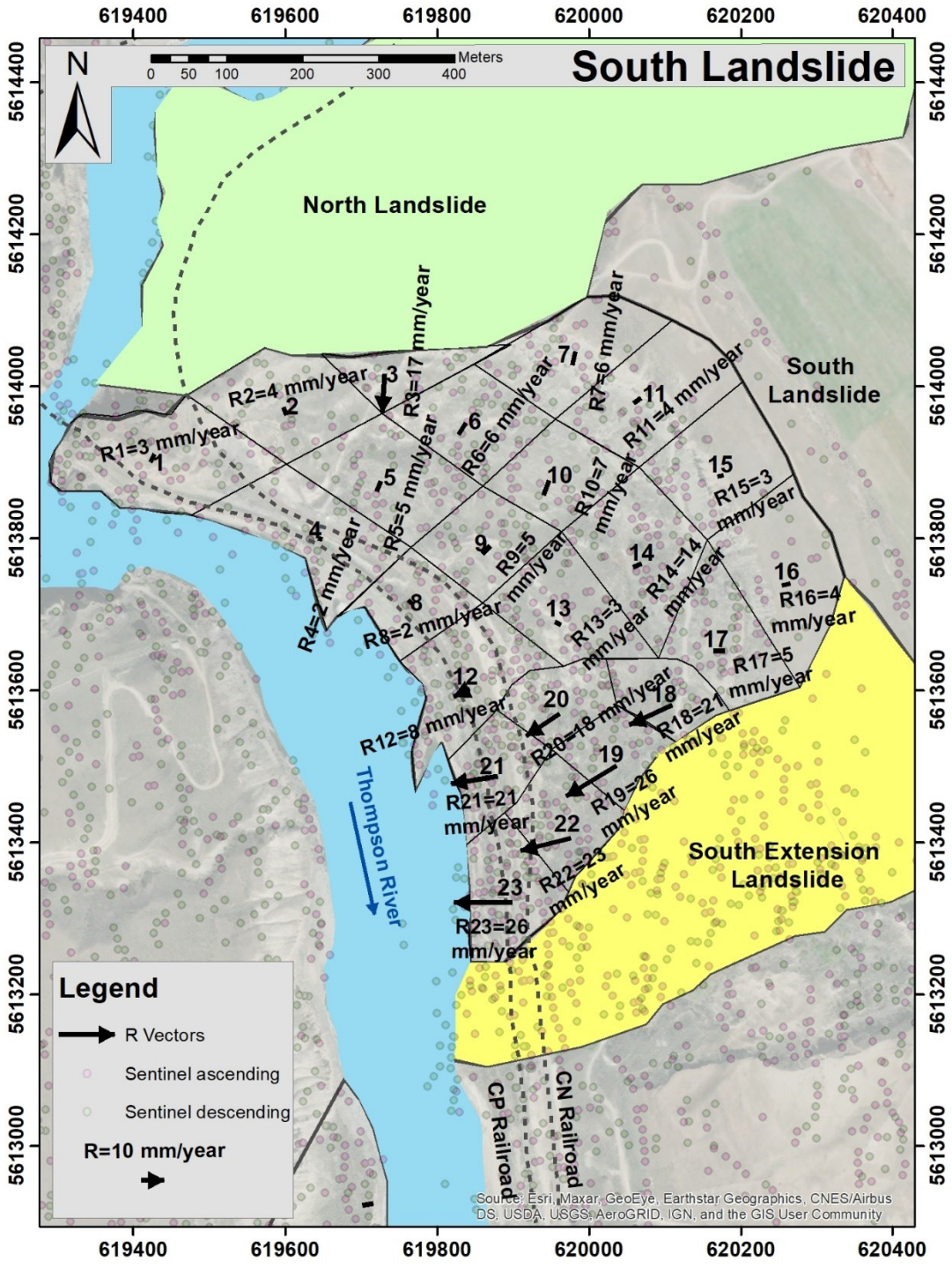

FIGURE 4-14- Calculated horizontal component of **R** vectors for divided parts within the South landslide extent in plan-view

- South landslide Section A

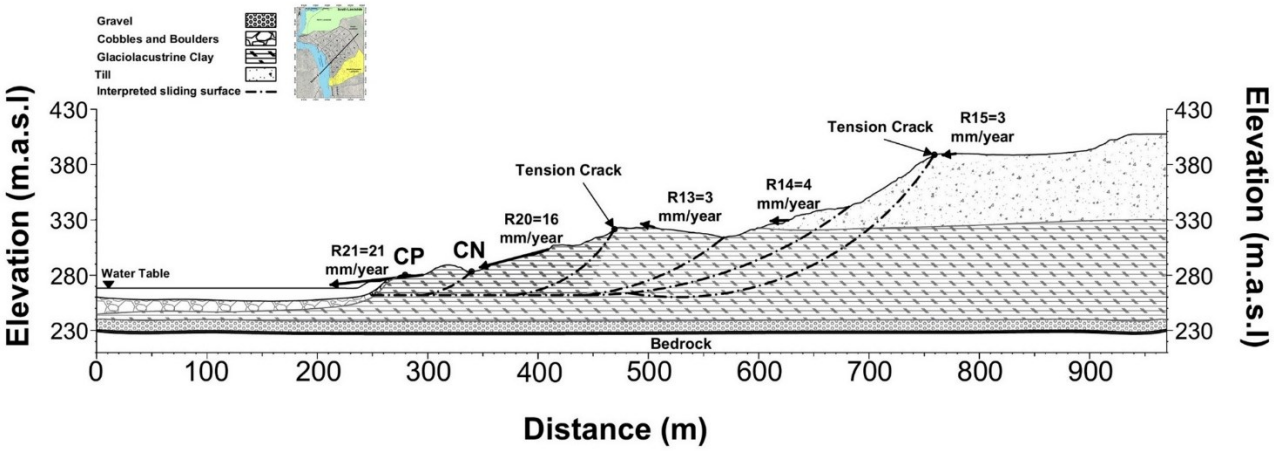

- South landslide Section B

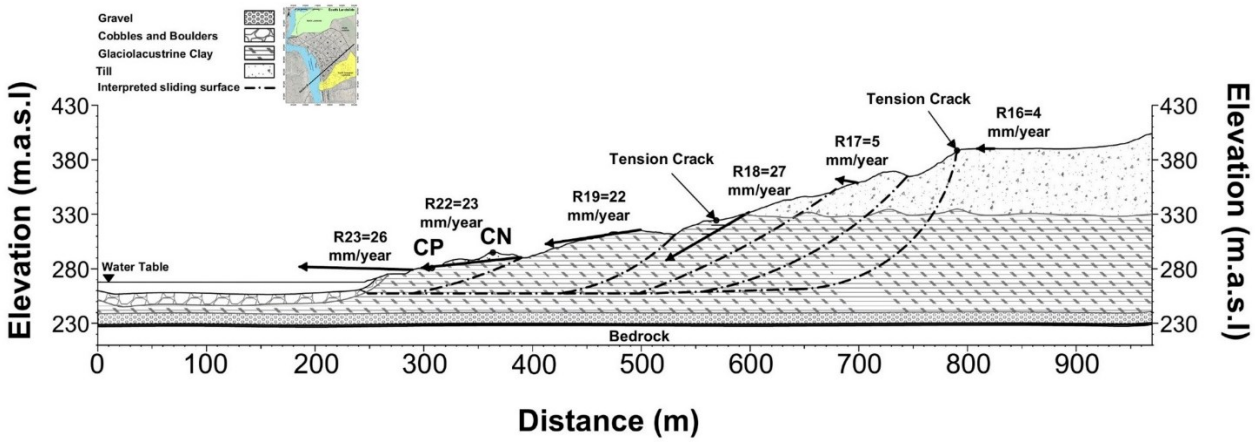

FIGURE 4-15- Calculated Vertical component of **R** for selected sectors on the South landslide

Area	Recorded date	Total Magnitude (mm/year)	Horizontal Magnitude (mm/year)	X direction component (mm/year)	Y direction component (mm/year)	Z direction component (mm/year)	Azimuth Angle (Degree)	Angle with Horizontal plane (Degree)
R1	May 2015 to May 2017	3	3	-1	-3	0	207	1
R2	May 2015 to May 2017	4	4	-2	4	0	157	4
R3	May 2015 to May 2017	17	17	-1	-17	-3	184	10
R4	May 2015 to May 2017	2	2	-1	-2	0	196	6
R5	May 2015 to May 2017	5	5	-2	-5	1	200	7
R6	May 2015 to May 2017	6	6	-3	-5	1	211	8
R7	May 2015 to May 2017	6	6	-1	-6	-3	192	26
R8	May 2015 To May 2017	3	2	-1	-2	3	222	49
R9	May 2015 to May 2017	5	5	-3	-5	-1	210	11
R10	May 2015 to May 2017	7	7	-2	-7	1	199	8
R11	May 2015 to May 2017	4	4	-3	-2	0	232	0
R12	May 2015 to May 2017	8	8	-7	-4	0	243	2
R13	May 2015 to May 2017	3	3	-3	1	1	295	13
R14	May 2015 to May 2017	4	4	-4	-2	0	247	2
R15	May 2015 to May 2017	3	3	-3	-1	0	258	7
R16	May 2015 to May 2017	4	4	-4	-1	1	270	11
R17	May 2015 to May 2017	5	5	-5	0	1	270	11
R18	May 2015 to May 2017	24	21	-19	-9	-11	245	27
R19	May 2015 to May 2017	26	26	-22	-13	-1	239	3
R20	May 2015 to May 2017	19	18	-15	-10	-4	236	12
R21	May 2015 to May 2017	21	21	-21	-3	-2	261	10
R22	May 2015 to May 2017	23	23	-22	-6	-4	256	10
R23	May 2015 to May 2017	26	26	-26	0	1	270	1

Table 4-5- Summary of calculated **R** magnitude and geometry for the South landslide

4.3.4 South Extension Landslide

The cumulative LOS displacement for the South Extension landslide is shown in figure 4-16. The South Extension landslide is located immediately south from the South landslide, and therefore its name. The landslide seems more active on sectors 1 to 8 (at and near the toe) while it seems the other sectors are less active. Figure 4-17 shows the time series of cumulative LOS displacement. It is shown that the cumulative LOS displacement does not exceed 10 mm for sectors 7, 8, 9, 10 and 11 for the ascending orbit and -10 for sectors 1, 9, 8, 10 and 11 for the descending orbit. The maximum cumulative 2-year LOS displacements are over 40 mm (ascending) and -50 mm (descending). There are also some observed periods of acceleration for sectors 2 to 7. Movements appear to accelerate in late summer and decelerate in spring, corresponding to river fluctuation (acceleration corresponds to river lows and a drawdown effect as identified for the Ripley Landslide in Hendry et al. 2015).

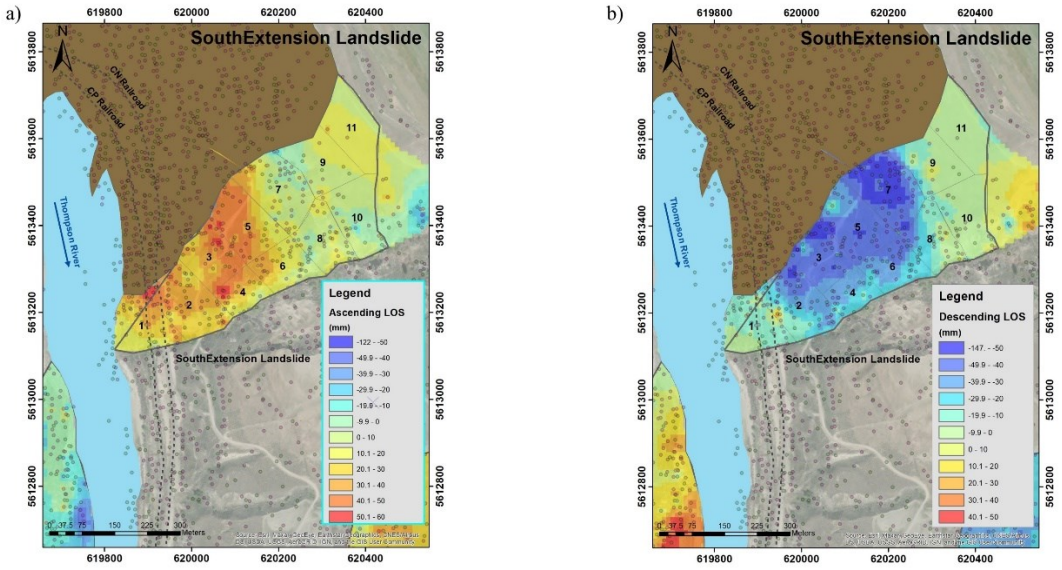

FIGURE 4-16- Cumulative 2-year LOS displacement for the South extension landslide for a) Sentinel ascending and b) Sentinel descending orbits.

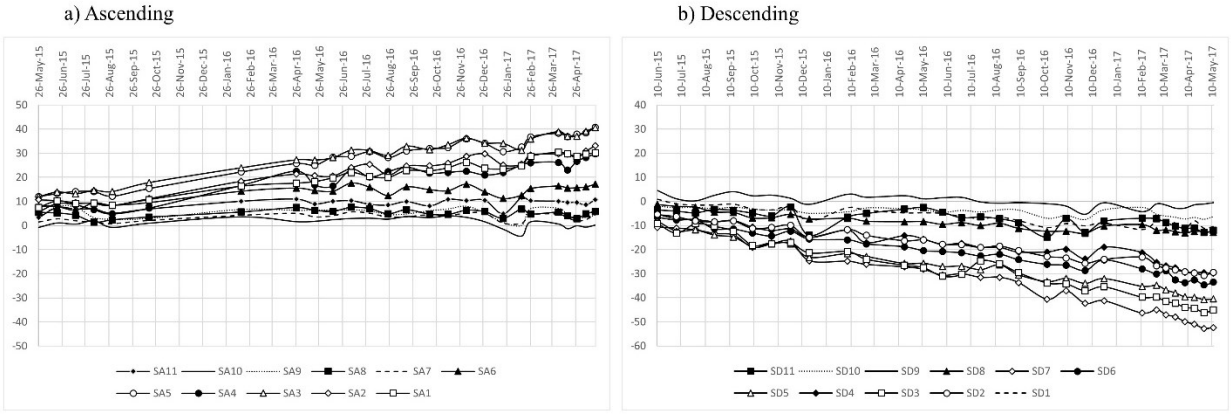

FIGURE 4-17- Cumulative LOS displacement between May 2015 and May 2017 at the South Extension landslide

The horizontal components of calculated **R** for the South Extension landslide are shown in Figure 4-18. The magnitude of the horizontal component of **R** varies between 3 mm/year for sector 9 on the Northeast area of the landslide, and 64 mm/year for sector 4 on the south boundary of the landslide.

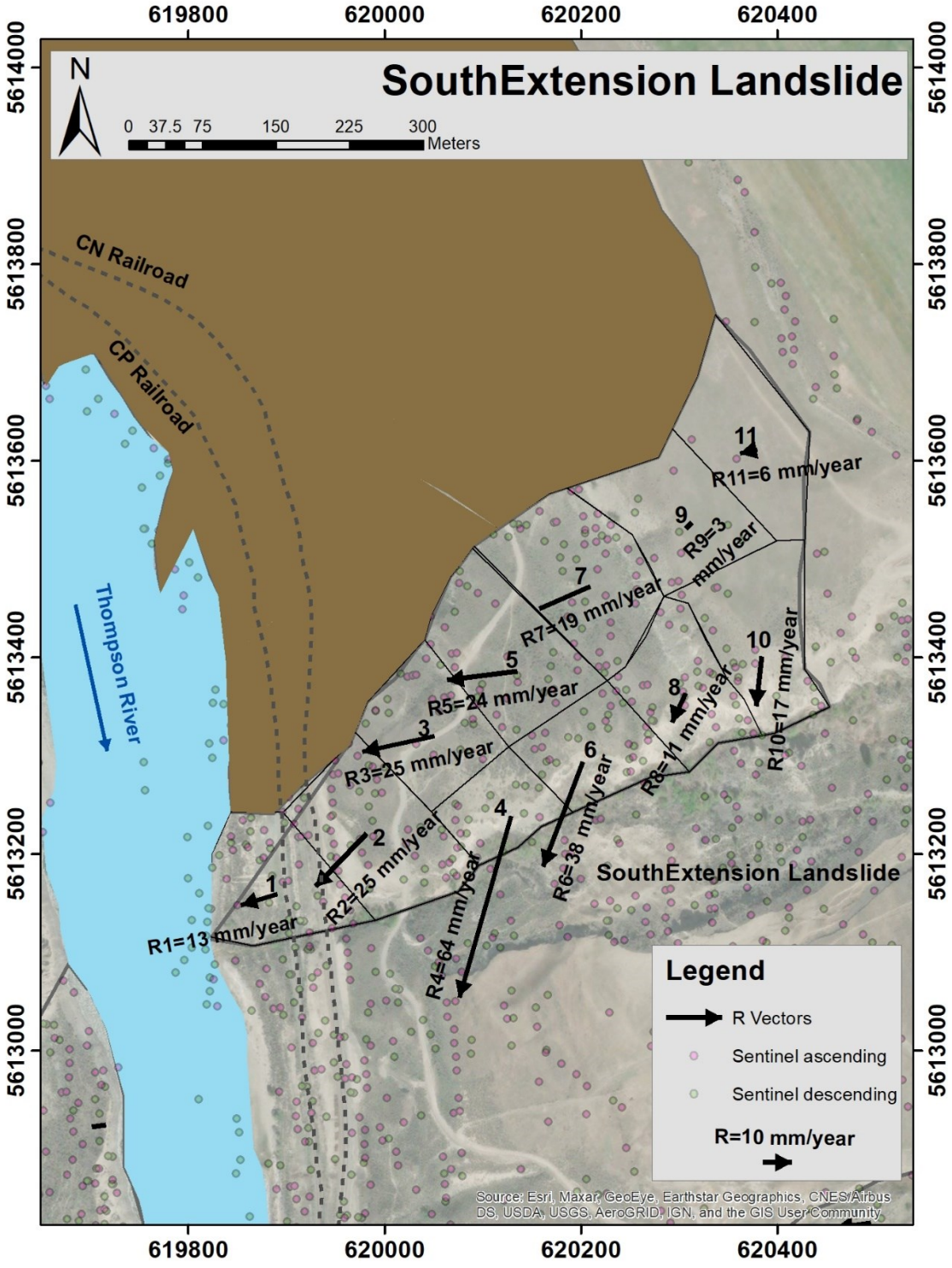

FIGURE 4-18- Calculated horizontal component of **R** within the South Extension landslide

The vertical components of **R** on the South Extension landslide are shown in Figure 4-19 for selected sectors of the landslide and selected cross sections. Movement is predominantly near horizontal near the toe of the landslide and some sectors upslope and near the back scarp show increased vertical component of movement. Movement is negligible behind the back scarp, suggesting no landslide retrogression beyond that elevation.

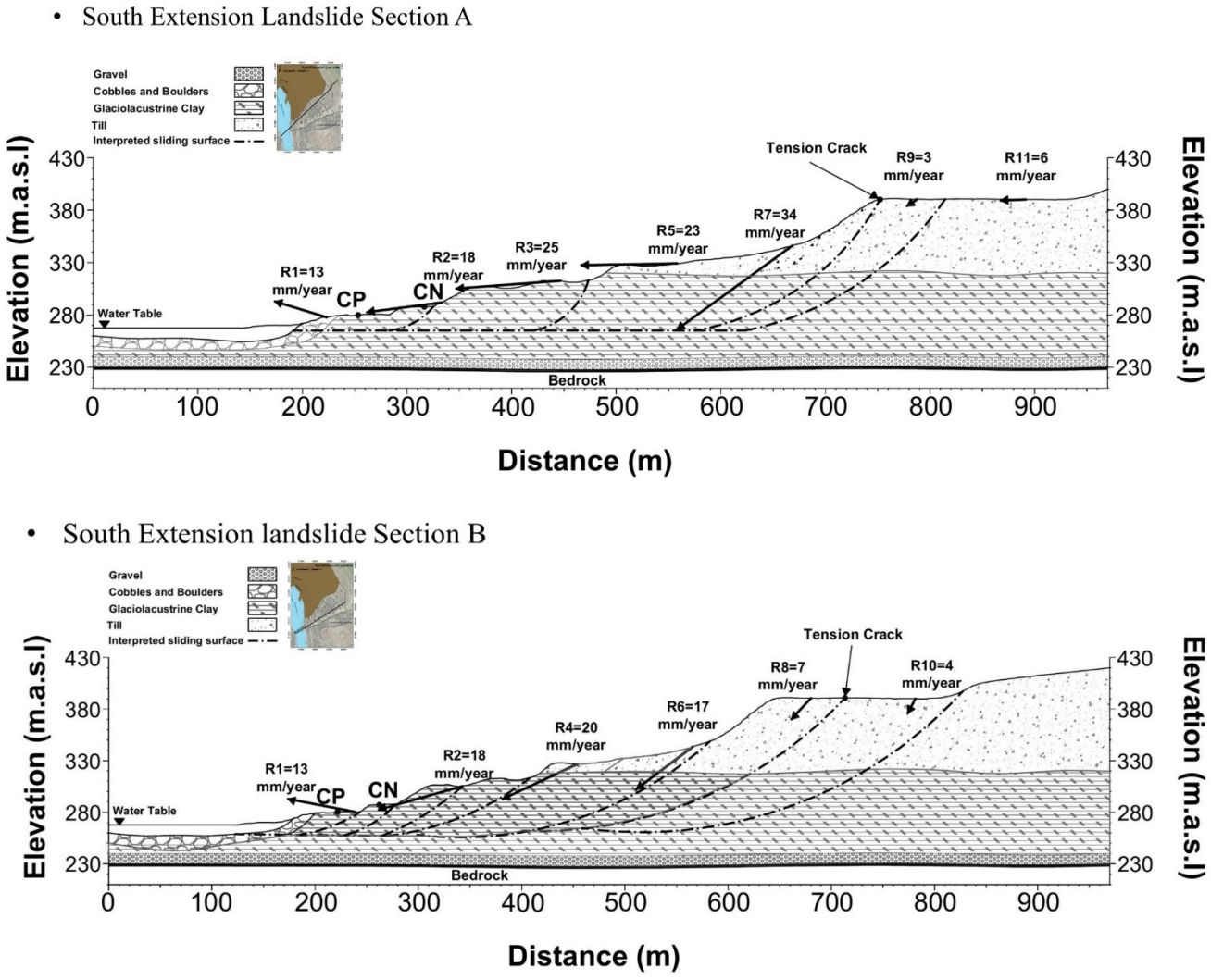

FIGURE 4-19- Calculated vertical component of **R** for selected sectors on the South Extension landslide

Table 4-6 presents the components of the calculated **R** for all sectors of the South Extension landslide, including the component magnitudes and the geometry of **R**.

Area	Recorded date	Total Magnitude (mm/year)	Horizontal Magnitude (mm/year)	X direction component (mm/year)	Y direction component (mm/year)	Z direction component (mm/year)	Azimuth Angle (Degree)	Angle with Horizontal plane (Degree)
R1	May 2015 to May 2017	14	13	-13	-4	4	253	16
R2	May 2015 to May 2017	25	25	-18	-18	-2	224	5
R3	May 2015 to May 2017	25	25	-25	-5	-2	258	4
R4	May 2015 to May 2017	65	64	-18	-62	-8	196	7
R5	May 2015 to May 2017	24	24	-23	-3	0	263	1
R6	May 2015 to May 2017	39	38	-14	-35	-10	201	15
R7	May 2015 to May 2017	23	19	-18	-8	-13	246	34
R8	May 2015 To May 2017	12	11	-5	-10	-5	205	24
R9	May 2015 to May 2017	4	3	-2	-2	-2	225	26
R10	May 2015 to May 2017	18	17	-2	-17	-4	186	12
R11	May 2015 to May 2017	6	6	-6	-1	0	257	2

Table 4-6- Summary of calculated **R** magnitude and geometry for the South Extension landslide

4.3.5 Barnard Landslide

The Barnard landslide cumulative 2-year LOS displacements are shown in Figure 4-20. The magnitudes of LOS displacements are larger at and near the toe of the landslide. The time series of the 2-year cumulative LOS displacements are shown in Figure 4-21 for all sectors of the Barnard landslide. The magnitude of the cumulative LOS displacement in these 2 years ranges between +30 and -30 for both orbits.

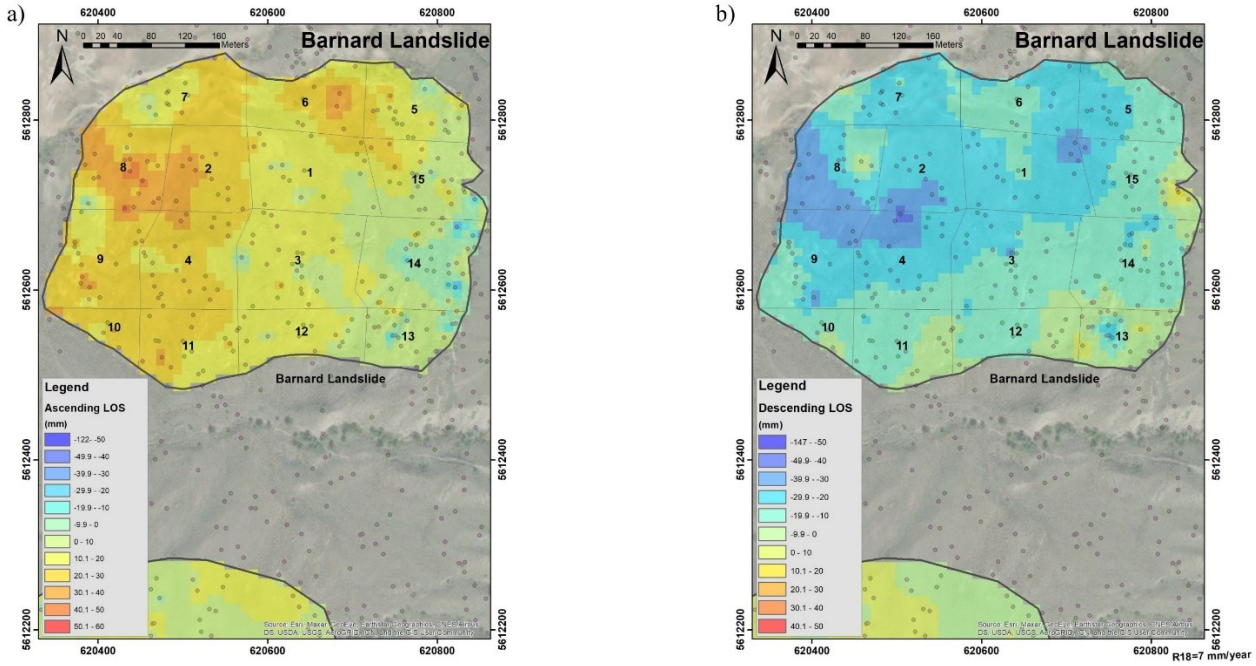

FIGURE 4-20- Cumulative 2-year LOS displacement for the Barnard landslide for a) Sentinel ascending and b) Sentinel descending orbits.

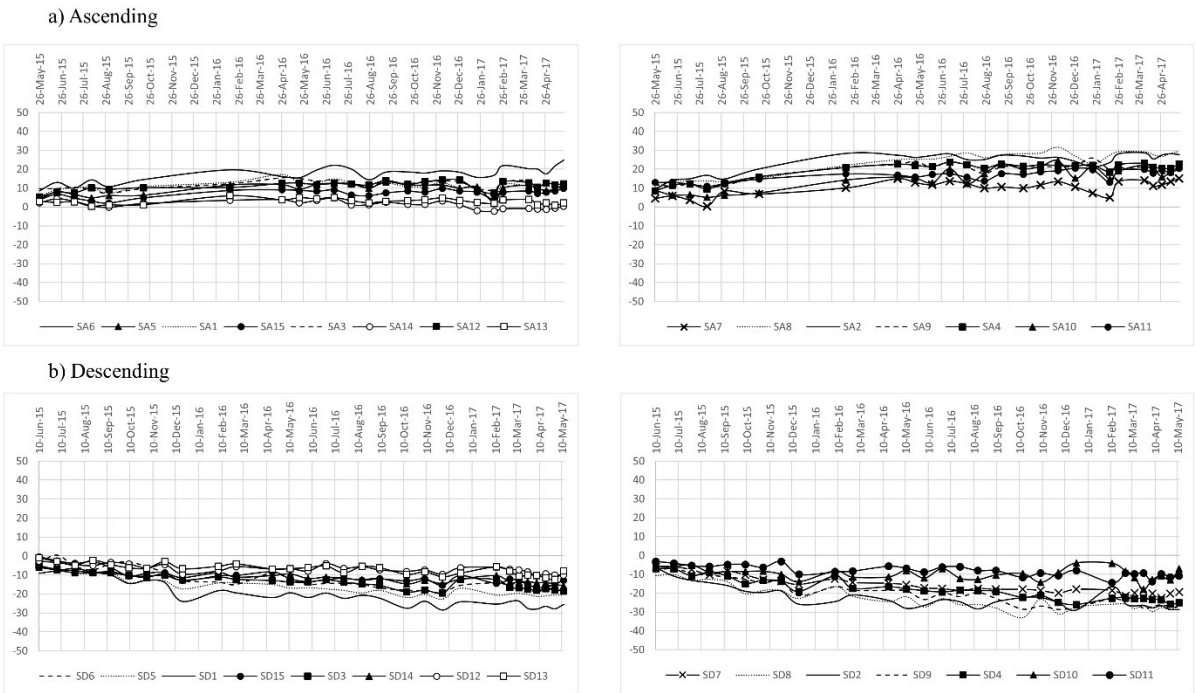

FIGURE 4-21- Cumulative 2-year LOS displacements at the Barnard landslide.

The calculated horizontal components of **R** on the Barnard landslide are shown in Figure 4-22. The magnitude of the horizontal displacements is between 2 and 18 mm/year, with the maximum horizontal displacement at sector 2, on the center of the landslide. The vertical components of **R** are shown in Figure 4-23. Ground displacements are near horizontal at or near the toe of the landslide while the vertical component of ground displacements increase in sectors to the east of the landslide. The higher vertical components of **R** near the crest, transitioning towards near horizontal movement and showing some upward component near the toe, suggests a predominantly circular kinematic of motion.

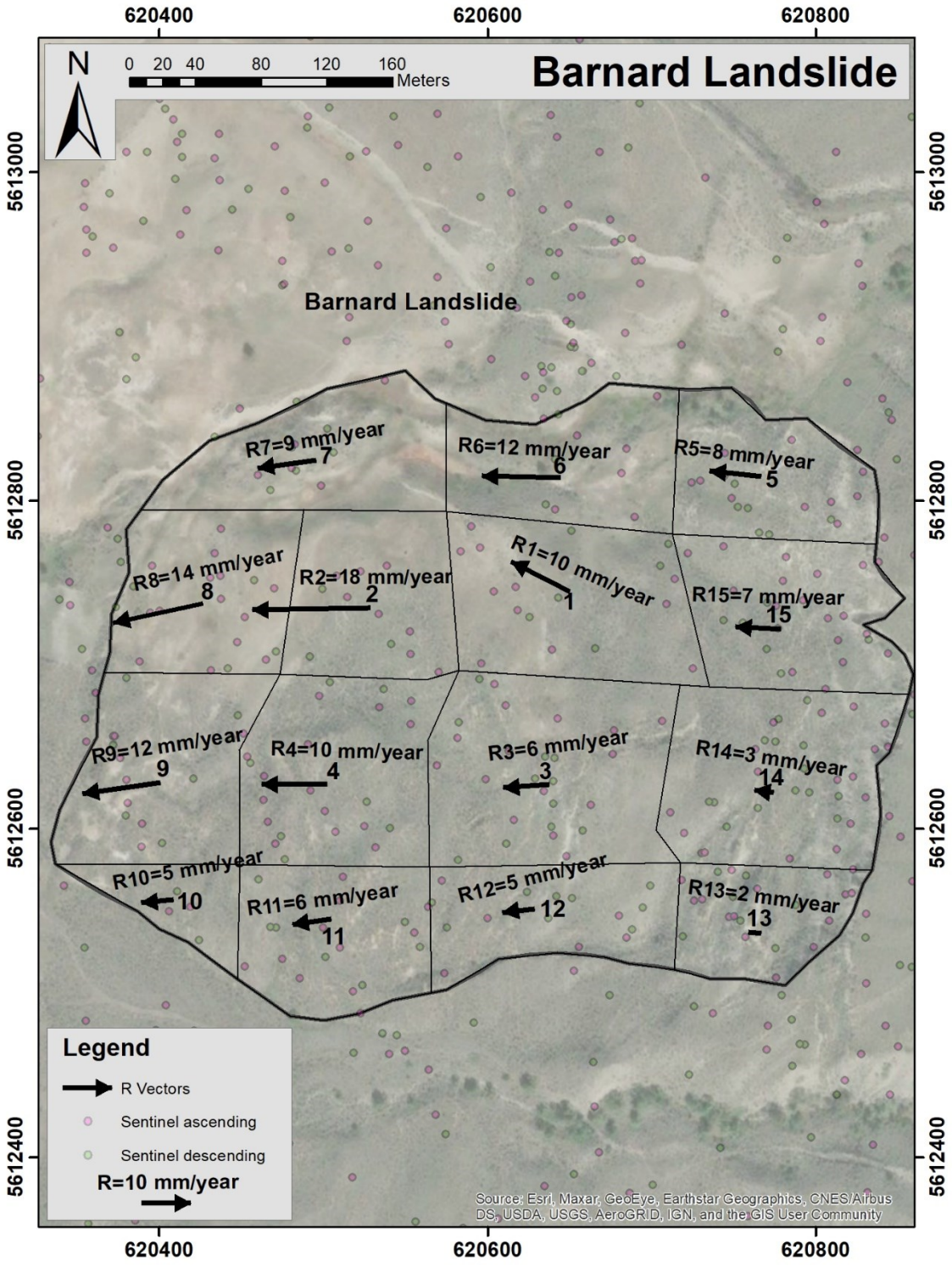

FIGURE 4-22- Calculated horizontal component of **R** within the Barnard landslide.

- Barnard landslide Section A

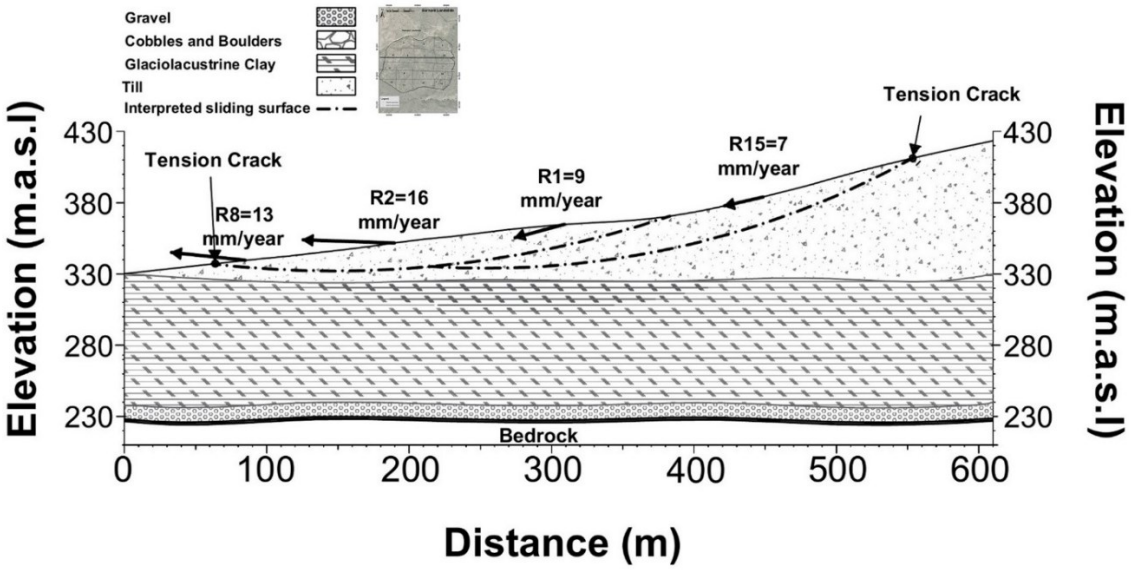

FIGURE 4-23- Calculated vertical component of **R** for selected sectors at the Barnard landslide.

Table 4-7 summarizes the components of calculated **R** and the geometry of these vectors.

Area	Recorded date	Total Magnitude (mm/year)	Horizontal Magnitude (mm/year)	X direction component (mm/year)	Y direction component (mm/year)	Z direction component (mm/year)	Azimuth Angle (Degree)	Angle with Horizontal plane (Degree)
R1	May 2015 to May 2017	10	10	-9	4	-3	297	15
R2	May 2015 to May 2017	18	18	-16	8	1	297	2
R3	May 2015 to May 2017	7	6	-6	0	-3	266	29
R4	May 2015 to May 2017	10	10	-10	0	-1	270	3
R5	May 2015 to May 2017	8	8	-8	1	-2	276	10
R6	May 2015 to May 2017	12	12	-12	0	1	271	6
R7	May 2015 to May 2017	9	9	-9	-1	-1	262	4
R8	May 2015 To May 2017	14	14	-13	-3	1	258	6
R9	May 2015 to May 2017	12	12	-12	-2	-3	262	14
R10	May 2015 to May 2017	7	5	-5	-1	4	264	37
R11	May 2015 to May 2017	6	6	-6	-1	0	262	1
R12	May 2015 to May 2017	5	5	-5	-1	0	263	0
R13	May 2015 to May 2017	3	2	-2	0	-2	275	44
R14	May 2015 to May 2017	5	3	-3	0	-4	278	48
R15	May 2015 to May 2017	7	7	-7	0	-2	273	13

Table 4-7- Summary of calculated **R** components magnitude and vector geometry at the Barnard landslide.

4.3.6 Redhill Landslide

The cumulative 2-year LOS displacements at the Redhill landslide are shown in Figure 4-24. The toe of the Redhill landslide appears to be the most active area of the landslide. The 2-year time series of cumulative LOS displacements are shown in Figure 4-25. The toe of this landslide is the

most active of all landslides in this paper. The cumulative LOS displacements exceed -100 mm (ascending) and 60 mm (descending). Sectors at the backscarp (11-20) have cumulative LOS displacements between -30 mm and +20 mm (considering both orbits).

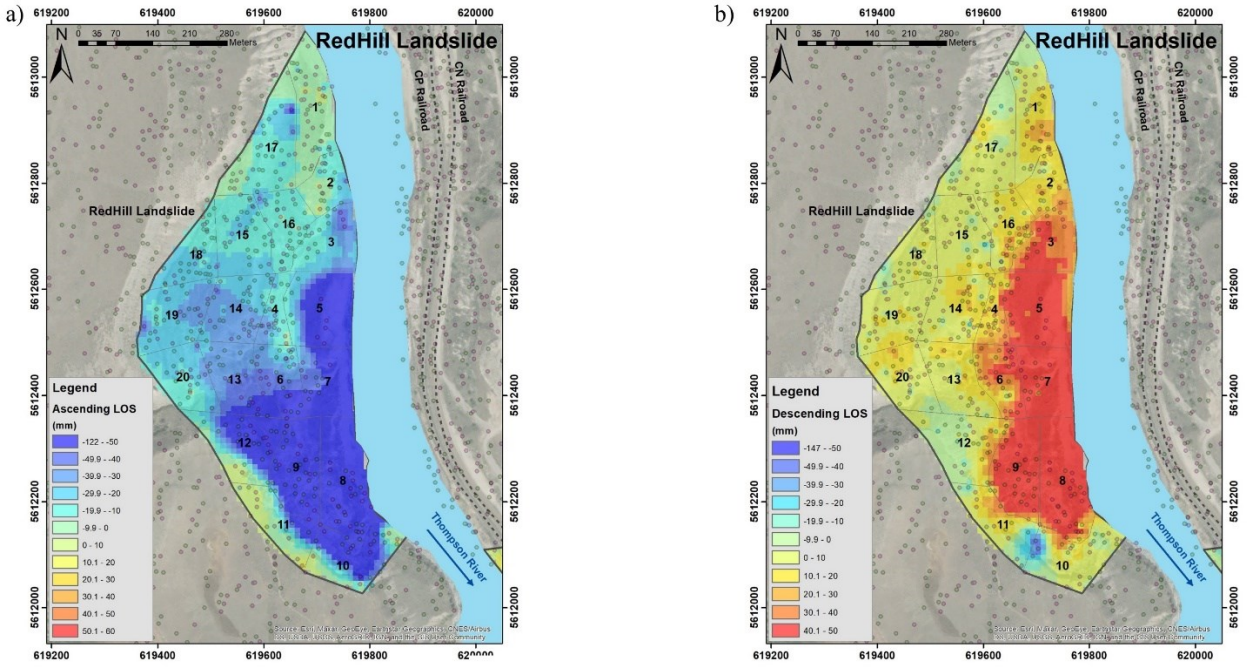

FIGURE 4-24- Cumulative 2-year LOS displacements at the Redhill landslide for a) Sentinel ascending and b) Sentinel descending orbits.

Figure 4-26 shows the horizontal component of calculated **R** for the Redhill landslide. Sectors 8 and 9 shows the most activity, with displacements of up to 52 mm/year. The magnitude of the horizontal component for other sectors of the landslide varies between 5 and 46 mm/year.

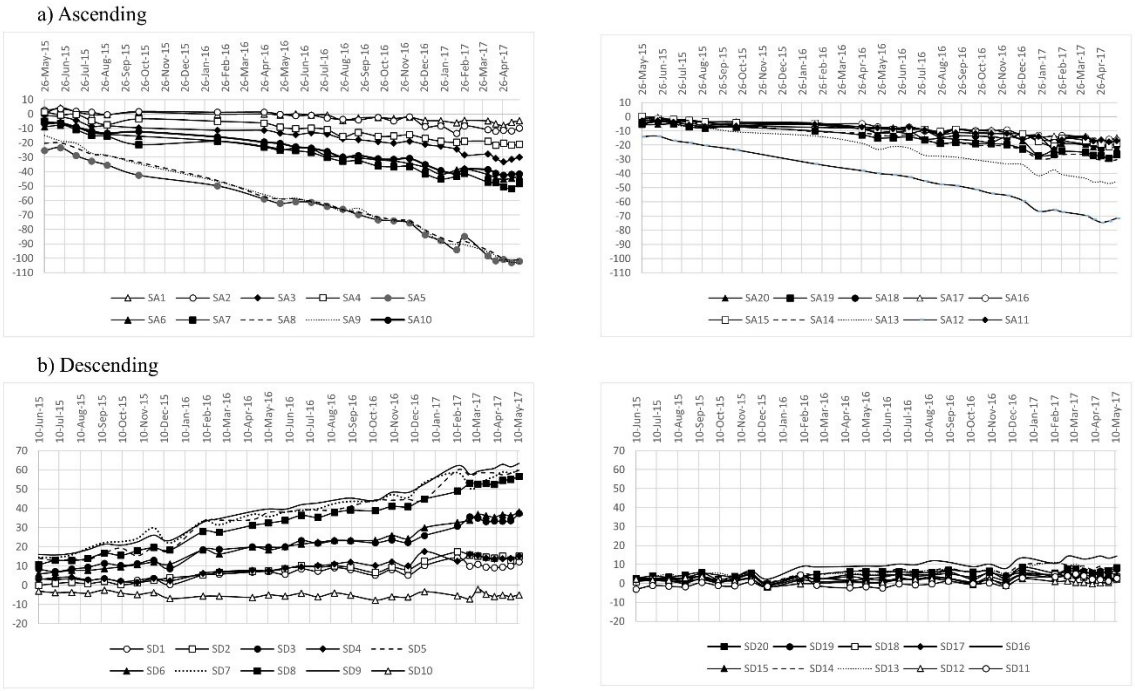

FIGURE 4-25- Cumulative 2-year LOS displacements at the Redhill landslide.

The vertical components of **R** for selected sectors of the landslide are shown in Figure 4-27. This figure show that ground displacements have a significant vertical component regardless of the distance from the toe or the back scarp, transitioning towards less vertical component near the toe. This would indicate that the toe of the landslide is likely well into the river bed that could not be captured by the Satellite InSAR data available. Table 4-8 summarizes the components and geometry of calculated **R**. The total magnitude of **R** is between 6 mm and 54 mm.

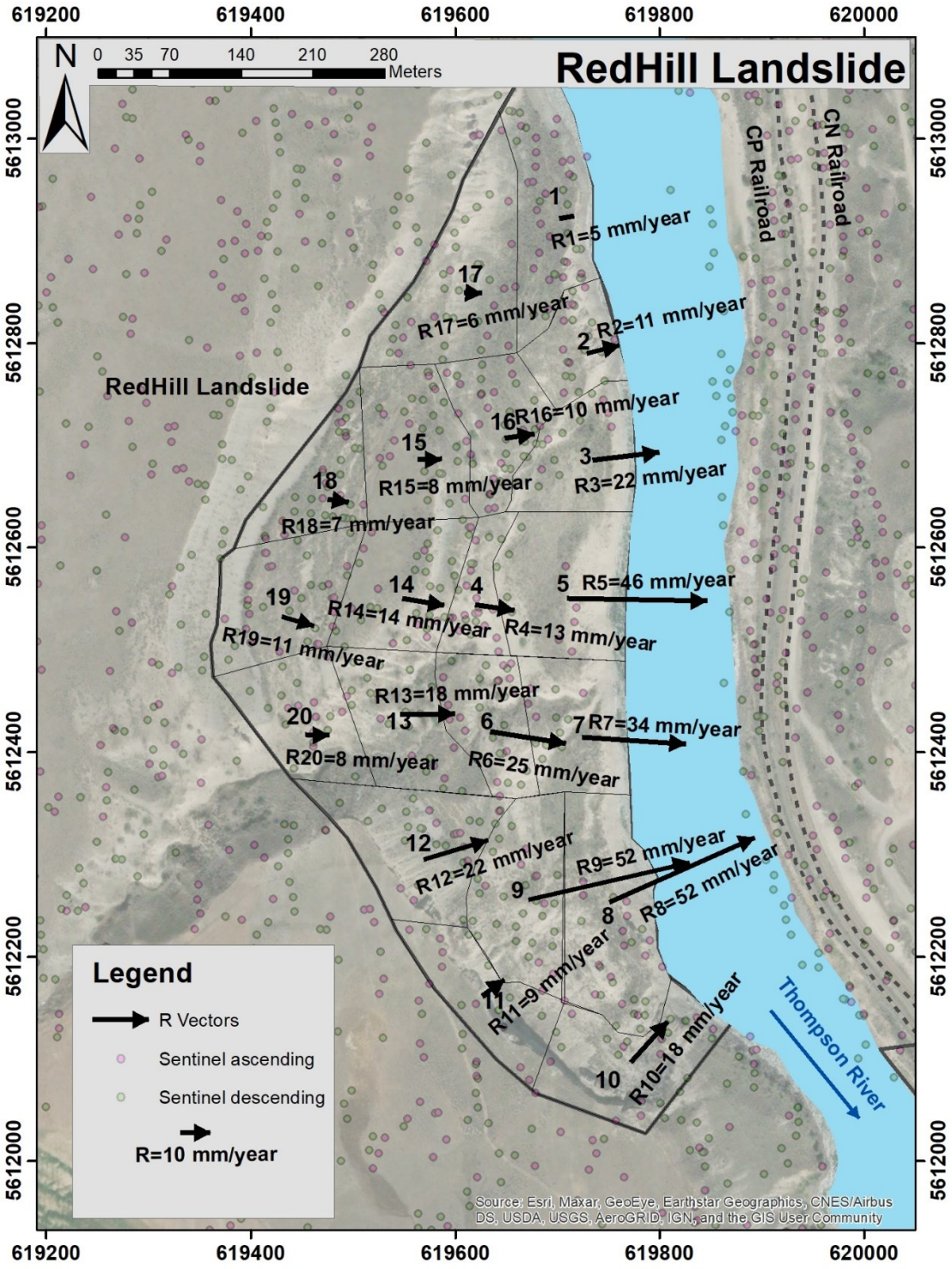

FIGURE 4-26- Calculated horizontal component of **R** on the Redhill landslide.

- Redhill landslide Section A

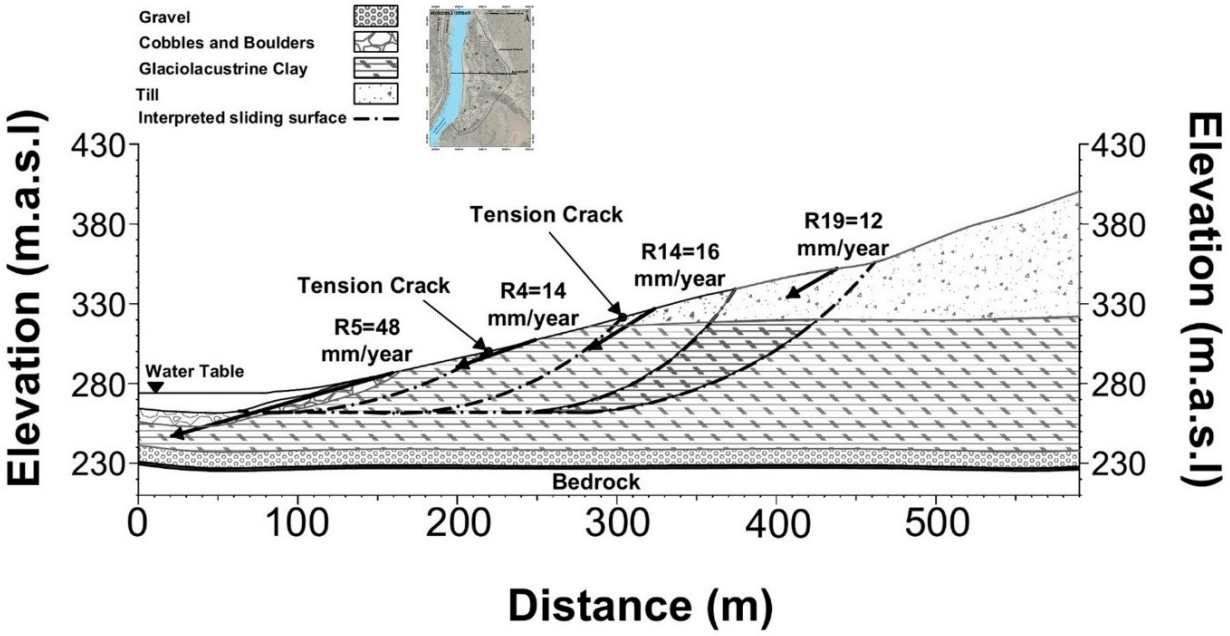

- Redhill landslide Section B

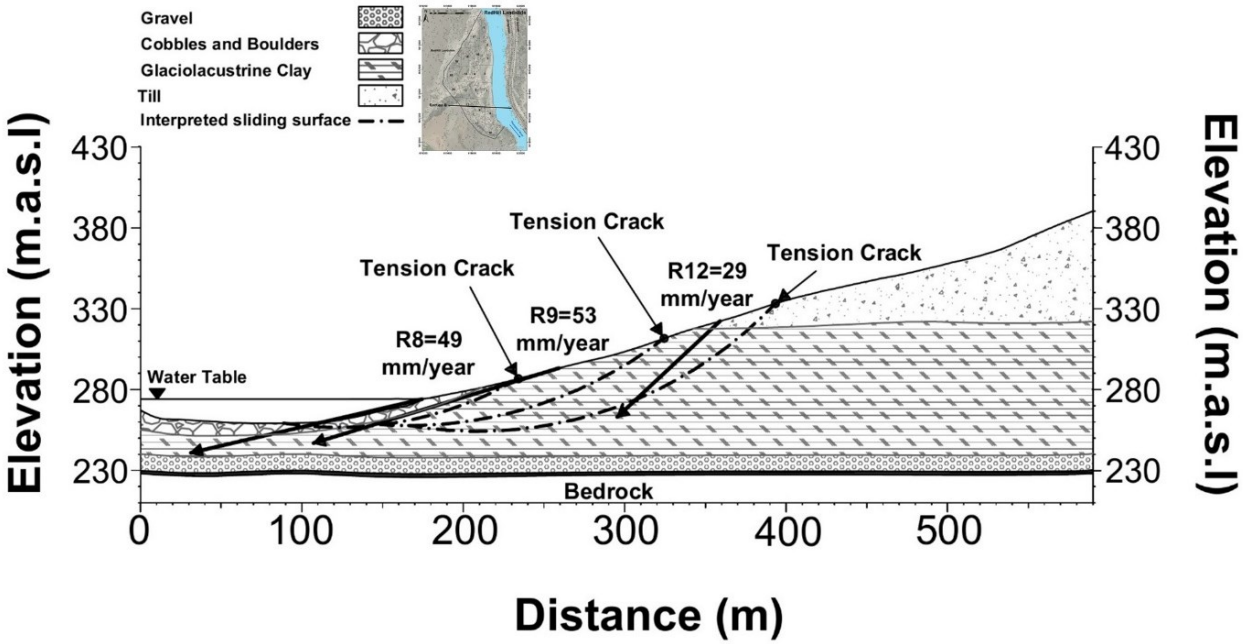

FIGURE 4-27- Calculated vertical component of **R** for selected sectors on the Redhill landslide.

Area	Recorded date	Total Magnitude (mm/year)	Horizontal Magnitude (mm/year)	X direction component (mm/year)	Y direction component (mm/year)	Z direction component (mm/year)	Azimuth Angle (Degree)	Angle with Horizontal plane (Degree)
R1	May 2015 to May 2017	6	5	5	1	1	81	11
R2	May 2015 to May 2017	11	11	10	3	1	75	4
R3	May 2015 to May 2017	22	22	22	3	-1	83	2
R4	May 2015 to May 2017	14	13	13	-2	-4	98	18
R5	May 2015 to May 2017	48	46	46	-1	-13	91	16
R6	May 2015 to May 2017	25	25	25	0	-2	89	4
R7	May 2015 to May 2017	34	34	34	-2	-1	94	2
R8	May 2015 To May 2017	53	52	48	21	-11	66	12
R9	May 2015 to May 2017	54	52	51	12	-15	77	16
R10	May 2015 to May 2017	21	18	12	13	-11	42	32
R11	May 2015 to May 2017	9	9	7	5	-2	54	14
R12	May 2015 to May 2017	29	22	21	6	-19	73	41
R13	May 2015 to May 2017	23	18	18	0	-14	89	37
R14	May 2015 to May 2017	16	14	13	-2	-8	99	31
R15	May 2015 to May 2017	10	8	8	0	-6	89	37
R16	May 2015 to May 2017	11	10	10	1	-2	82	9
R17	May 2015 to May 2017	8	6	6	0	-5	93	40
R18	May 2015 to May 2017	8	7	7	-1	-5	99	36
R19	May 2015 to May 2017	13	11	11	-3	-6	106	29
R20	May 2015 to May 2017	9	8	8	0	-4	91	64

Table 4-8 Summary of calculated **R** magnitude, components and geometry on the Redhill landslide.

4.4 Summary and Discussion

Although the density of gathered data are different for each landslide in the research area, Figure 4-3 shows the data density guided selection of landslide sectors to balance information adequacy and availability for kinematic analysis. Density was enough for all defined sectors of each landslide to calculate the **R** vectors except for sector 2 of the Goddard landslide with lack of descending orbit data.

Figures 4-4 and 8 show low activity recorded by Sentinel 1 (LOS) for most parts of Goddard and North landslides, with increased activity on sectors 1, 2 and 3 on the toe of the North landslide. Figure 4-12 shows low activity for South landslide, except for sectors 18 to 23. The South extension landslide is more active according to Figure 4-16 on those sectors that have a common boundary with South landslide, suggesting the south extension is likely a lateral retrogression of the South Landslide. Figure 4-20 illustrates two different trends of the activity measured on the west and east sectors of the Barnard landslide. However, this landslide shows low activity generally on all its sectors and trends are likely masked by the limits of detection of the technology and assumptions in this work, combined. The activity of the Redhill landslide is relatively high specially at its toe near to the Thompson River in sectors 3 to 12 from both satellite orientations as it is shown in Figure 4-24.

Despite the absence of a clear seasonal displacement trend in most landslide displacement data, this was likely due to the low cumulative LOS and measurement precision of the data (Figures 4-5, 4-9, 4-13, 4-17, 4-21 and 4-25), precluding definitive interpretation of seasonal trends; movements appear to accelerate in late summer and decelerate in spring, corresponding to river fluctuation (acceleration corresponds to river lows and a drawdown effect as identified for the Ripley Landslide in Hendry et al. (2015) and Huntley (2021).

The horizontal component of **R** vectors for all sectors of the research area do not exceed 64 mm/year which means all landslides in this area are classified as very slow-moving landslides based on velocity classification by Curden and Vernes (1996) (Hungr et al., 2014). The horizontal component of calculated ground movement for the Goddard landslide is between 2 and 29 mm/year (Figure 4-6) with the maximum movement calculated for sector 7. Figure 10 shows the magnitude of horizontal movement between 2 and 35 mm/year in the research timeline for the North landslide with the maximum movement in sector 1 on the landslide's toe. This is consistent with previous findings (Huntley et al., 2021). Figure 4-14 and Figure 4-18 show the horizontal component of **R** vectors vary between 2 to 26 mm/year for South landslide and 3 to 64 mm/year for the South extension landslide as well. The more active parts of the South landslide are located near the boundary with the South Extension landslide, suggesting this extension is likely a lateral retrogression of the South landslide. The maximum displacement is observed for sector 4 of the South extension landslide and the direction of **R** vectors in horizontal plane are different in north and south parts of this landslide due to their different aspects. Air imagery inspection suggests that this change in displacement attitude is likely due to the presence of a gully at the south boundary of the South Extension landslide, allowing for the kinematics of the landslide to develop a southward trend of motion, however this aspect is matter of further investigation as the assumptions of the horizontal direction of movement directly define this directionality solely on a topographic basis. The reported magnitudes for these areas are consistent with previous findings (D. Huntley, 2021).

Figure 4-22 show the horizontal movements of the Barnard landslide between 2 and 18 mm/year with the more active areas concentrated on the central sectors of the landslide and extending to the west, closer to the River. Figure 4-26 shows the horizontal movement at the Red Hill

landslide between 5 and 52 mm/year, with highest activity in sectors 8 and 9 at the toe of the landslide. The magnitude and activity is also consistent with previous studies (D. Huntley, 2021).

Generally, the vertical component of the terrain movement changes based on both distance from the river and the magnitude of movements for each specific sector of each landslide. It is observed in Figure 4-7 that the Goddard landslide is moving more vertically on the toe of the landslide on sectors 1, 3 and the back scarp for sectors 10 and 11 despite their lower movement. The movement is more horizontal on other sectors (15, 16 and 17). Figure 4-11 shows horizontal movement on the North landslide for almost all sectors except those ones at the toe which are moving with larger vertical components. Vertical components of **R** vectors on the South landslide in Figure 4-15 also show small horizontal movement at the back scarp with more pronounced vertical components when compared to the toe of the landslide. Figure 4-19 also shows that for the South Extension landslide, the vertical components are relatively negligible for sectors at the toe in comparison to sectors closer to the back scarp. These results are consistent with compound kinematics of landslides, commonly defined by the presence of a sub horizontal weak layers that act as base sliding surfaces. Previous research had identified the presence of silt and clay layers with sub-horizontal bedding which would be responsible for the landslide activity in this valley (Clague and Evans 2003; Eshraghian et al. 2007; Journault 2018), and the kinematics observed through the results of this study support the hypothesis of compound mechanisms. This landslide mechanism based on the recent results show this compound kinematic with soil masses moving on sub-horizontal basal sliding surfaces and being pushed by upslope driving wedges on near-planar to semi-circular sliding surfaces (e.g. the South landslide and the toe of the South Extension landslide).

Figure 4-26 illustrates almost horizontal movement for sectors of Barnard landslide which are closer to the river on the west part of this landslide while the vertical components are more notable for sectors on the east side of the Barnard landslide. The shear interpreted surfaces using the reported **R** vectors in this figure suggest a rotational retrogressive landslide in this area with lower depth than other landslides in the research area due to the direction of movements of each sector and the locations of tension cracks observed in ground features.

The vertical component of **R** is consistent for most sectors within the Redhill in sections of the figure 4-27. The vertical and horizontal components of **R** in the section views suggest a retrogressive, rotational movement for the Redhill landslide which is consistent with previous research. (D. Huntley, 2021).

4.5 Conclusions

Six landslides with most significant impacts on the CNR and CPR railways are investigated in this research. These landslides are Goddard, North, South, South extension, Barnard and Redhill which are located from the north of the Thompson River valley to South respectively. This valley is one of the most important transportation corridors in Canada which experienced several landslides in its history. This paper presents a new understanding of landslides' displacement and kinematic in this area using InSAR monitoring data gathered by Sentinel 1 satellite from May 2015 to May 2017 from both ascending and descending orbits. To obtain more detailed displacements of each landslide, they are divided to different sectors to better understand their kinematics. A method is proposed where the horizontal component of movement is considered parallel to the slope azimuth in order to calculate an approximation of the three-dimensional ground displacement vector (R) using InSAR data from two orientations. The method was

validated for a landslide in the study area against recorded GPS results on the Ripley landslide (Soltanieh and Macciotta, in press).

All landslides in this research are classified as very slow landslides according to velocity classification by Curden and Vernes (1996) (Hungr et al., 2014). The total magnitude of movement in this area is reported between 2 and 64 mm/year for all landslides in this research. Table 4-9 shows a summary of movements for each landslide studied. The maximum movement occurred in the South Extension landslide with a velocity of 64 mm/year while the Barnard is the slowest with a maximum velocity of 18 mm/year. The Redhill landslide also is one of the most active landslides in this research with maximum velocity of 52 mm/year.

Landslide	Monitoring Timeline	Maximum Velocity (mm/year)	Minimum Velocity (mm/year)	Velocity Classification	Type of Landslide's kinematic
Goddard	May2015 to May 2017	2	29	Very Slow	Retrogressive rotational
North	May2015 to May 2017	2	35	Very Slow	Rotational on the toe
South	May2015 to May 2017	2	26	Very Slow	transitional
South Extension	May2015 to May 2017	3	64	Very Slow	Transitional on the toe + Retrogressive rotational
Barnard	May2015 to May 2017	2	18	Very Slow	Rotational retrogressive
Redhill	May2015 to May 2017	8	56	Very Slow	Retrogressive rotational

Table 4-9- Summary of all monitored landslides along the Thompson River valley

Ground displacements measured outside the known-active landslide areas were very low, suggesting minimum to no retrogression activity (except for the interpretation discussed for the South Extension landslide).

The approach presented for landslide investigation based on combining Satellite InSAR orientations, assumptions of landslide horizontal displacement direction based on topographic

characteristics, and averaging for space and time inconsistencies between different LOS orientation acquisition; provides valuable additional insight to common interpretation of East-West and vertical components. The work in this paper illustrates how the added benefits of the approach include enhanced characterization of landslide kinematics and state of activity. It is important to note that the assumption of landslide directionality needs to be evaluated on a case-by-case, as surface topographic characteristics could mislead the horizontal orientation of movement for complex mechanisms.

Acknowledgments

The authors would like to acknowledge Canadian Pacific Railway (CP) and TRE Altamira for providing the InSAR monitoring results used in this study. This research was performed within the umbrella of the Railway Ground Hazards Research Program (RGHRP), which is funded by the Natural Sciences and Engineering Research Council of Canada (NSERC), Canadian Pacific Railway, Canadian National Railway, and Transport Canada; and is a collaboration that incudes Queen's University, the Canadian Geological Survey and the University of Alberta.

5. Summary, General Conclusion and recommendation

5.1. Summary

7 landslides along 10 kilometers of the Thompson River Valley, south of town of Ashcroft, British Columbia, which can impact the Canadian National Railways (CNR) and Canadian Pacific Railways (CPR), have been investigated in this research. Landslides in this corridor always threaten the transportation infrastructures of these two lines which play significant role for Canada's economy due to their importance for the transportation system of Canada. CNR and CPR continuously invest in landslide investigations along this valley as a basis to understand and mitigate the risk of possible landslide acceleration events.

Remote sensing technology was employed in this thesis to enhance the interpretation of landslides kinematics within the area of research. Satellite radar information capture by the Sentinel 1 constellation, in both ascending and descending orbits, was processed by TRE Altamira group to provide line of sight (LOS) ground displacements for each orbit between May 2015 to May 2017. This data was the basis for the development of the methods to estimate true displacement vectors and the geotechnical interpretation in this thesis.

A method was presented that combines changes of LOS distance between the radar sensor and each sector of landslides and the assumption that the horizontal component of the ground movement is subparallel to the slope aspect, to estimate the true landslide displacement vector. This approach was validated a the Ripley Landslide Ripley landslide in the area of research, which confirm the results of the method were consistent with the known landslide deformation behaviour.

The verified method was applied to other landslides along the Thompson River Valley in order to enhance the interpretation of the kinematics of these landslides. The final results of this method also were compared with other available outcomes of other investigations by other researchers on the landslides of the research area.

5.2. General Conclusions

Specific conclusions have been presented in Chapter 3 and Chapter 4 of this thesis, which correspond to the detailed outcome from the methods and results at the landslides within the study area. The results of the applied method in this research on different landslides along the Thompson River valley confirm slow to extremely slow movement for all landslides within the area of research according to the classification by Cruden and Varnes, 1996. The results also agree with the previous investigation's results.

The results of the satellite InSAR ground deformation monitoring for the Ripley landslide show the maximum velocity of 82 mm/year that is the most active landslide which was investigated in this research. The velocity for different sectors of the Ripley landslide is reported between 2 to 82 mm/year based on the results of the applied method. The sectors near the Thompson river, on the toe of the slide, are more active than others within the extent of the Ripley landslide. This landslide is classified as slow to very slow (depending on the different sectors) based on the Cruden and Varnes, 1996 classification. The GPS results for this landslide supports these results. An updated interpretation of this landslide's kinematic confirms a compound landslide with an upper wedge pushing the toe over a weak sub-horizontal surface. This agrees previous investigations.

The South Extension landslide, which is an extension of the South landslide, is the second most active landslide investigated in this research. The velocity of different sectors on this landslide vary between 3 and 64 mm/year which is classified as a very slow landslide. The results of ground movement support the South Extension landslide as a translational landslide at its toe and central section with more retrogressive rotational movement towards the back scarp of the landslide.

The Redhill landslide is the third most active landslide in the area with a maximum velocity of 56 mm/year on the toe of the landslide. The slowest velocity for selected sectors within this landslide is 8 mm/year and the Redhill landslide also is classified as a very slow landslide base on the results of the applied method in this research. The interpreted kinematic of this landslide supports Retrogressive rotational movement on the Redhill landslide.

The North landslide movements range between 2 and 35 mm/year which put this landslide in very slow class in the Cruden and Varnes 1996 classification. The activity of the North landslide is lower than other 3 landslides above, the kinematic of this landslide suggests rotational mechanism is active at the toe of the North landslide with very low activity behind this section. The results of the estimated real displacement vectors for the Goddard landslide vary between 2 and 29 mm/year, classified as very slow. The interpretation of the landslide kinematics supports retrogressive rotational movements. The Barnard landslide was the less active landslide part of the study, with a maximum velocity of 18 mm/year. This landslide is more active at the center of its extent and it is inactive in other parts of landslide. The minimum velocity within this landslide is only 2 mm/year.

Although there are no obvious seasonal displacement trends for most parts of the landslides based on the results in this research, it is interpreted that these were obscured due to the low

cumulative LOS and measurement precision of the data as well as the assumptions behind the method to estimate the real displacement vectors. Other research has identified that the movements in the Ripley landslide accelerate in late summer to Fall and decelerate in spring. This has also been observed to some extent for other landslides (Hendry et al., 2015; Huntley 2021). A brief summary of landslides activity within the research area is presented in Table 5-1.

The approach presented for landslide investigation based on combining Satellite InSAR orientations, assumptions of landslide horizontal displacement direction based on topographic characteristics, and averaging for space and time inconsistencies between different LOS orientation acquisition; provides valuable additional insight to common interpretation of East-West and vertical components. The work in this paper illustrates how the added benefits of the approach include enhanced characterization of landslide kinematics and state of activity. It is important to note that the assumption of landslide directionality needs to be evaluated on a case-by-case, as surface topographic characteristics could mislead the horizontal orientation of movement for complex mechanisms.

5.3. Recommendations for future research

The method presented in this research to estimate the true displacement vectors of landslides suggests an accurate, reliable and cost-efficient method to monitor ground movement in the region of study where it was validated. This assumes specific kinematics, and if the method is to be applied for many landslides all around the world, it should be noted that the assumption of horizontal movement in the average slope's aspect direction needs to be evaluated at other localities and for other landslide types. Furthermore, surface topographic characteristics could mislead the horizontal orientation of movement for complex mechanism, when the scale of the landslide sectors and landslide features (e.g. scarps) are such that the aspect of the slope becomes

misleading with regards to the overall downslope direction, or when basal sliding surfaces have different dip directions than the overall surface slopes. The accuracy of this method should be evaluated for these other contexts.

The other recommendation is about the monitoring of ground behind the known back scarps of the landslides in the area of research. Despite the very slow movements detected behind te back scarp areas of all landslides, these movements could be within the limit of detection of the applied method and we cannot discard precursors to further retrogression of these landslides. Therefore, continuous InSAR monitoring and other complementing techniques (e.g. LiDAR and change detection, in-place instrumentation) up slope from the known active area of each landslide could allow identifying any ongoing landslide retrogression.

Landslide	Monitoring Timeline	Maximum Velocity (mm/year)	Minimum Velocity (mm/year)	Velocity Classification	Type of Landslide's kinematic
Goddard	May2015 to May 2017	2	29	Very Slow	Retrogressive rotational
North	May2015 to May 2017	2	35	Very Slow	Rotational on the toe
South	May2015 to May 2017	2	26	Very Slow	transitional
South Extension	May2015 to May 2017	3	64	Very Slow	Transitional on the toe + Retrogressive rotational
Barnard	May2015 to May 2017	2	18	Very Slow	Rotational retrogressive
Redhill	May2015 to May 2017	8	56	Very Slow	Retrogressive rotational
Ripley	May2015 to May 2017	2	82	Very Slow	Compound Landslide

Table 5-1- Summary of key deformation characteristics for all monitored landslides along the Thompson River valley

References

1. Abe, T.; Iwahana, G.; Efremov, P. v.; Desyatkin, A. R.; Kawamura, T.; Fedorov, A.; Zhegusov, Y.; Yanagiya, K.; & Tadono, T. Surface displacement revealed by L-band InSAR analysis in the Mayya area, Central Yakutia, underlain by continuous permafrost. Earth, Planets and Space. **2020** 72(1), 138.
2. Charrière, M.; Humair, F.; Froese, C.; Jaboyedoff, M.; Pedrazzini, A.; & Longchamp, C. From the source area to the deposit: Collapse, fragmentation, and propagation of the Frank Slide. Geological Society of America Bulletin. **2020**, B31243.1.
3. Choe, B.-H.; Blais-Stevens, A.; Samsonov, S.; & Dudley, J. Sentinel-1 and RADARSAT Constellation Mission InSAR Assessment of Slope Movements in the Southern Interior of British Columbia, Canada. Remote Sensing. **2021**, 13(19), 3999.
4. Clague, J. J.; & Evans, S. G. (n.d.). Geologic Framework of Large Historic Landslides in Thompson River Valley, British Columbia. **2003**, 9 (3): 201-212.
5. Cruden, D. M.; & Martin, C. D. Before the Frank Slide. Canadian Geotechnical Journal. **2007**, 44(7), 765–780.
6. D. Huntley, D. R.-C. R. C. J. J. and P. B.Understanding plateau and prairie landslides: annual report on landslide research in the Thompson River valley, British Columbia, and the Assiniboine River valley, Manitoba-Saskatchewan **2020-2021**
7. Hendry, M. T.; Macciotta, R.; Martin, C. D.; & Reich, B. Effect of Thompson River elevation on velocity and instability of Ripley Slide. Canadian Geotechnical Journal. **2015**, 52(3), 257–267.
8. Hungr, O.; Leroueil, S.; & Picarelli, L. The Varnes classification of landslide types, an update. Landslides. **2014**, 11(2), 167–194.

9. Huntley, D.; Bobrowsky, P.; Hendry, M.; Macciotta, R.; Elwood, D.; Sattler, K.; Best, M.; Chambers, J.; & Meldrum, P. Application of multi-dimensional electrical resistivity tomography datasets to investigate a very slow-moving landslide near Ashcroft, British Columbia, Canada. Landslides. **2019a**, 16(5), 1033–1042.
10. Huntley, D.; Rotheram-Clarke, D.; Pon, A.; Tomaszewicz, A.; Leighton, J.; Cocking, R.; & Joseph, J. Benchmarked RADARSAT-2, SENTINEL-1 and RADARSAT Constellation Mission Change-Detection Monitoring at North Slide, Thompson River Valley, British Columbia: ensuring a Landslide-Resilient National Railway Network. Canadian Journal of Remote Sensing. **2021**, 47(4), 635–656.
11. Journault, J.; Macciotta, R.; Hendry, M. T.; Charbonneau, F.; Huntley, D.; & Bobrowsky, P. T. Measuring displacements of the Thompson River valley landslides, south of Ashcroft, BC, Canada, using satellite InSAR. Landslides. **2018**, 15(4), 621–636.
12. Macciotta, R.; Hendry, M.; & Martin, C. D. Developing an early warning system for a very slow landslide based on displacement monitoring. Natural Hazards. **2016**, 81(2), 887–907.
13. Macciotta, R.; Hendry, M. T.; & Martin, D.; Lan, H. Monitoring of the Ripley Slide in the Thompson River Valley, BC. **2014**. https://doi.org/10.13140/2.1.2811.7125
14. Mancini, F.; Grassi, F.; & Cenni, N. A Workflow Based on SNAP–StaMPS Open-Source Tools and GNSS Data for PSI-Based Ground Deformation Using Dual-Orbit Sentinel-1 Data: Accuracy Assessment with Error Propagation Analysis. Remote Sensing. **2021**, 13(4), 753.

15. Mei, S.; Poncos, V.; & Froese, C. Mapping millimetre-scale ground deformation over the underground coal mines in the Frank Slide area, Alberta, Canada, using spaceborne InSAR technology. Canadian Journal of Remote Sensing. **2008**, 34(2), 113–134.
16. Rodriguez, J.; Macciotta, R.; Hendry, M. T.; Roustaei, M.; Gräpel, C.; & Skirrow, R. UAVs for monitoring, investigation, and mitigation design of a rock slope with multiple failure mechanisms—a case study. Landslides. **2020**, 17(9), 2027–2040.
17. Vallee, M. Falling in Place: Geoscience, Disaster, and Cultural Heritage at the Frank Slide, Canada's Deadliest Rockslide. Space and Culture. **2019**, 22(1), 66–76.
18. Xu, D.; Hu, X.-Y.; Shan, C.-L.; & Li, R.-H. Landslide monitoring in southwestern China via time-lapse electrical resistivity tomography. Applied Geophysics. **2016**, 13(1), 1–12.
19. Rodriguez, J.; Deane, E.; Hendry, M.; Macciotta, R.; Evans, T.; Gräpel, C.; Skirrow, R.Practical evaluation of single-frequency dGNSS for monitoring slow-moving landslides. Landslides. **2021**, 18, 3671-3684.
20. Macciotta, R.; Hendry, M. Remote sensing applications for landslide monitoring and investigation in Western Canada. Remote Sensing. **2021**, 13(3): 366
21. Lan, H.; Zhao, X.; Macciotta, R.; Peng, J.; Li, L.; Wu, Y.; Zhu, Y.; Liu, X.; Zhang, N.; Liu, S.; Zhou, C.; Clague, J.J. The cyclic expansion and contraction characteristics of a loess slope and implications for slope stability. Scientific Reports. **2021**, 11:2250
22. Woods, A.; Macciotta, R.; Hendry, M.; Stewart, T.; Marsh, J. Updated understanding of the deformation characteristics of the Checkerboard Creek rock slope through GB-InSAR monitoring. Engineering Geology. **2020**, 281:105974

23. Macciotta, R.; Grapel, C.; Skirrow, R. Fragmented rockfall volume distribution from photogrammetry-based structural mapping and discrete fracture networks. Applied Sciences. **2020**, 10:6977
24. Deane, E.; Macciotta, R.; Hendry, M.; Grapel, C.; Skirrow, R. Leveraging historical aerial photographs and digital photogrammetry techniques for landslide investigation – a practical perspective. Landslides. **2020**, 17, 1989-1996.
25. Hendry, M.; Macciotta, R.; Martin, C.D.; Reich, B. Effect of Thompson River elevation on velocity and instability of Ripley Slide. Canadian Geotechnical Journal. **2015**, 52(3): 257-267
26. Huntley, D.; Bobrowsky, P.; Hendry, M.; Macciotta, R.; Best, M. Multi-technique Geophysical Investigation of a Very Slow-moving Landslide Near Ashcroft, British Columbia, Canada. Journal of Environmental and Engineering Geophysics. **2019b**, 24(1):87–110
27. Huntley, D.; Holmes, J.; Bobrowsky, P.; Chambers, J.; Meldrum, P.; Wilkinson, P.; Donohue, S.; Elwood, D.; Sattler, K.; Hendry, M.; Macciotta, R.; Roberts, N. Hydrogeological and geophysical properties of the very slow-moving Ripley Landslide, Thompson River valley, British Columbia. Canadian Journal of Earth Sciences. **2020**, 57 (12): 1371-1391.
28. Sattler, K.; Elwood, D.; Hendry, M.T.; Huntley, D.; Holmes, J.; Wilkinson, P.B.; Chambers, J.; Donohue, S.; Meldrum, P.I.; Macciotta, R.; Bobrowsky, P.T. Quantifying the contribution of matric suction on changes in stability and displacement rate of a translational landslide in glaciolacustrine clay. Landslides. **2021**, 18, 1675- 1689.

29. Schafer, M. 2016. Kinematics and controlling mechanics of the slow moving Ripley landslide. MSc Thesis, University of Alberta, Canada.
30. Eshraghian A.; Martin D.; Cruden D. Complex Earth Slides in the Thompson River Valley, Ashcroft, British Columbia. Environmental & Engineering. **2007**, 13 (2); 161-181.
31. Porter M.J.; Savigny K.W.; Keegan TR.; Bunce CM.; MacKay C. Controls on stability of the Thompson River landslides. 55th Canadian Geotechnical Conference, Niagara Falls, Canada. **2002**.
32. Huntley D.H.; Bobrowsky P. Surficial geology and monitoring of the Ripley slide, near Ashcroft, British Columbia, Canada. Geological Survey of Canada. **2014**, 7531, 21 p.
33. Herrera G.; Gutierrez F.; Garcia-Davalilo J.C; Guerrero J.; Notti D.; Galve JP.; Fernandez-Merodo JA.; Cooksley G. Multi-sensor advanced DInSAR monitoring of very slow landslides: The Tena Valley case study (Central Spanish Pyrenees). Remote Sensing of Environment. **2012**, 381-387, 08037.
34. Colesanti C.; Wasowski J. Investigating landslide with space-borne Synthetic Aperture Radar (SAR) interferometry. Engineering Geology. **2006**, 88, 173- 199.
35. Vadivel S.K.P.; Kim D.J.; Kim Y.C. Time-series InSAR Analysis and post-processing Using ISCE-StaMPS package for Measuring Bridge Displacements. Korean Journal of Remote Sensing. **2020**, 36, 4, 527-534.
36. Motagh M.; Shamshiri R.; Haghighi MH.; Wetzel HU.; Akbari B.; Nahavandchi H.; Roessner S.; Arabi S. Quantifying groundwater exploitation induced subsidence in the Rafsanjan plain, southeastern Iran, using InSAR time-series and in situ measurements. Engineering Geology. **2017**, 218, 152-161.

37. Hooper A.; Bekaert D.; Spaans K.; Arikan M. Recent advances in SAR interferometry time series analysis for measuring crustal deformation. Technophysics. **2011**, 514-517.
38. Chen B.; Zhenhong L.; Zhang C.; Ding M.; Zhu W.; Zhang S.; Han B.; Du Y.; Cao Y.; Zhang C.; Liao Z.; Wang J.; Peng J. Wide Area Detection and Distribution Characteristics of Landslides along Sichuan Expressways. Remote Sens. **2022**, 14 (14), 3431.
39. Liu Y.; Yao X.; Gu Z.; Zhou Z.; Liu X.; Chen X.; Wei S. Study of the Automatic Recognition of Landslides by Using InSAR Images and the Improval Mask R-CNN Model in the Eastern Tibet Plateau. Remote Sens. **2022**, 14(14), 3362.
40. Mastro P.; Masiello G.; Serio C.; Pepe A. Change Detection Techniques with Synthetic Aperture Radar Images Experimens with Random Forests and Sentinel-1 Observations. Remote Sens. **2022**, 14(14), 3323.
41. Abdel-Hamid A.; Dubovyk O.; Greve K. The potential of Sentinel-1 InSAR coherence for grasslands monitoring in Eastern Cape, South Africa. International Journal of Applied Earth Observations and Geoinformation. **2021**, 98, 102306.
42. Dumka K.R.; SuriBabu D.; Malik K.; Prajapati S.; Narain P. PS-InSAR derived deformation study in the Kachchh, Western India. Applied Computing and Geosciences. **2020**, 8, 100041.
43. Castellazzi P, Schmid W. Interpreting C-band InSAR ground deformation data for large-scale groundwater management in Australia: Journal of Hydrology. Regional Studies. **2020**, 34, 100774.

44. Soltanieh A.; Macciotta R. Updated understanding of the Ripley landslide kinematics using satellite InSAR. Geosciences. **(In press)** (2)

45. Ferretti A.; Fumagalli A.; Novali F.; Prati C.; Rocca F and Rucci A. A new algorithm for processing interferometric data-stacks: SqueeSAR IEEE Trans. Geosci. Remote Sens. **2011**

46. Eshraghian A.; Martin D.; Cruden D. Complex Earth Slides in the Thompson River Valley, Ashcroft, British Columbia: Environmental & Engineering. **2007**. (2)

47. Eshraghian A.; Hazard Analysis of Reactivated Earth Slides in the Thompson River Valley, Ashcroft, British Columbia. PHD Thesis, University of Alberta. **2007** (2)

48. Lévy S.; Jaboyedoff M.; Locat J.; Demers D. Erosion and channel change as factors of landslides and valley formation in Champlain Sea Clays: The Chacoura River, Quebec, Canada. Geomorphology. **2011**, 145-146, 12-18.

49. Arbanas Z.; Vivoda Prodan M.; Mihalić Arbanas S.; Peranić J. Identification, monitoring and simulation of landslides in the Rječina River Valley, Croatia. STAREPS Conference paper. **2014**.

50. Guzzetti F.; Reichenbach P.; Ghigi S. Rockfall Hazard and Risk Assessment Along a Transportation Corridor in the Nera Valley, Central Italy. Environmental Management. **2004**, 34, 191-208.

51. Hunger, O.; Evans, S.G.; Hazzard, J. Magnitude and frequency of rock falls and rock slides along the main transportation corridors of southwestern British Columbia. Geological Survay of Canada. **1999**.

52. Giannecchini, R.; Galanti, Y.; D'Amato Avanzi, G. Critical rainfall thresholds for triggering shallow landslides in the Serchio River Valley (Tuscany, Italy). Natural Hazards and Earth System Sciences. **2012**, 12,829-842.
53. Jaiswal, P.; Van Westen, C.J..Use of quantitative landslide hazard and risk information for local disaster risk reduction along a transportation corridor: a case study from Nilgiri district, India. Nat Hazards. **2012**, 65, 887-913.
54. Weidner, L.; DePrekel, K.; Oommen, T.; Vitton, S. Investigating large landslides along a river valley using combined physical, statistical, and hydrologic modeling. Engineering Geology. **2019**, 105169.
55. Tonini, M.; Pedrazzini, A.; Penna, I.; Jaboyedoff, M. Spatial pattern of landslides in Swiss Rhone Valley. Nat Hazards. **2014**, 73, 97-110.
56. Bradley, K.; Mallick, R.; Andikagumi, H.; Hubbard, J.; Meilianda, E.; Switzer, A.; Du, N.; Brocard, G.; Alfian, D.; Benazir, B.; Feng, G.; Yun, S.; Majewski, J.; Wei, S.; M. Hill, E. Earthquake-triggered 2018 Palu Valley landslides enabled by wet rice cultivation. Nature Geoscience. **2019**, 12, 935-939.
57. Wang, B.; Paudel, B.; Li, H. Retrogression characteristics of landslides in fine -grained permafrost soils, Mackenzie Valley, Canada. Landslide. 2009, 6. 121-127
58. TRE ALTAMIRA Group. 2018. Ground Deformation InSAR Analysis over the Thompson Canyon, British Columbia Technical Details. Published August 10, 2018.